

T-2617

GEOLOGY, ALTERATION AND GENESIS OF THE NG
ALUNITE AREA, SOUTHERN WAH WAH RANGE,
SOUTHWESTERN UTAH

By

Albert H. Hofstra

ProQuest Number: 10782367

All rights reserved

INFORMATION TO ALL USERS

The quality of this reproduction is dependent upon the quality of the copy submitted.

In the unlikely event that the author did not send a complete manuscript and there are missing pages, these will be noted. Also, if material had to be removed, a note will indicate the deletion.



ProQuest 10782367

Published by ProQuest LLC (2018). Copyright of the Dissertation is held by the Author.

All rights reserved.

This work is protected against unauthorized copying under Title 17, United States Code
Microform Edition © ProQuest LLC.

ProQuest LLC.
789 East Eisenhower Parkway
P.O. Box 1346
Ann Arbor, MI 48106 – 1346

A thesis submitted to the Faculty and the Board of Trustees of the Colorado School of Mines in partial fulfillment of the requirements for the degree of Master of Science (Geology).

Golden, Colorado

Date April 10, 1984

Signed: Albert H. Hofstra

Albert H. Hofstra

Approved: P. J. LeAnderson

Dr. P. J. LeAnderson
Thesis Advisor

Golden, Colorado

Date 4/11/84

J. J. Finney

Dr. J. J. Finney
Head, Department of Geology

ABSTRACT

The NG Alunite Area is one of the largest alunite deposits in the U.S. with reserves of 630 million metric tons of >30% alunite (>10% Al_2O_3).

Oligocene calc-alkaline ignimbrites, overlying Paleozoic carbonates, are pervasively altered to dominantly quartz and alunite to form four large tabular to funnel-shaped deposits. These altered volcanics are zoned horizontally from silica at the center, outward through quartz-alunite, kaolinite-hematite, montmorillonite-chlorite-pyrite and chlorite-calcite zones. The vertical pattern grades from silica at the top through quartz-alunite to quartz-alunite-sericite-pyrite at a depth of 250-300 meters.

The altered areas are associated with a system of normal faults, and are arranged concentrically about three small Miocene porphyritic rhyolite plugs. Monoclinial flexures and tilted fault blocks may reflect the presence of a shallow-level intrusion. A K-Ar age date of 22.5 m.y. on alunite is contemporaneous with rhyolites in this part of the Great Basin.

The isotopic composition of S in alunite of +1.45 per mil is indicative of magmatically derived S. Fluid inclusions in quartz veins formed prior to pervasive alteration have homogenization temperatures of 275-325°C and salinities of <2 eq. wt. % NaCl in the silica and quartz-alunite zones. Inclusions in alunite veinlets,

formed during the episode of pervasive alteration, consist only of small, vapor dominant inclusions which were too small for microthermometric analysis. Mineral stability relations indicate the fluids depositing alunite consisted of an aqueous solution of H_2SO_4 .

These features suggest that H_2S -bearing fluids, possibly evolved from a shallow-level intrusion, rose and mixed with circulating meteoric waters which eventually crossed the boiling curve, near to or at the paleoground water table, resulting in the formation of vigorously boiling hydrothermal systems at the sites of fluid upwelling. At, and above the boiling water table, H_2S and other exsolved gases were oxidized by atmospheric oxygen to form H_2SO_4 and other compounds which altered the host rocks to alunite.

The deposits at NG probably reflect the action of only the near surface part of a larger hydrothermal system. Possible sites for sulphide mineralization at depth within the hydrothermal system at NG include: (1) porphyry-type mineralization in the contact zone of the shallow-level intrusion, (2) skarn-type mineralization in the superjacent rocks above the intrusion, and (3) vein and/or replacement mineralization along fluid pathways. In addition, if current models of precious metal mineralization in epithermal systems apply, then the potential for precious metal mineralization at the level where boiling occurred is also possible.

Rock samples obtained from the acid-altered areas have uniformly low trace element contents of Mo, Cu, Zn, Pb, Ag, and Au. Samples

T-2617

from quartz-sericite-pyrite veins and from jasperoid occurring locally in the area yield anomalous Cu and Zn-Ag values, respectively.

Samples from the porphyritic rhyolite plugs have uniformly low trace element contents of Mo, Cu, Zn, Pb, Ag, Au, As, Sn, W, and F. These data suggest that if buried mineralization occurs in the area it may be composed of Cu, Zn, and Ag sulphides or associated elements.

TABLE OF CONTENTS

	Page
ABSTRACT	iii
LIST OF FIGURES.	vii
LIST OF TABLES	ix
LIST OF PLATES	x
ACKNOWLEDGMENTS.	xi
INTRODUCTION	1
REGIONAL METALLOGENY	13
GEOLOGIC SETTING AND STRATIGRAPHIC HISTORY	18
GEOLOGY OF THE NG ALUNITE AREA	23
ALTERATION AND MINERALIZATION.	47
TRACE ELEMENT GEOCHEMISTRY	61
FLUID INCLUSIONS	67
ISOTOPIC COMPOSITION OF SULFUR	85
SUMMARY AND GENETIC MODEL.	88
REFERENCES CITED	97
APPENDIX A	107
APPENDIX B	118

LIST OF FIGURES

	Page
Figure 1. Location Map.	2
Figure 2. Geologic Map of the Southern Wah Wah Range.	3
Figure 3. Cross-section through the Southern Wah Wah Range.	5
Figure 4. Locations of Alunite Reserves and Resources in the Conterminous United States.	7
Figure 5. Oblique Aerial View of the NG Alunite Area.	10
Figure 6. Regional Geologic and Metallogenic Features	14
Figure 7. Generalized Geologic Column	24
Figure 8. Joint Frequency Data.	43
Figure 9. Vein and Alteration Paragenesis	49
Figure 10. Cross Section through NG Area C.	56
Figure 11. Phase Relations in the System $K_2O-Al_2O_3-SiO_2-SO_3$	59
Figure 12. Fluid Inclusion Data	68
Figure 13. Primary Liquid-Dominant Inclusion in Calcite	70
Figure 14. Secondary Liquid-Dominant Inclusion in Calcite	71
Figure 15. Primary Liquid-Dominant Inclusion in Quartz.	72
Figure 16. Secondary Liquid-Dominant Inclusion in Quartz.	73
Figure 17. Primary Vapor-Dominant Inclusion in Quartz	74
Figure 18. Primary Vapor-Dominant Inclusion in Alunite.	75
Figure 19. Pseudosecondary Vapor-Dominant Inclusion in Alunite.	76
Figure 20. Lateral Temperature Gradient Based Upon Fluid Inclusions	80
Figure 21. Hypothetical Evolution of the Hydrothermal System.	91

	Page
Figure B-1. Percent Frequency Histogram and Cumulative Percent Frequency Plot - Gold.	124
Figure B-2. Percent Frequency Histogram and Cumulative Percent Frequency Plot - Silver.	125
Figure B-3. Percent Frequency Histogram and Cumulative Percent Frequency Plot - Lead.	126
Figure B-4. Percent Frequency Histogram and Cumulative Percent Frequency Plot - Zinc.	127
Figure B-5. Percent Frequency Histogram and Cumulative Percent Frequency Plot - Copper.	128
Figure B-6. Percent Frequency Histogram and Cumulative Percent Frequency Plot - Molybdenum.	129
Figure B-7. Percent Frequency Histogram and Cumulative Percent Frequency Plot - Copper, Zinc, and Lead Product.	130

LIST OF TABLES

	Page
Table 1. Modal Estimates for Volcanic Rocks.	25
Table 2. Alteration Pattern, NG Alunite Area	48
Table 3. Trace Element Geochemistry, NG Alunite Area	63
Table 4. Summary of Physical and Chemical Conditions Attending Alteration and Mineralization	89
Table A-1. Results of Heating Freezing Calibration Runs.	110
Table A-2. Fluid Inclusion Data.	111
Table B-1. Analytical Results - Trace Element Geochemistry . . .	119
Table B-2. Analytical Procedure - Cone Geochemical Inc..	122
Table B-3. Analytical Procedure - Bondar-Clegg Inc..	123

LIST OF PLATES

- Plate 1. Geologic Map
- Plate 2. Geologic Cross Section
- Plate 3. Alteration and Mineralization
- Plate 4. Trace Element Geochemistry and Fluid Inclusion
Sample Locations
- Plate 5. Trace Element Geochemistry

ACKNOWLEDGMENTS

I would like to thank Canyon Resources Corporation for providing financial support during the field work, and in particular, Bill Walker for his continued encouragement and support. I would like to extend my appreciation to Charles Bower at Earth Sciences, Inc. for his help in locating information in the company files which contributed to the body of this report. Many thanks are also extended to Skip Cunningham at the U.S. Geological Survey for his part in getting the Survey to perform sulphur isotope and K-Ar age determinations on alunite from the NG area. I would also like to thank Robert L. Harris, whose support permitted the completion of this research. Finally, I would like to thank my thesis committee, Bill Walker, Dr. R. C. Epis, and Dr. L. G. Closs, and especially my thesis advisor, Dr. Jim LeAnderson, for their critical review and suggestions which considerably improved the manuscript.

INTRODUCTION

The NG Alunite Area is located approximately 30 air miles southwest of Milford, Utah on the southern end of the Wah Wah Mountain Range in southwestern Utah. (Figs. 1 and 2).

Previous geologic investigations in the southern Wah Wah Mountains and vicinity have been extensive, but not extremely detailed in nature. Miller (1966) examined the structure and stratigraphy of the sedimentary rocks in the area, but largely neglected the stratigraphy and structure of the volcanics. Armstrong (1968) dealt with the large-scale structural and stratigraphic relations of the sedimentary rocks occurring in the region. Mackin (1960), Armstrong (1970), Anderson (1971), Best et al. (1973), Best and Brimhall (1974), Anderson and Rowley (1975), Shuey et al. (1976), Mehnert (1978), Rowley et al. (1978a), and Steven et al. (1979) have dealt extensively with the stratigraphic relations, structural framework, and geochronology of the Tertiary volcanic rocks occurring in the region. Recent local mapping by Lindsey and Osmonson (1978), Best and Keith (1979), and Lemmon and Morris (1979), of the volcanic rocks in areas adjacent to the thesis area have defined the stratigraphic relations of locally derived volcanics. The relation of ore deposits to tectonics, magmatism, and geophysical anomalies in this region have been reviewed extensively by Shawe and Stewart (1976), Stewart, Moore and Zietz (1977), and by Rowley et al. (1978b).

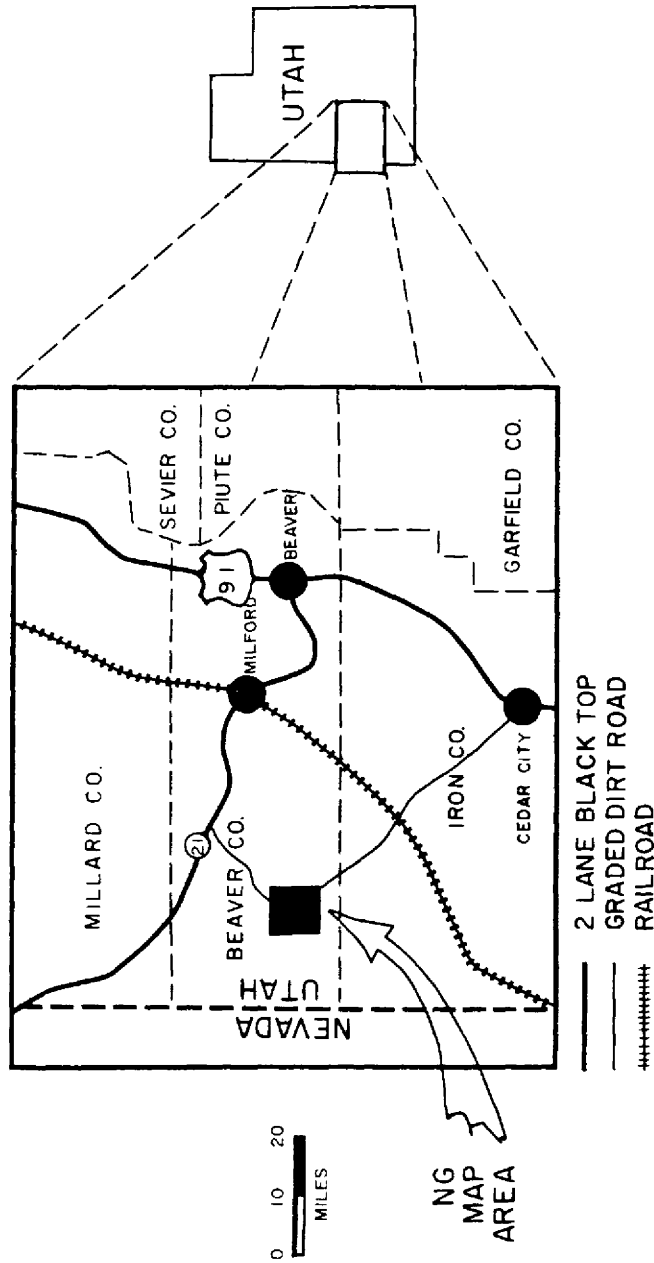


FIGURE 1. LOCATION MAP OF THE NG ALUNITE AREA

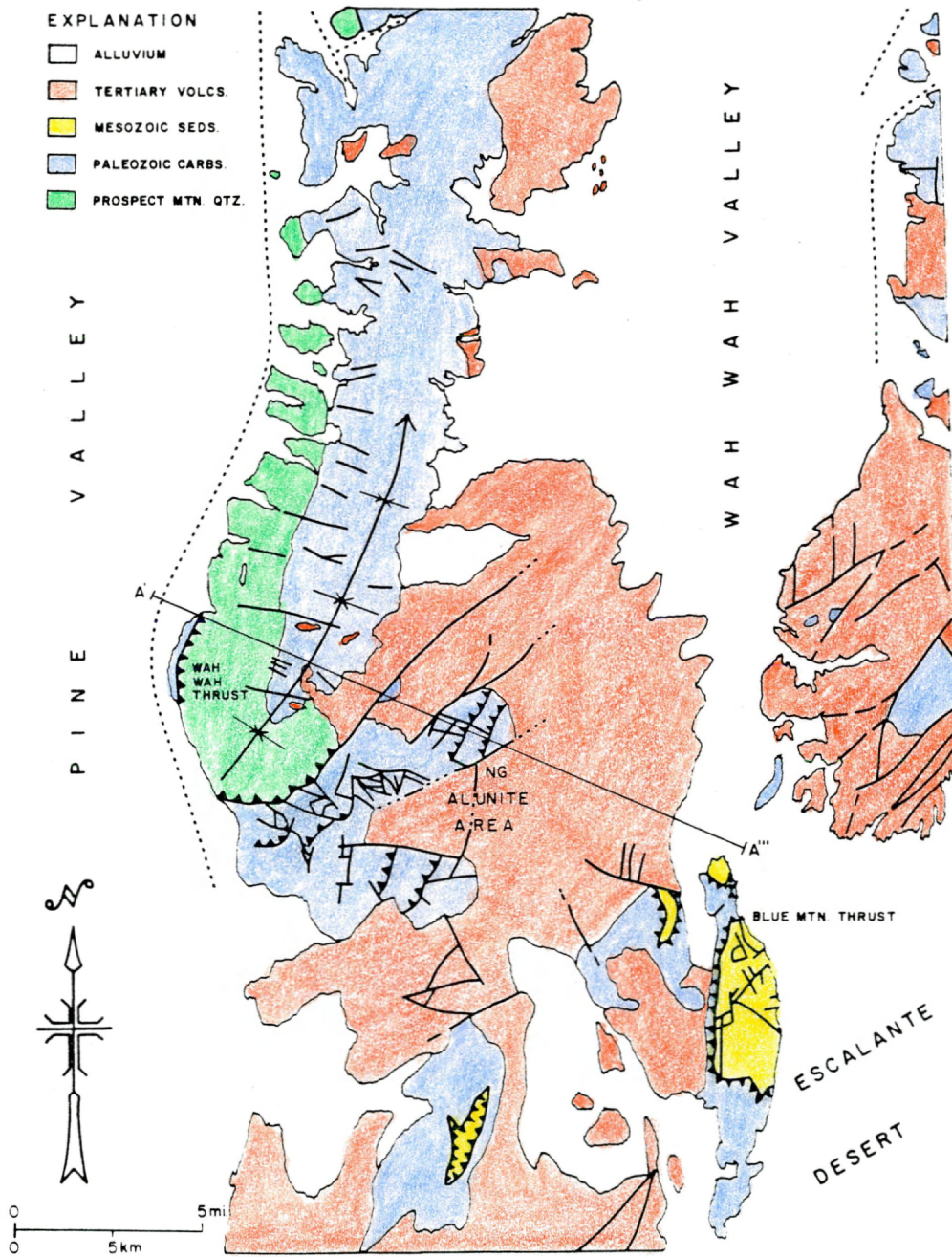


FIGURE 2, GEOLOGIC MAP OF THE SOUTHERN WAH WAH RANGE, SOUTHWESTERN UTAH (Adapted from STEVEN et al,1978)

The Wah Wah Mountains form a northtrending range bounded by alluviated valleys near the eastern margin of the Basin and Range Province. The Wah Wah Range is the topographic expression of a tilted fault block bounded by west-dipping listric normal faults, developed as a result of regional east-west extension during the Miocene. The core of the range consists of Paleozoic carbonates and quartzites (Figs. 2 and 3) which were thrust faulted and folded into a syncline during the Sevier Orogeny. The southern end of the range is covered by Cenozoic volcanics, predominantly calc-alkaline ignimbrites of Oligocene through Miocene age. These volcanics have been intensely faulted and altered to dominantly quartz and alunite. The alunite deposits at the NG Alunite area form one of the largest and highest grade deposits known in the world.

The stoichiometric formula for pure alunite is $KAl_3(SO_4)_2(OH)_6$, with a theoretical composition of 36.92 percent Al_2O_3 , 11.37 percent K_2O , 38.66 percent SO_3 , and 13.05 percent H_2O , although most natural alunite contains at least a small amount of Na in substitution for K (Cunningham, 1976) and sometimes Fe in place of Al (Botinelly, 1976 and Brophy et al. 1962). With the development of economic metallurgical methods for processing alunite bearing rocks, alunite deposits have become important as a potential nonbauxite source of aluminum with byproduct potassium sulfate fertilizer and sulfuric acid (Hall, 1978). Considering the United States' near total dependence on imported

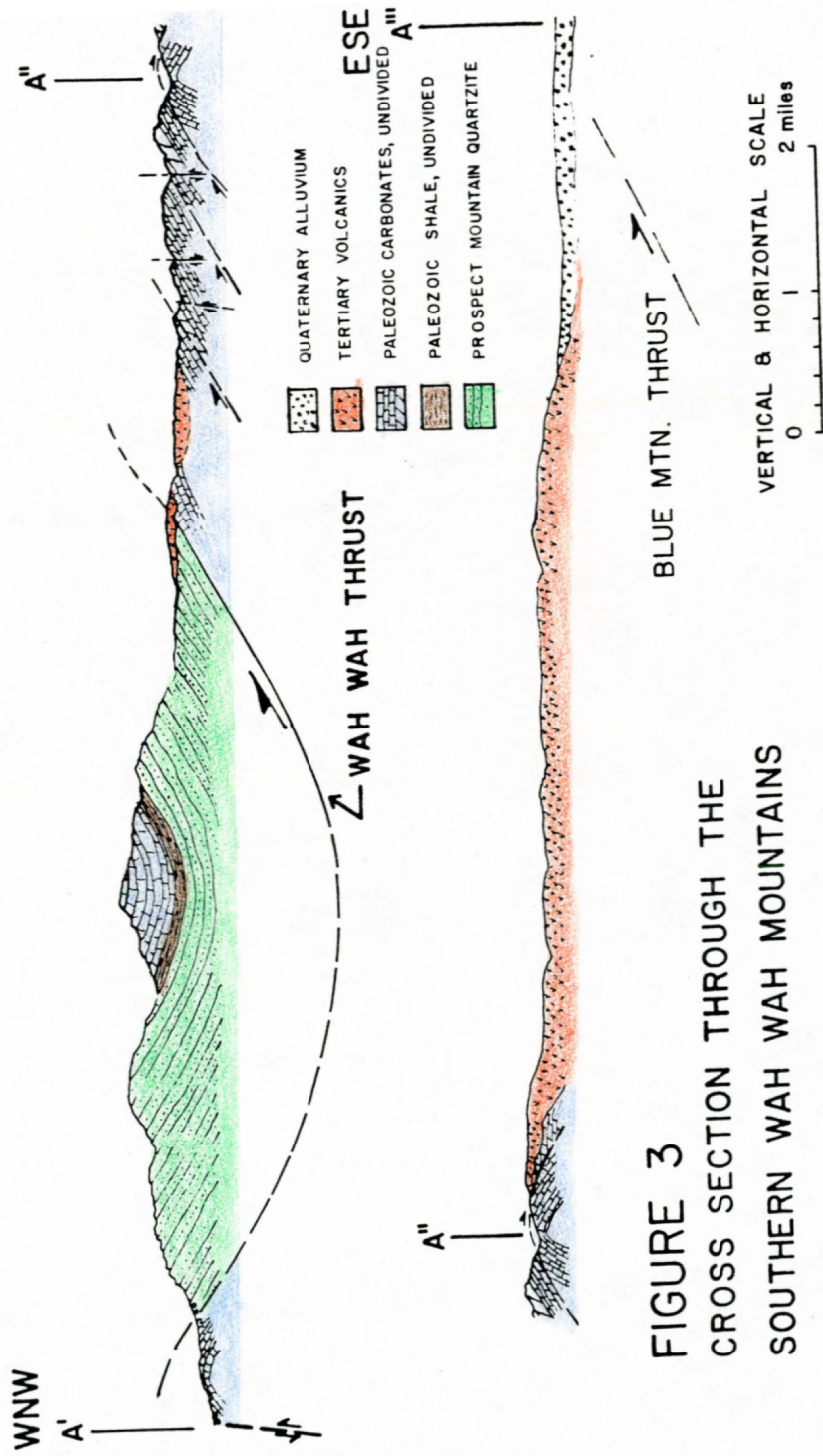


FIGURE 3
CROSS SECTION THROUGH THE
SOUTHERN WAH WAH MOUNTAINS

BLUE MTN. THRUST

ADAPTED FROM G. M. MILLER, 1966

bauxite and alumina, alunite deposits are valuable as a strategic resource of alumina.

Alunite occurs in two main types of deposits: (1) hydrothermal deposits as veins and replacements; and (2) supergene sedimentary deposits formed in clay rich rocks and lacustrine sediments (Hall, 1978). Figure 4 shows the distribution of these deposits in the conterminum United States. Hydrothermal vein and replacement deposits are formed during advanced argillic alteration at low pH's (Hemley et al. 1969). The host for these deposits are typically volcanic rocks of rhyolitic to dacitic composition (Hall, 1978). Replacement deposits constitute the bulk of the alunite resources, both in the United States and the rest of the world (Hall, 1978). Although these deposits rarely contain more than 30 percent alunite, equivalent to only 11 percent Al_2O_3 , Hall (1978) reports that they can be mined by large-scale, low-cost, open-pit methods.

The history of the development of alunite as a strategic mineral resource and one of economic value is given by Hall (1978). Alunite has been mined, in Italy since the 15th Century and in China since the 17th Century, as a raw material for making alum. During World War I, the supply of potash fertilizer from Germany was interrupted, prompting several companies to attempt to develop the alunite veins of the Marysvale district, Utah as a source of potassium sulfate fertilizer. Extraction of alumina from alunite was not attempted, except on a laboratory scale, until World War II when the supply of imported bauxite

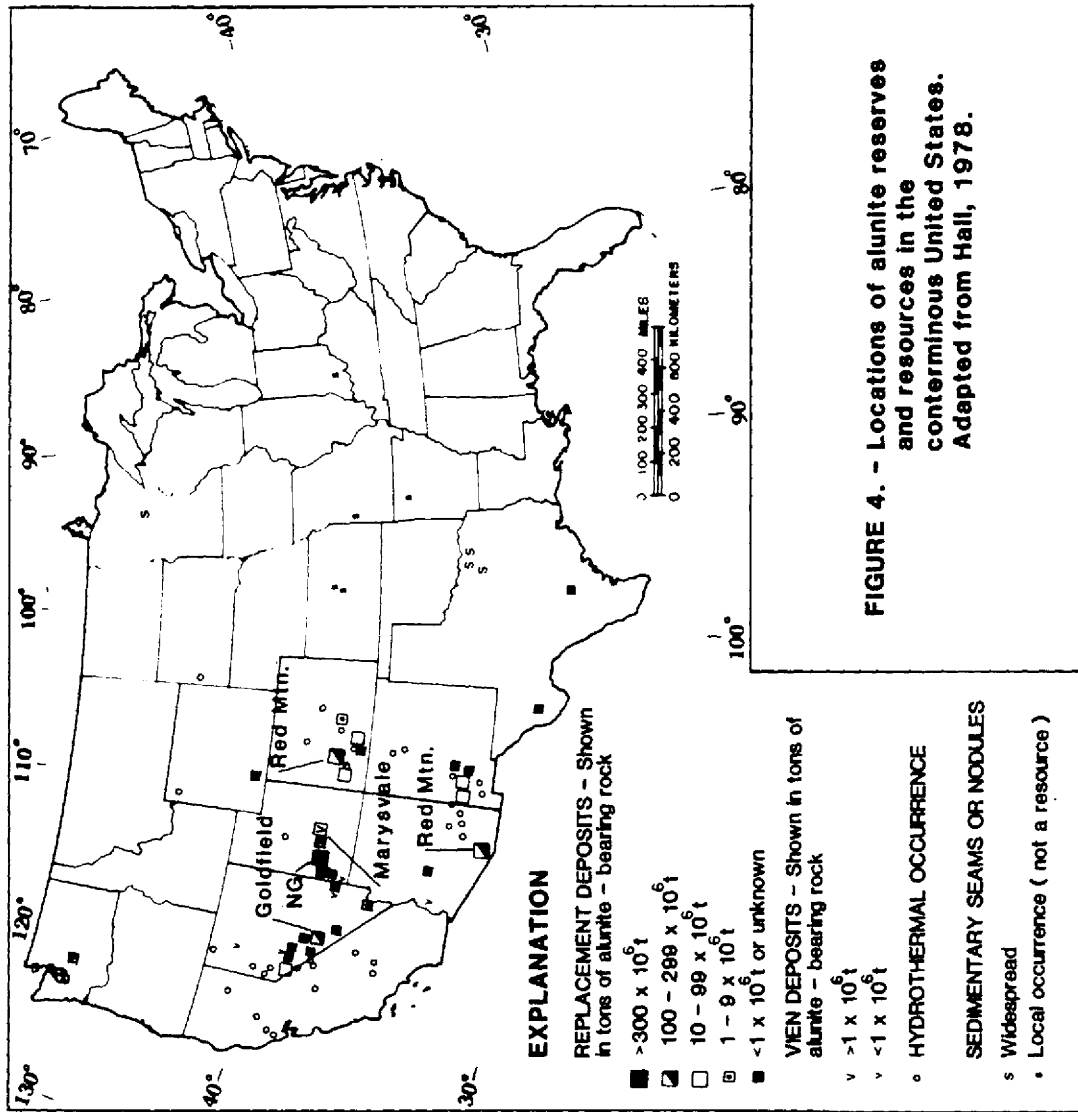


FIGURE 4. - Locations of alunitite reserves and resources in the conterminous United States. Adapted from Hall, 1978.

from Surinam and other sources was threatened. The alunite veins at Marysvale were again exploited, this time as a source of alumina with potassium sulfate as a byproduct. During the same period, an experimental plant in Japan produced several thousand tons of alumina from alunite-rich rocks mined in South Korea. Both operations succeeded technologically but were economic failures. No permanent operations resulted and after the war, alunite was relegated to the status of a potential, submarginal aluminum resource. Since then, only large-tonnage, low-grade replacement deposits are deemed to have sufficient reserves to support an alumina industry based on alunite. Hall (1978) reports that a potentially exploitable deposit should contain at least 90 million metric tons having an alunite content of at least 30 percent. Presently, the only plant in the world extracting alumina from these large-tonnage low-grade deposits is in Azerbaijan, U.S.S.R. This plant has the capacity to produce 200,000 tons of alumina per year, although it is questionable whether or not this operation would be competitive in an open market economy.

The principle domestic alunite reserves and potential resources occur in the Great Basin and Rio Grande Rift provinces of the western U.S. (Fig. 4). The most important alunite resource areas in this region (Hall, 1978) include: (1) the deposits at Goldfield, Nevada (Fig. 4) with identified resources of up to 300 million metric tons containing between 10 and 20 percent alunite; (2) the deposit at Red Mountain, near Patagonia, in southern Arizona (Fig. 4) with 200 million

metric tons containing roughly 25 percent alunite; (3) the deposit at Red Mountain, near Lake City, Colorado (Fig. 4) with 250 million metric tons containing between 30 and 40 percent alunite; and (4) the deposits at the NG Alunite Area, in the southern Wah Wah Mountains, Utah (Fig. 4) with 630 million metric tons containing greater than 30 percent alunite. Although alunite deposits are common in the western U.S., only the deposits at Red Mountain, Colorado and the NG Alunite Area have sufficient reserves and grades to potentially support an alunite based alumina industry.

The alunite at NG is concentrated in four discrete deposits, designated Areas A, B, C, and D, which form four resistant ridges (Fig. 5). Investigations of the area to date (Walker, 1971; Walker and Stevens, 1972; Perry and Walker, 1974; and Perry et al. 1977) by the Alumet Partnership (Southwire Company, Earth Sciences, Inc., and National Steel Corporation) have been exclusively oriented towards evaluating the economic potential of the alunite-rich altered volcanics as a source of smelter grade alumina. Drilling in recent years by the Alumet Partnership has proven reserves of 91 million metric tons containing 35 to 40 weight percent alunite in NG Area C, and indicated and inferred reserves of 544 million metric tons containing greater than 30 percent alunite from the remaining Areas B, C, and D. The Alumet group has overcome most of the metallurgical problems encountered in previous attempts to extract alumina from these low-grade deposits and propose to establish a commercial mine and mill

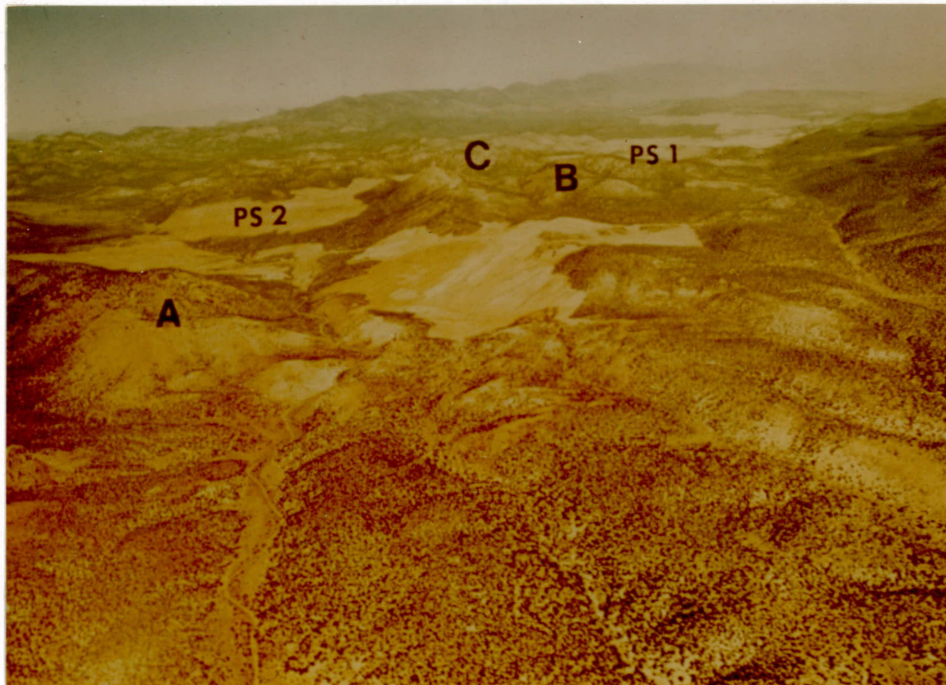


Figure 5. Oblique Aerial View of the NG Alunite Area, looking north. The letters A, B, and C mark major ridges of alunite altered volcanic rocks. Area D is located outside the field of view near the left margin of the photograph. PS₁ and PS₂ are proposed sites for future power stations. Photo courtesy Earth Sciences Inc.

designed to produce cell-grade alumina (alumina suitable for reduction to aluminum) along with by-product potassium sulfate fertilizer and sulfuric acid. The activities of the Alumet consortium have revived interest in alunite as a potential nonbauxite source of aluminum.

Alunite mineralization is also important because it is often reported to occur in association with other types of mineralization. For example, alunite is a well-developed alteration product at several hot-springs Hg deposits (White, 1981) and in many epithermal Au-Ag deposits such as at Goldfield, Nevada (Tolman and Ambrose, 1934) and Pueblo Viejo, Dominican Republic (Kesler et al. 1981). It has also been reported to occur at the tops of porphyry systems (Sillitoe, 1973) in the Andean Cu-belt of South America and in the southern Arizona Cu-province (Knight, 1977), including the Cu-Mo porphyry at Red Mountain, Arizona.

The NG Alunite Area, in particular, may also be related to several other types of mineral deposits. Topaz rhyolites, rich in F and lithophile elements, present at the Tetons just south of the project area (Lindsey and Osmonson, 1978) have been linked to: fluorspar-uranium mineralization, which occurs at the Staatz Mine south of Area D; Climax-type porphyry molybdenum mineralization, such as the Pine Grove deposits occurring on the western flank of the southern Wah Wah Range, 10 km northwest of the field area; and San Juan-type base and precious metal deposits rich in F and Mn (Burt, et al. 1982). Slack (1980) proposed that the alunite deposits at Red Mountain, near

Lake City, Colorado, represent the near-surface expression of the volcanic hosted epithermal system which deposited precious metals at the Golden Fleece mine and precious and base metals in nearby mines at deeper levels in the system. Secondary hematite-uraninite-pyrite mineralization is often associated with the San Juan-type deposits (Burt et al. 1982), and occurs in fault zones at the Blawn Mountain uranium deposit south of Area D and in lesser concentrations throughout the field area. Similar secondary uranium deposits associated with alunite mineralization also occur at Marysvale, Utah (Cunningham and Steven, 1979a, and Steven et al. 1980).

The purpose of this investigation is to determine the physico-chemical conditions necessary for the genesis of the NG alunite deposits and their relationship to: (1) other types of mineralization occurring in the area and (2) recent models of hydrothermal systems published in the literature. To achieve this purpose, observations on structure and alteration mineralogy were combined with fluid inclusion studies, trace element geochemistry, and S isotope compositions and K-Ar age dates recently provided by the U.S. Geological Survey.

REGIONAL METALLOGENY

Mineral deposits in the Great Basin Epigenetic Ore Province (Shawe and Stewart, 1976) can be separated into an eastern group dominated by base-metal deposits and a western group dominated by precious-metal deposits, although both areas have produced precious- and base-metals and tungsten. The division between these two sub-provinces is approximately parallel to the boundary between miogeoclinal and eugeoclinal rocks of the Paleozoic Cordilleran Orogenic Belt (Fig. 6), and may be due to the presence of Precambrian basement under the miogeoclinal or eastern part of the Great Basin.

Shawe and Stewart (1976) found that the mineral deposits occurring in the Great Basin tend to occur in clusters along linear trends, and that these belts of mineral deposits were most clearly developed in the eastern base-metal subprovince. The east-trending mineral belts in the base-metal subprovince also appeared to be more clearly related to features such as aeromagnetic anomalies, igneous activity, and structural discontinuities than the northwest trending mineral belts of Nevada (Fig. 6). The Pioche Mineral Belt in southwestern Utah and eastern Nevada (line Q-R on Fig. 6) exhibits the clearest relationship to geologic and geophysical features. It differs from other mineral belts in the base-metal sub-province in that it contains deposits of molybdenite, fluorspar, uranium, and alunite, (Shawe and Stewart, 1976). Geologic features associated with this belt as determined by Shawe

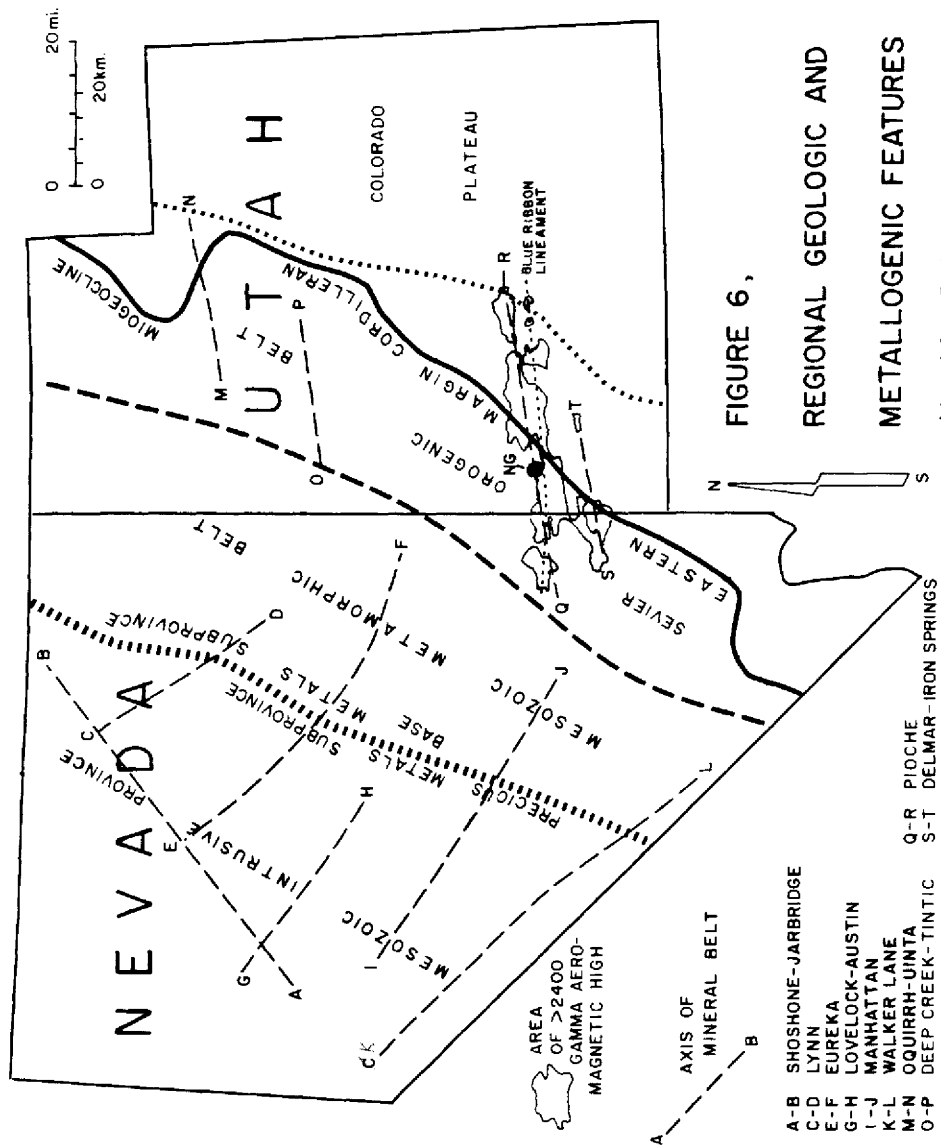


FIGURE 6,

REGIONAL GEOLOGIC AND METALLOGENIC FEATURES

Adapted from Rowley et al., 1978b, Stewart et al., 1977, and Shaws and Stewart, 1976.

and Stewart (1976), and Stewart et al. (1977) include: a broad system of positive aeromagnetic anomalies; porphyritic calc-alkaline volcanic and intrusive rocks; rhyolite lava flows of Miocene to Holocene age in the Utah portion; and a series of northeast to east-northeast trending faults which are locally en echelon. In the opinion of Shawe and Stewart (1976) these faults reflect a shear zone of left-lateral displacement in the basement. Stewart et al. (1977) found that the calc-alkaline igneous rocks, which occur in east-west patterns in eastern Nevada and western Utah, become successively younger to the south. They proposed that the east-west patterns are the result of a southward migrating front of igneous activity related to a southward propagating structural warp in a subducting plate. The scarcity of calc-alkaline igneous rocks and aeromagnetic anomalies between successive east-trending volcano-plutonic belts are thought to be due to the presence of competent rock between the weak east-trending pre-Tertiary structural zones in the crust which focused igneous activity.

In a later study, Rowley et al. (1978b) recognized a younger east-trending linear element within the Pioche Mineral Belt--the Blue Ribbon Lineament (Fig. 6). They found the lineament to be a fault zone based upon the alignment of features such as range terminations, valleys, aeromagnetic contours, a series of middle Miocene and younger rhyolite eruptive centers, and several hot springs associated with the major east-west faults. The deeper level of erosion north of the lineament and lower topography south of the lineament demonstrated that

the cumulative displacement across the lineament is down to the south. Rowley et al. (1978b) showed that the Blue Ribbon Lineament is also the site of a series of altered and mineralized rocks of middle Miocene to Pliocene age, which are commonly associated with rhyolites of the same age. The distinctive occurrences of Mo, F, U, and alunite deposits within the eastern part of the Pioche Mineral Belt appear to be more closely related to the younger Blue Ribbon Lineament and, based upon studies by Burt et al. (1982), to continentally derived topaz rhyolites. The rhyolites occurring along the lineament are middle Miocene and younger in age, correlative to the period of bimodal volcanism, indicating that the lineament developed coincidental with extensional rifting of the eastern Great Basin. The presence of hot springs areas along the lineament demonstrates that it has been a persistent geologic feature since the middle Miocene. The lineament apparently served as a channelway for magmas and hydrothermal solutions along much of its extent.

In the southern Wah Wah Range, the geology reflects the influence of the Blue Ribbon Lineament as exemplified by the presence of east-trending faults and several rhyolite intrusive and eruptive centers, some of which are associated with mineral deposits. The largest deposits include the porphyry molybdenite deposit at Pine Grove, fluor-spar at the Staats Mine, uranium at Blawn Mountain, and alunite at NG.

All of these relations suggest that the clustering of ore deposits in the Pioche Mineral Belt and Blue Ribbon Lineament is related to

deep-seated structural zones in basement rocks which have variously influenced the locus and character of structural, igneous, and hydrothermal activity much as the Precambrian shear zone influenced the locus of these features in the Colorado Mineral Belt during the Tertiary.

GEOLOGIC SETTING AND STRATIGRAPHIC HISTORY

The NG Alunite Area is located on the southeastern flank of the north-trending Wah Wah Range, a block-faulted range typical of the Basin and Range province. Most of the Wah Wah Range is composed of a conformable sequence of miogeoclinal sediments including quartzite, limestone, dolomite, and minor shale (Miller, 1966). According to Armstrong (1968), these sediments were deposited under relatively quiescent conditions, beginning sometime before the appearance of Cambrian fossils and continuing into the Triassic. Deposition took place near the eastern margin, or hingeline, of the Cordilleran miogeocline (Fig. 6) where the thick sequences of basin, slope, and rise sediments thin onto the Paleozoic continental shelf to the east. Precambrian metamorphic rocks 1.5 b.y. in age underlie the shelf sediments (Armstrong, 1968) as far west as the hingeline (Fig. 6) (Burchfiel and Davis, 1972).

In the Wah Wah Range, Precambrian metamorphic rocks are not exposed, but Paleozoic miogeoclinal sediments in excess of 10,000 feet have been measured and described by Miller (1966). The lower one-third of this sequence is composed of the basal clastic Eocambrian to Cambrian Prospect Mountain quartzite which is a prominent ridge former in the Wah Wah Range. The upper two-thirds of the sequence is composed of Cambrian to Triassic limestone and dolomite with minor intercalated shales.

Due to the lack of regional unconformities within the miogeoclinal rocks (Miller, 1966), it appears that in southwestern Utah sedimentation was not disrupted by the Antler orogeny occurring to the west, nor by the uplift of the Ancestral Rocky Mountains to the east, although both of these orogenic areas contributed clastics to the miogeocline.

Armstrong (1968) determined that Triassic marine sediments were the last to be deposited in the Cordilleran miogeocline due to uplift associated with the Sonoman orogeny occurring to the west. This uplift of the Great Basin region caused a major westward shift of the continental margin and resulted in the development of subaerial continental conditions over much of this area. Armstrong recognized that the site of the greatest uplift associated with the Jurassic Sonoman orogeny was located in the western part of the miogeocline (Nevada) where the accumulation of miogeoclinal sediments had been the thickest. Clastics derived from this highland area were spread as far east as the Colorado Plateau. However, beginning in the early Cretaceous, the major source of clastic material shifted to the east (Armstrong, 1968), at the previous location of the eastern margin of the Paleozoic miogeocline. Uplift along this belt was accomplished by a series of east-directed thrusts and minor folds which piled the thick sequence of miogeoclinal rocks onto the Paleozoic continental platform. Armstrong (1968) was the first to realize that these folds and thrusts represented the southern continuation of the Foreland Fold and Thrust Belt and referred

to this area as the Sevier orogenic belt. He found the major thrust sheets in this belt to have displacements of greater than 25 miles (40 km) and to be underlain by major, low-angle decollement surfaces. In southern Utah, Armstrong (1968) estimated the amount of shortening across the belt to be greater than 40 miles (65 km).

In the Wah Wah Range, two major thrusts related to the Sevier Orogeny are present. The western most Wah Wah thrust places Eocambrian to Cambrian Prospect Mountain quartzite over Cambrian to Jurassic carbonate and clastic rocks. This thrust sheet contains over 7,000 feet (2,250 meters) of resistant Prospect Mountain quartzite which forms prominent ridges along the western flank of the Wah Wah Range (Miller, 1966). The topographically lower Blue Mountain thrust places Cambrian and younger age carbonates over Jurassic clastic rocks (Miller, 1966). This thrust sheet is internally disrupted by a series of imbricate thrusts which in turn place older units over younger ones. At the NG Alunite Area, the carbonate rocks composing the Blue Mountain thrust sheet underlie the altered volcanic rocks, which are the subject of this investigation. A generalized cross-section through the Wah Wah Range at NG is presented in Figure 3.

In southwestern Utah, the Sevier highland was largely reduced to a peneplain by the middle Eocene (Armstrong, 1968). Consequently, the area became the site of deposition of the continental-lacustrine and conglomeratic sediments of the Claron Formation (Anderson and Rowley, 1975). The accumulation of the Claron Formation marked the

end of the long period of nondeposition which began in this area with the Triassic uplifts associated with the Sonoman orogeny.

Deposition of the Claron Formation continued until the late Oligocene, approximately 35 m.y. ago, when this area became the site of voluminous eruptions of calc-alkaline magma. Anderson and Rowley (1975) reported that the largest eruptions resulted in the formation of a sequence of regionally conformable ash-flow tuff units which are separated by volcanics of local origin. They suggested that these volcanic rocks were laid down on a surface of low relief as evidenced by the large lateral extent of some of the more voluminous units. In southwest Utah, the Needles Range Formation, Isom Formation, and Quichapa Group ignimbrites described by Anderson and Rowley (1975) and Mackin (1960) form the sequence of regionally extensive ashflow tuffs. Members from each of these formations are represented in the thesis area as well as an older basal ash-flow of more local origin. These rocks are described in detail in a later section on volcanic stratigraphy.

The character of volcanism changed in the Miocene (Anderson and Rowley, 1975), about 23 m.y. ago, with the eruption of a bimodal suite of basalt and rhyolite which has continued into the Holocene. Unlike the calc-alkaline volcanic rocks deposited during the earlier episode of volcanism, the rhyolites and basalts deposited during this episode were erupted from scattered local centers and produced flows of small lateral extent. Several workers, e.g., Anderson and Rowley, 1975;

Rowley et al. 1978a; Mehnert, 1978; and Best and Brimhall, 1974, have demonstrated that the beginning of block faulting in the Basin and Range is not only synchronous with, but also genetically related to the eruption of both basalts and rhyolites which began in this area about 23 m.y. ago. Normal faults in southwestern Utah, such as the Hurricane fault, are known to be older than the Basin and Range faults. These faults are related to the structural differentiation of the Colorado Plateau Province which began about 26 m.y. ago (Rowley et al. 1978a).

The period of bimodal volcanism is represented in the NG Alunite Area by the complex Formation of Blawn Wash of Best and Keith (1979), and by the younger Basalt of Brimstone Reservoir (Lemmon and Morris, 1979). These units are described in the section on volcanic stratigraphy. It was during this period of volcanism that the Wah Wah Range became a structurally distinct unit separated from the adjacent valleys. Since the eruption of the youngest basalt flows, about 13 m.y. years ago, the southern Wah Wah Range has been the site of erosion, and deposition of colluvial and alluvial deposits during the Quaternary.

GEOLOGY OF THE NG ALUNITE AREA

The volcanic stratigraphy of the NG Alunite Area is dominated by ignimbrites which were deposited over much of southwestern Utah and eastern Nevada during Oligocene and Miocene times. Ignimbrites of regional distribution present at NG include all four members of the Needles Range Formation, the Baldhills member of the Isom Formation, and the Bauers Tuff member of the Condor Canyon Formation of the Quichapa Group. Volcanics of local extent or derivation include the Lamerdorf Tuff member of the Escalante Desert Formation, the basalt and rhyolite members of the Formation of Blawn Wash, and the Basalt of Brimstone Reservoir. The relative chronology between the ignimbrites, tuffs, and flows are shown on the geologic column for the area (Fig. 7). The map symbol, age, thickness, and detailed descriptions of the volcanic lithologies are presented below along with radiometric ages obtained from the literature. Thicknesses were derived trigonometrically from the dip of compaction foliation and/or bedding and length perpendicular to strike mapped in the area. Table 1 shows the estimated mineral mode for each unit.

The detailed stratigraphy and structure of the Paleozoic sedimentary rocks, which underlie the volcanics, have been studied previously by Miller (1966) and will not be presented here.

Tel Lamerdorf Tuff Member, Escalante Desert Formation (Best and Keith, 1979)

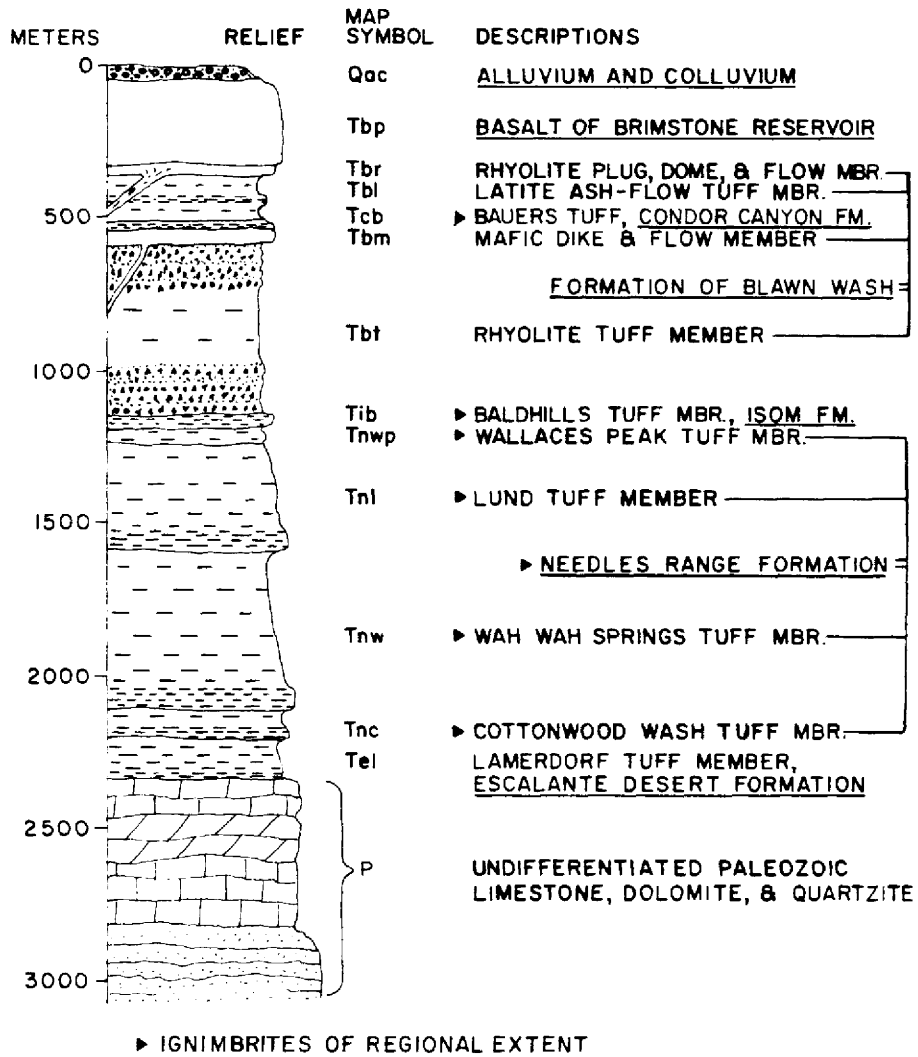


FIGURE 7, GENERALIZED GEOLOGIC COLUMN NG ALUNITE AREA

Table 1.--Modal Estimates for Volcanic Rocks

Member	NG ALUNITE AREA (Volume Percent)										
	Quartz	Sanidine	Plagioclase	Biotite	Hornblende	Clinopyroxene	Olivine	Opaque Oxides	Trace Minerals	Lithic Fragments	Groundmass
Tbp*			10		Tr	2	3	Tr			85
Tbr*	5	3	2	Tr				Tr			90
Tbl*		20		Tr					Tr		80
Tcb**		5	8	2					Tr		85
Tbm*			7		Tr	3		1	Ze		90
Tbt*	3	3		2				Tr	Gt	20	70
Tib**			9	Tr		1		Tr			90
Tnwp**	2	Tr	23	4	4			Tr	Sph, Ap, Zc		65
Tnl**	7	Tr	23	3	4	Tr		Tr	Sph, Ap, Zc		60
Tnw**	1	Tr	25	4	9	Tr		Tr			60
Tnc**	3	Tr	28	6	2	Tr		Tr			60
Tel*	1	Tr	11	3	Tr			Tr	Zc, Ap	Tr	85

Tr = Trace; Ap = apatite; Zc = zircon; Ze = zeolite; Gt = garnet; Sph = sphene

* Visual estimate

** Point count

Age: Oligocene, 34-29 m.y. Bracketed by the age of the Needles Range Formation dated at 29.7 m.y. (Armstrong, 1970) and the Horn Silver Andesite dated at 30.8 and 34.1 m.y. (Lemmon and Morris, 1979).

Thickness: May reach 300 feet (100 meters).

Description: Lavender, to gray, to dark olive-green and brown; plagioclase-biotite, moderately welded vitric-crystal ash-flow tuff. Probably quartz-latitude in composition. Locally, a lavender to gray flow unit may be present (especially common south of the map area) which contains more and larger phenocrysts of plagioclase and biotite. This unit characteristically weathers into hackly plates and grus.

Deposition of the Lamerdorf Tuff member of the Escalante Desert Formation was the first episode of volcanism in the area. This event marked the beginning of calc-alkaline volcanism in the field area. The lateral extent of the Lamerdorf Tuff and several of the other members of this formation is fairly limited (Best and Keith, 1979), and thicknesses often vary considerably. Whether this is due to erosion or non-deposition over local areas of high relief is unclear.

Tn Needles Range Formation (Best et al. 1973; Mackin, 1960)

Age: Oligocene, Armstrong (1970) showed that there were no

significant differences in age between the four members, each dated at 29.7 m.y.

Thickness: The overall thickness may exceed 3,000 feet (1,000 meters) in the field area.

Description: The Formation is composed of four nearly identical members, each composed of gray to greenish-brown to purplish-brown, plagioclase-hornblende-biotite-quartz, crystal-vitric, moderately welded, ash-flow tuff. The lower three members each vary from a dark-colored basal vitrophyre to a lighter divitrophyred zone, to a light gray and light olive green weakly welded upper part. The upper member lacks a basal vitrophyre. Conspicuous features of each of the four units are described below in the order of their deposition. On the basis of major element analyses, Anderson and Rowley (1975) classified the Needles Range Formation as a dacite.

Mackin (1960) originally defined the Needles Range Formation and divided it into two members, the Wah Wah Springs Tuff and the Minersville Tuff. Later, detailed studies by Best et al. (1973), and Shuey et al. (1976) resulted in a revision of Mackin's definition to include four members in the Needles Range Formation--the Cottonwood Wash Tuff, Wah Wah Springs Tuff, Lund Tuff, and Wallaces Peak Tuff. The revised nomenclature is adopted in this report.

The Needles Range Formation is distinctive in its great lateral extent covering a rectangular area of more than 33,600 sq km in southwestern Utah and eastern Nevada (Best et al. 1973). Shuey et al. (1976) explained the rectangular shape of the outcrop area by calling upon eruption from a source area centered on the northtrending Sevier highland resulting in downhill flow on both sides of the ridge. Based upon estimates of the volume of material ejected during the eruption of the Wah Wah Springs Tuff alone, Shuey et al. (1976) found this would require crustal subsidence that should have resulted in the formation of a caldera on the order of 72 km across and 1 km deep. To date, no such caldera has been located.

Shuey et al. (1976) found the Wah Wah Springs Tuff to be thickest in parts of the Needles Range where its thickness is on the order of 350 meters compared to an average of about 100 meters over most of its extent. They considered the source area to be nearby, possibly in the area of the Escalante Desert (Fig. 2) and the southern Needles Range. The thickness of the Wah Wah Springs Tuff in the field area of approximately 525 meters indicates that the southern Wah Wah Range is close to the eruptive source and it supports the contention of Shuey et al. (1976) that the nearby Escalante Desert may be the site of the eruptive source and caldera. The thickness of the Lund Tuff of about 350 meters is slightly thicker than that reported at

the type locality northwest of Lund, Utah (Best et al. 1973), also possibly indicating a nearby eruptive source.

Tnc Cottonwood Wash Tuff Member

Thickness: Varies from zero to 300 feet (100 meters) in thickness.

Description: Euhedral biotite phenocrysts up to 8 mm in diameter and sparse quartz phenocrysts as much as 4 mm in diameter are typical. Plagioclase phenocrysts are abundant and large. Hornblende is inconspicuous in hand sample.

Tnw Wah Wah Springs Tuff Member

Thickness: 1,650 feet (525 meters).

Description: Pumice lapilli are more abundant, and the average crystal size is less than the Cottonwood Wash Member. Abundant 1-2 mm phenocrysts of hornblende are the most prominent feature. Biotite phenocrysts are 3 to 4 mm across and quartz is not visible in hand specimen.

Tnl Lund Tuff Member

Thickness: 1,100 feet (350 meters).

Description: This unit is most easily identified by the presence of up to 15 percent phenocrysts of quartz 2 to 3 mm across. Apatite and sphene are present in most thin sections.

Tnwp Wallaces Peak Tuff Member

Thickness: The only recognized exposure in Blawn Wash reached a maximum of about 100 feet (30 meters).

Description: Conspicuous, large, white, pumice lapilli, which make up 10 to 20 percent of the rock, are diagnostic as well as the moderate degree of welding and compaction. This member did not develop a densely welded basal portion. Quartz phenocrysts are less common and are smaller than in the Lund Member. Zircon, apatite, and sphene are conspicuous in thin sections.

Tib Baldhills Member of the Isom Formation (Anderson and Rowley, 1975; Mackin, 1960)

Age: Miocene, Armstrong (1970) dated the Baldhills Member at 25.0 m.y., and Fleck et al. (1975) at 25.2 m.y.

Thickness: Less than 50 feet (15 meters).

Description: Dark reddish, to purplish, to chocolate-brown, vitric-crystal, densely welded ash-flow tuff with less than 15 percent phenocrysts of plagioclase and minor augite and opaque oxide minerals. Locally intensely compressed and stretched lenticles of light-colored pumice are present. Characteristically, this unit shows a strong platy parting and a blocky fracture which forms a grus composed of roughly cubic granules. Anderson and Rowley (1975) report the composition to be that of an average quartz latite.

The Baldhills Tuff is one of the most distinctive units occurring in the map area. In unaltered areas the member characteristically forms resistant ridges capping the less resistant, weakly welded Wallaces Peak Tuff and upper weakly welded part of the Wah Wah Springs Tuff. In areas of altered rock, the member is distinguished by its lack of phenocrysts, and especially by its strong platy parting and blocky "cubic" fracture. Even though the Baldhills Tuff is quite thin, less than 15 meters thick, it is continuous across the map area, suggesting that it was deposited on a surface of very little relief. The distinctive character and continuous nature of the member made it an ideal marker bed during mapping. Anderson and Rowley (1975) considered the eruptive source of the Baldhills Tuff to lie somewhere in the Escalante Desert near the northern Iron Springs District and southern Black Mountains, where they found numerous cooling units of only local extent.

Tb Formation of Blawn Wash, of Best and Keith (1979)

Age: Middle Miocene; the Formation ranges in age from about 25-20 m.y.

Thickness: The aggregate thickness may reach 2,000 feet (650 meters) in Blawn Wash.

Description: A complex sequence of dominantly rhyolitic intrusions, flows, ash-flows, airfall tuffs, base-surge deposits,

volcanic sandstones, and mafic dikes and flows. Conspicuous features of each member are described below in the order of their deposition.

Tbt Rhyolite Tuff Member, Formation of Blawn Wash (Best and Keith, 1979)

Age: Miocene; relationships to other units indicate an age of 25 to 22 m.y. Westra and Keith (1981) report an age date of 20 m.y. on the correlative Pine Grove porphyry.

Thickness: As much as 900 feet (300 meters) of this unit is exposed in Blawn Wash (Best and Keith, 1979).

Description: A varied sequence of light-colored, loosely consolidated, vitric-lithic-crystal, ash-flow and airfall tuffs with intervening beds of stratified base-surge deposits, volcanic sandstones, and conglomerates. A typical sequence starts with a tan, green, or reddish-brown, stratified, volcanic breccia with graded bedding, which rests atop the underlying Isom Formation. This unit is overlain by a light olive green, unconsolidated vitric-lithic-crystal ash-flow tuff containing fragments of the Lund Tuff Member of the Needles Range Formation. This unit is in turn overlain by an unwelded vitric-crystal ash-flow tuff unit which is white to pink in color. This unit is the most voluminous, and makes up about 1/2 to 2/3 of the member. Sparsely disseminated

throughout the upper 1/2 of this unit are euhedral phenocrysts of dark reddish-brown garnet 1 to 2 mm in diameter, and lithic fragments of quartzite and chert. In the southern part of the map area, a reddish-brown, stratified volcanic breccia overlies the Mafic Dike and Flow Member, which contains numerous conspicuous euhedral phenocrysts of dark reddish-brown garnet.

The basal part of the Rhyolite Tuff member consists exclusively of fragments of what appear to be devitrified, vitric, ash-flow tuff, or possibly a flow, which forms a repetitive sequence of well-sorted, layered, graded beds, which are locally crossbedded. This part of the Rhyolite Tuff member is considered to represent a deposit of base-surge origin as described by Sheridan and Updike (1975). Breccia fragments as much as 5 cm across, present in this unit, do not resemble any of the ash-flow tuffs in the map area. This suggests the presence of an eruptive source area nearby, but outside the map area.

The next portion of this member contains up to 50 percent fragments, usually less than 2 cm across, of the Lund member, of the Needles Range Formation. In areas of altered rocks, this unit is easily mistaken for the Lund Member. Best and Keith (1979) found fragments up to 25 cm across in this unit to the south of the map area, suggesting a source to the south.

Above these breccia units is an unwelded rhyolite ash-flow tuff. The mineralogy of the lower part of this unit is typical of silicic alkalic rhyolites occurring along the Blue Ribbon Lineament. The upper part, however, contains distinctive euhedral phenocrysts of spessartine garnet which are sparsely disseminated throughout. The garnet-bearing part of the member is thought by the present investigator to be correlatable with the garnet-bearing ash-flow tuff from the Mo-rich Pine Grove porphyry.

The uppermost portion of the Rhyolite Tuff member resembles the lowermost breccia unit with the exception that it contains euhedral garnet phenocrysts identical to those in the ash-flow tuff unit underlying it. The source area of this part of the Rhyolite member may also be the Pine Grove porphyry.

The euhedral character of the garnets, occurring in parts of the Rhyolite Tuff Member, indicates they were derived directly from a silicate melt system or a silicate melt-aqueous fluid system with which they were in equilibrium. In Climax-type systems, such as the Pine Grove porphyry (Westra and Keith, 1981), aluminous phases such as garnet may form by the evolution of a vapor phase rich in alkalis and volatiles which effectively depletes the silicate melt of its alkali content (Clarke, 1981). Clarke (1981) classified aluminous rhyolites of this derivation as endogenic (origin as a result of internal processes within

the silicate melt-aqueous fluid system) hyperaluminous rhyolite. Hyperaluminous granitic intrusions are often accompanied by alkali metasomatic aureoles (Clarke, 1981) such as occur in the potassic alteration zone of the Pine Grove porphyry Mo deposit.

Tbm Mafic Dike and Flow Member, Formation of Blawn Wash (Best and Keith, 1979)

Age: Miocene, 23 m.y. (Best, 1981, written commun.).

Thickness: May reach 300-600 feet (100-200 meters) locally. For the most part it is about 100 feet in thickness.

Description: Gray, with phenocrysts of augite and labradorite in a matrix of plagioclase, ferro-magnesium silicates, magnetite and glass. Weathers brown with individual blocks exhibiting characteristic, red, liesegang banding. Very sparse zeolite amygdules are also characteristic. The unit ranges from 55-60 weight percent SiO_2 and 2.4-4.0 percent K_2O (Best and Keith, 1979), which indicates a basaltic andesite composition. Like the rhyolites, the eruption of basalts was synchronous with the beginning of block faulting in this part of the Great Basin (Anderson and Rowley, 1975).

The Mafic Member of the Formation of Blawn Wash is of local origin, as evidenced by exposures along Blawn Wash (Pl. 1), where the flow descends into one or more dikes. Smaller dikes of

this member are locally present to the west across the southern part of the map area, typically in the outcrop area of the Rhyolite Tuff Member.

Tcb Bauers Tuff Member of the Condor Canyon Formation, Quichapa Group, (Anderson and Rowley, 1975; Mackin, 1960)

Age: Middle Miocene. Armstrong (1970) obtained dates of 21.3 m.y. and 21.6 m.y. for the Bauers Tuff; Fleck et al. (1975) a date of 22.1 m.y.

Thickness: Less than 50 feet (15 meters).

Description: Dark reddish-brown, plagioclase-sanidine-biotite, vitric-crystal, welded tuff. The ash-flow is present in only a few places within the map area. Locally, a basal black to dark green vitrophyre is present, which is less than 10 feet thick, and contains sparse, red spherulites. In the southern portion of the map area, the vitrophyre is devitrified and gray, to light brown, to pink in color. The middle, dark reddish-brown welded zone is overlain by an upper light gray to olive green, nonfoliated, partially welded zone. Anderson and Rowley (1975), on the basis of a major element analyses, consider the Bauers Tuff to be a calc-alkaline rhyolite. The Swett Tuff Member of the Condor Canyon Formation was not observed in the map area.

The Bauers Tuff originally covered an area of more than 25,000 sq. km (Anderson and Rowley, 1975) from the extreme western Markagunt Plateau in Utah to the Seaman and Pahrangat Ranges in Nevada. In the map area, a complete section was observed only southwest of Area B. Elsewhere the tuff is largely absent. It was impossible to determine whether this was due to erosion or nondeposition related to the structural development of topographic features. The source area of the Bauers Tuff is not known, although its greatest thickness, 35 meters, occurs in the southwestern Black Mountains, possibly near the vent area (Anderson and Rowley, 1975).

Age: Middle Miocene. Best (1981, personal commun.) estimates the age to be between 20 and 22 m.y.

Thickness: Less than 600 feet (300 meters).

Description: Light pink to pink, vitric-crystal, densely welded ash-flow tuff. Contains less than 20 percent phenocrysts of sanidine with traces of plagioclase, biotite, and hornblende. The lower and upper portions of the unit are only slightly welded, if at all. These portions are characterized by abundant and conspicuous, equidimensional pumice lapilli 1 cm or less in diameter. The densely welded and devitrified central part of the unit has a thickness less than 2/3 of the total thickness of the unit.

The apparent latite composition seems to indicate that this unit may be more closely associated with the earlier calc-alkaline period of volcanism. Even though this member may be contemporaneous with the regionally extensive ash-flows erupted at this time, it apparently is of local origin.

Tbr Rhyolite Plug, Dome, and Flow Member, Formation of Blawn Wash.

Age: Middle Miocene. Mehnert (1978) obtained an age date of 20.16 ± 0.86 m.y. from topaz rhyolite at the nearby Staats Mine. Rhyolites at Mt. Belknap, near Marysvale, range in age from 20-18 m.y. (Cunningham, 1979b). In addition, the field area lies along a northeast-trending belt of rhyolite intrusive and eruptive centers of early Miocene age 23 to 18 m.y., defined by Best and Mehnert, (1983). The rhyolite at NG is probably of similar age.

Thickness: The flows do not exceed 125 feet (40 meters) in thickness and are often much thinner and of limited extent.

Description: Light gray, pink, lavender, or brown; devitrified porphyritic, silicic-alkalic rhyolite. Contains less than 10%, 1 mm phenocrysts of quartz, sanidine, and plagioclase in a microcrystalline matrix. Generally flow layered and locally lithophysal. In the southeastern part of the map area it is locally perlitic in texture. Rhyolites in this part of the Great Basin have been found to be generally synchronous with

a northeast-trending block faulting event, 22 to 18 m.y. ago, (Best and Mehnert, 1983) indicative of northwest-southeast crustal extension.

The Rhyolite Plug, Dome, and Flow Member of the Formation of Blawn Wash is typical of many silicic-alkalic rhyolite flows and intrusions occurring along the Blue Ribbon Lineament. This unit, however, appears to vary in thickness across the map area suggesting the existence of topographically high and low areas prior to deposition, due to faulting, erosion, or both. The flows in the area vary from white porcelaneous or perlitic in texture to dark purple, devitrified flows containing sparse phenocrysts of feldspar, quartz, and biotite. Unlike the variation between flows, the three intrusive rhyolites located near the center of the map area (Pl. 1) are very similar to one another. All contain sparse phenocrysts of feldspar and quartz with traces of biotite and opaque oxide minerals; they exhibit prominent flow banding and platy fracture. The foliation of the westernmost plug is variously oriented, but vertical; whereas, in the intrusion to the east, the foliation dips toward the east at 30 to 60 degrees, suggesting a plug-dome or flow-dome character. The rhyolite intrusion to the southeast is the smallest and has less well-developed flow banding than the others. This plug, and the westernmost one, both exhibit banded intrusion breccias near

their margins with vertical elongation of smeared breccia fragments. Similar brecciated and banded rock was not observed near the margin of the plug-dome, although exposures are poor. The existence of thin perlitic flows, less than 10 feet thick, more than a mile from the nearest possible vent area may indicate the magma had relatively low viscosity, and therefore, high water content. Initially, however, the water content had to have been low for the magma to have reached the surface without first becoming water saturated and crystallizing. The formation of intrusive breccia along the margins of the westernmost plug, evidence of explosive forces, may be due to either a high volatile content of some of the magma or perhaps interaction with ground waters at the margins of the magma column.

- Tbp Basalt of Brimstone Reservoir Area (Lemmon and Morris, 1979)
Age: Pliocene, 13 m.y. Best, M. G., (1981, personal commun.).
Thickness: May reach as much as 1,650 feet (550 meters) to the east of the map area (Lemmon and Morris, 1979); however, it is less than 500 feet thick at the eastern margin of the map area.
- Description: Dark gray to black, locally vesicular, porphyritic-aphanitic, augite-hornblende-andesine basalt flow. One millimeter phenocrysts of augite, hornblende, and andesine

occur in a felted matrix of labradorite, glass, and magnetite. May approach augite andesite (mugearite) in composition.

The Basalt of Brimstone Reservoir, the last volcanic episode in the area, occurred about 7 m.y. after the last eruption of rhyolite. This unit outcrops along the eastern margin of the map area.

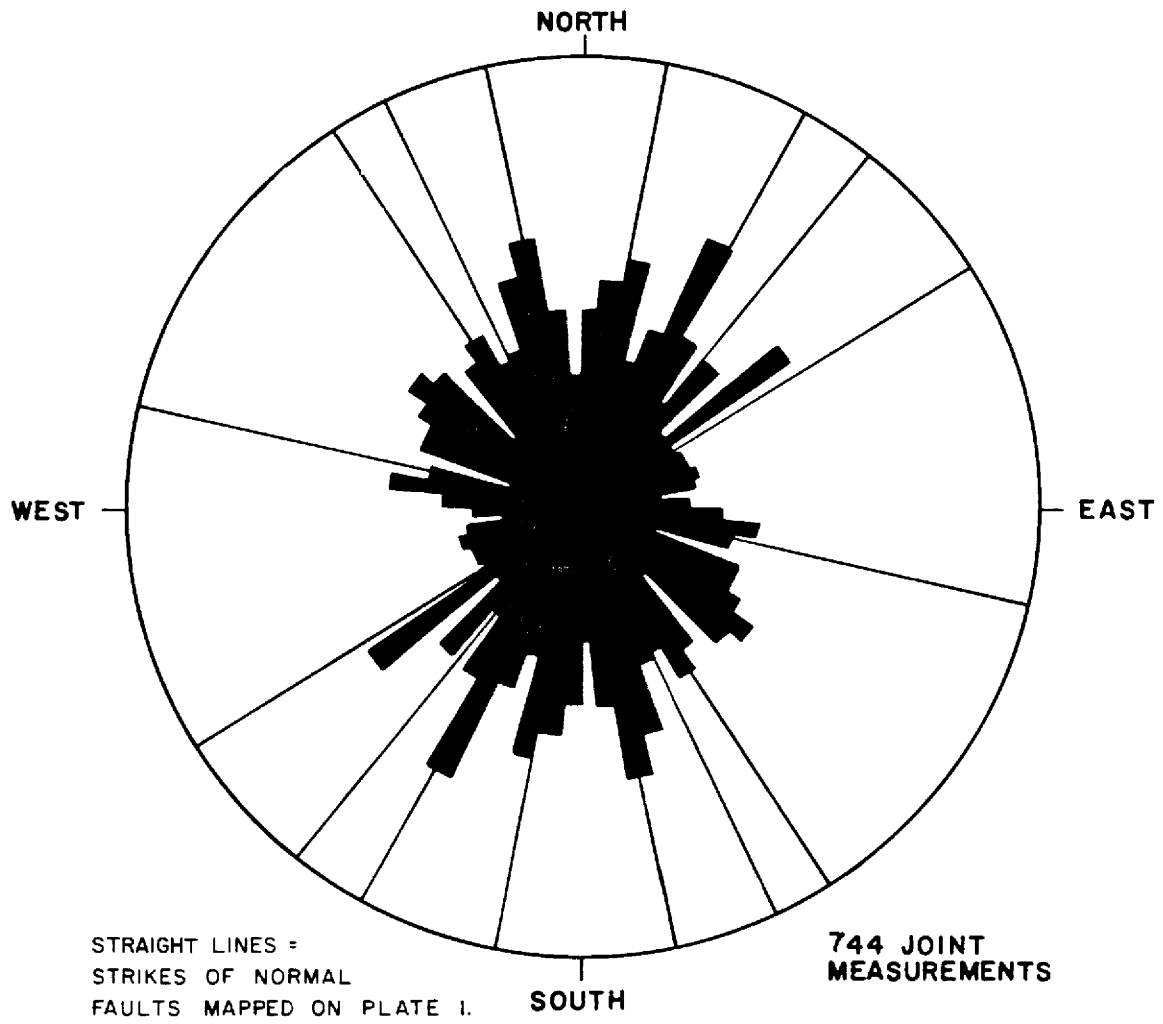
All of the volcanic rocks older than the Rhyolite Plug, Dome and Flow Member have been variously altered or mineralized, placing the age of alunite mineralization at about 20 m.y. The U.S. Geological Survey obtained a preliminary K-Ar age of 22.5 m.y. on vein alunite from the north end of NG Area C, (Cunningham, written commun. 1982). This date is not consistent with the stratigraphic relations, or the K-Ar age determinations on the volcanic rocks.

The three silicic-alkalic rhyolite intrusions, approximately 20 m.y. in age, which happen to be centrally located with respect to the alunite altered volcanics in Areas A, B, C, and D (Pls. 1 and 3) are apparently later volcanic phases, not related to the episode of alunite alteration, but centered on the proposed intrusive complex thought to be responsible for the alteration.

Immediately to the north and several miles south of the NG Alunite Area, the volcanic rocks are disrupted by only a few faults and structural relations are much simpler. In both of these areas, the faults are approximately parallel to the front of the north-trending

Wah Wah Range. These faults were probably formed under the same stress regime that was responsible for the formation of local Basin and Range structure. In the NG Alunite Area, several of the major faults are similarly oriented in northerly directions, and are considered to be coeval with those faults occurring to the north and south. East-West trending faults also occur at NG which may be related to the Blue Ribbon Lineament described in an earlier section. In addition, the fault density in the NG area is greater than it is in the areas to the north, (Lemmon and Morris, 1979) and south, (Best and Keith, 1979).

Figure 8 is a plot of joint orientations measured throughout the area. The plot shows that north-trending joints are the most frequent. These joints are parallel to several major north-trending faults (Fig. 8) and were presumably formed under the influence of the same east-west to northwest-southeast tensional stress regime. The east-west trending joints may be related to the Blue Ribbon Lineament. Tension joints with other orientations are of two origins; (1) cooling joints, formed during cooling and contraction of the volcanic rocks immediately following deposition, and (2) tectonic joints, formed under tensional stresses of local origin. In the field, cooling and tectonic joints are indistinguishable. Tectonic joints not related to east-west extension or the Blue Ribbon Lineament may have formed in response to a vertically oriented principle stress regime developed during local uplift.



STRIKE OF NORMAL FAULTS
AND ROSE DIAGRAM OF JOINT ORIENTATIONS

FIGURE 8, JOINT FREQUENCY DATA

The structural features of the NG Alunite Area indicate that much of the area was subjected to upflexing, upfaulting, and extension prior to the episode of alunite mineralization. In the southeastern part of the map area (Pl. 1) the volcanic strata form a monoclinial flexure that dips to the east, southeast, and south, away from the central portion of the map area. The fault block on the south end of Area B, also centrally located relative to the alunite altered volcanics, is uplifted relative to the surrounding rocks. Elsewhere throughout the map area, the volcanic rocks are disrupted by variously oriented systems of normal faults often arranged in dominantly antithetic patterns indicative of local extension.

The anomalous structural features of the volcanic rocks at NG may have formed during the emplacement of a shallow level intrusion. A number of geologists working in the Basin and Range Province, notably Mackin (1960), Mehnert (1978) and Best, (Pers. Commun.), have described similar structures in the wall rocks surrounding high-level intrusions. These intrusions commonly make room for themselves by up-flexing and up-faulting their roofs. Monoclinial flexures are commonly developed around the margins of the intrusions which serve the same purpose in the room-making process (Mackin, 1960). The silicic-alkalic rhyolite plugs and the structural features observed at NG may be related to the emplacement of an intrusion at depth.

Based upon the work of Mackin (1960), and Mehnert (1978), the intrusion(s), if present, may be a laccolith. They found that many

of the shallow-level intrusions in southwestern Utah are laccoliths which were emplaced along low-dipping planes of easy parting; and, that in areas of complex structure, they are often found to be emplaced along flat thrusts such as the flat-lying Blue Mountain thrust underlying the field area (Fig. 3). It is possible, therefore, that if an intrusion is present, it is laccolithic in shape and was emplaced along the Blue Mountain thrust. The deep structural relations presented on Plate 2 were drawn on the basis of this inference. According to Mackin (1960), the lateral extent of these shallow-level intrusives is spatially related to the overlying area of structural disturbance. At NG, the distribution of structurally anomalous and altered volcanic rocks coincide, and are thought to reflect the presence of a buried intrusive complex which was responsible for the structural patterns, the rhyolite plugs, and the heat required for the development of the hydrothermal system which produced the alunite alteration.

Based upon the distribution of structure and mineralization mapped by Lindsey and Osmonson (1978) another intrusion may underlie the area immediately to the south of the field area as well. At the Staats Mine, a topaz rhyolite plug is emplaced in Paleozoic carbonates. The carbonate rocks in this area are locally altered to jasperoid (Lindsey and Osmonson, 1978). To the south these Paleozoic carbonates are overlain by south-dipping volcanic rocks which may mark the approximate southern limit of structural influence of the proposed shallow-level intrusion. The two topaz rhyolite plugs of the Tetons

are located in this area of south-dipping volcanics. The volcanic rocks present even farther to the south have relatively simple structural relations, although they were subjected to low intensity alteration.

If the limit of these shallow-level, possibly laccolithic, intrusions are accurately defined by the relations cited above, they have a combined north-south dimension of at least 6 miles with an east-west dimension of about 3 miles. In other words, the area of influence of the proposed shallow level intrusive complex is much larger than the distribution of eruptive centers mapped at the surface.

ALTERATION AND MINERALIZATION

The NG Alunite Area is dominated by four topographically high areas, designated Areas A, B, C, and D (Fig. 5 and Pls. 1 and 3), in which the volcanic rocks have been predominantly altered to quartz and alunite. Less intensely altered and unaltered volcanics are found in the valleys between the four ridges. The distribution and mineralogy of the altered rocks at NG have been studied in great detail by Earth Sciences, Inc. in their efforts to define bodies of ore. They performed hundreds of X-ray diffraction runs on samples from both the surface and subsurface. Most of the samples were from the areas of alunite-altered rocks, although many samples were analyzed from the less intensely altered zones. The mineralogy of the less intensely altered rocks was studied by the present investigator using the petrographic microscope. Based upon X-ray diffraction and petrographic work, several alteration zones have been defined. The distribution of these alteration zones across the NG Alunite Area is presented on Plate 3. Table 2 outlines the mineralogy and textures characteristic of each zone.

In addition to the main stage of alunite-related alteration, several episodes of vein mineralization were recognized in the map area. Figure 9 outlines the paragenesis of veining and alteration at NG. The relative timing of each of these events is based upon cross cutting relationships observed in the field, as well as

Table 2.--Alteration Pattern, NG Alunite Area

<u>Alteration Zone</u>	<u>Mineralogy</u>	<u>Texture</u>
Silica Zone	Quartz ± opal, ± cristobolite, and ± tridymite.	Varies from massive replacement to spongy siliceous sinters. Original rock textures are gone.
Quartz-Alunite Zone	quartz and alunite, ± cristobolite, ± kaolinite, ± pyrophyllite, ± boehmite, ± hematite and ± goethite.	Pervasive; the original rock textures are mostly obliterated and can be discerned only with great difficulty.
Hematite-Clay Zone	Hematite, kaolinite, chlorite, montmorillonite, ± alunite, ± sericite, ± pyrophyllite, ± goethite.	Original textures are preserved. Hematite occurs often as disseminations and in bands. Biotite and K-feldspar are locally preserved.
High Propylitic Zone	Chlorite, montmorillonite, sericite, epidote, ± kaolinite, ± pyrite, ± quartz and ± calcite.	Original textures are easily observed. K-feldspar, biotite, plagioclase, and hornblende are present.
Low Propylitic Zone	Chlorite, calcite, ± epidote, ± pyrite, and ± quartz.	Very weak alteration; virtually fresh rock.

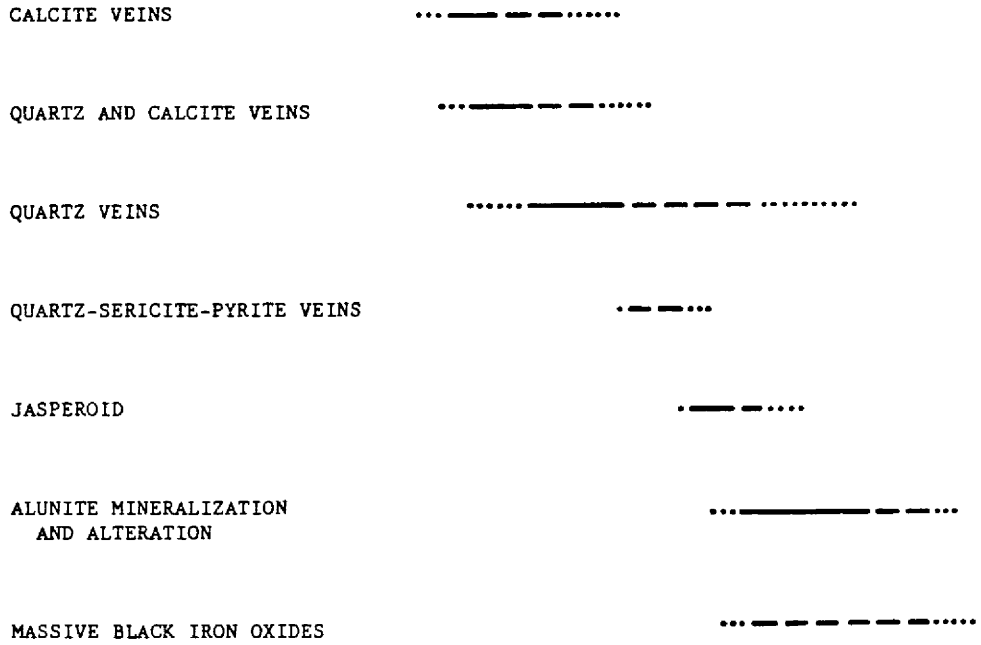


Figure 9. Vein and Alteration Paragenesis, NG Alunite Area.
Solid, dashed, and dotted lines indicate approximate
quantity in decreasing order

textural characteristics of individual complex veins. In general, early calcite veins are followed and replaced by quartz veins followed by the main stage of alteration that deposited the alunite. Locally, quartz-sericite-pyrite veins and/or jasperoids are present that formed prior to the main stage of alunite-related alteration but later than the episode of quartz veining (Fig. 9). Massive deposits of iron oxides also occur locally (Plate 3) that formed during and/or after main stage alunite alteration. The remainder of this section describes each type of mineral occurrence and, on the basis of textural relationships and phase relations published in the literature, attempts to place restrictions on the conditions attending each episode of mineralization.

Calcite and calcite-quartz veins are present most commonly in low intensity, propylitically-altered rocks. Characteristically, chlorite, calcite, and pyrite occur in the thin selvage of altered rock surrounding the veins. A few coarse-grained lamellar calcite veins up to 2 feet (0.6 meters) across were located in the area (Plate 3), although most are less than 1 cm in width. Most veins were discontinuous and traceable for no more than a few tens or, locally, hundreds of feet.

Holland and Malinin (1979) have shown that the precipitation and solution of calcite in meteoric hydrothermal systems is mainly a function of temperature, pH, and CO_2 fugacity. The solubility of calcite decreases with (1) increasing temperature, (2) increasing pH, and (3) decreasing CO_2 fugacity. Waters of meteoric origin

containing calcium and carbon species resulting from equilibration with volcanic wallrocks will tend toward saturation (1) during descent into deeper, higher temperature rocks, (2) via hydrolysis or, possibly, redox reactions with silicate wallrocks which reduce the H⁺ concentration, and (3) by loss of CO₂ during boiling. The occurrence of chlorite and calcite in the altered zone around the veins suggests the hydrothermal fluids were near neutral to slightly alkaline in composition (Rose and Burt, 1979).

Quartz veins were most often observed in the propylitically altered areas, although they are also present in each of the higher intensity alteration zones. Calcite veins are less prominent in areas where quartz veins are well developed. Where calcite veins were replaced by quartz, boxy and slotted textures formed by replacement along cleavage planes in calcite are present. One such quartz vein more than 2 feet (0.6 meters) across was located in the valley northwest of Area A (Plate 3), but most are much smaller. Otherwise, the quartz veins typically contain drusy quartz and are usually less than a few centimeters across. Few veins were traceable for more than a few tens or, locally, hundreds of feet.

Experimental studies in the SiO₂-H₂O system, summarized by Holland and Malinin (1979), have shown that the solubility of quartz in aqueous solutions increases with increasing temperature and is virtually independent of pH and concentration of dissolved salts, although they have a strong effect on exchange reactions between the fluids and

wallrocks which liberate silica. Therefore, cooling of the hydrothermal fluids as they rose towards the surface may have contributed to quartz deposition. The replacement of earlier formed calcite veins by quartz is consistent with this idea because calcite solubility increases in cooling fluids. Episodic boiling of the fluids would also have contributed to the deposition of quartz. Loss of volatiles during boiling increases the silica concentration of the residual fluid, thus promoting quartz deposition. The source of silica was probably from exchange reactions with siliceous wallrocks, possibly augmented by emanations from a magmatic source. The walls of these veins exhibit weak alteration characterized by clay minerals, sericite, and pyrite. These minerals are normally deposited from hydrothermal fluids with neutral to slightly acid pH's (Rose and Burt, 1979).

Green, fine-grained, quartz-sericite-pyrite veins were observed in only seven places (Pl. 3). These veins varied from about 6 inches (0.2 meters) to 3 feet (1 meter) in width and are discontinuous, usually less than a few tens or, locally, hundreds of feet in length. The surrounding wallrocks are locally silicified and phyllically altered to the point where the contact between the vein-filling and wallrocks is difficult to discern. The conditions attending this stage of mineralization are not accurately known, although experimental studies of phase relationships in hydrous potassium aluminum silicate systems, summarized in Rose and Burt (1979), suggest that in potassic rocks sericite is stable only at temperatures of greater than about 130°C and at weakly acidic to near neutral pH's.

The gradational boundary along the margins of these veins, a result of intense pervasive alteration and replacement of the wall-rocks, indicates these fluids were out of equilibrium and highly reactive with the surrounding wallrocks. Mineral precipitation may have been promoted by reaction of the fluid with the wallrocks, boiling, temperature increase, or other influences.

Jasperoid was observed in the southern and northwestern portions of the map area (Pl. 3), usually near the margins of alunite-altered rocks. It varies in color from milky white to dark reddish-brown and is found to occur near, and sometimes along, faults. They commonly form dike-like bodies resistant to erosion which are often traceable over fairly long distances (Pl. 3). One jasperoid body, southeast of Area B, occurs in the silicic-alkalic rhyolite plug located there; however, its genetic relation to the plug is not known. Lindsey and Osmonson (1978) reported many areas of jasperoid south of Area D, in sedimentary carbonates, which may be similar to those described here.

Lovering (1977) determined that the prerequisites for jasperoid formation are: (1) an adequate source of silica, (2) solutions that can transport silica, and (3) conditions such that the hydrothermal fluids are able to both promote the solution of host rocks and inhibit the solubility of silica. Possible sources of silica at NG include the silica-bearing volcanic rocks and also siliceous fluids exsolved from cooling magma at depth. As mentioned earlier, silica solubility increases with increasing temperature. As a result, waters

associated with volcanic geothermal systems have the highest concentrations of silica compared to other naturally occurring waters. The simultaneous dissolution of wallrocks and precipitation of silica, as evidenced by relict host rock textures, indicates that the fluids responsible for jasperoid formation were able to approach equilibrium with the wallrocks only via extensive amounts of chemical exchange. The occurrence of jasperoid in the carbonate rocks south of the map area suggests that cooling of the fluids during ascent towards the surface was a factor, because this would promote both the solution of calcite and the precipitation of silica. Fluids with pH less than neutral may have also promoted carbonate dissolution.

The jasperoids occurring at NG are often yellow, red, and brown due to the presence of iron oxide minerals. Occasionally, boxwork textures suggestive of pyrite are present. The iron oxide minerals occurring in most jasperoids have been shown by Lovering (1972) to be secondary oxidation products of originally reduced iron species. This is important because it indicates that the solutions depositing jasperoid were generally able to stabilize pyrite as were the fluids depositing each episode of mineralization thus far. This contrasts with the next two stages of mineralization in which hematite is the stable form of excess iron.

The formation of broad areas of altered rocks associated with alunite mineralization was the most intense episode of hydrothermal activity affecting the area. The widespread alteration occurring

during this episode may have obliterated many of the veins deposited during earlier episodes as only a few quartz veins are present in these altered areas.

Examination of Plate 3 reveals that each of the major altered areas exhibits a concentric zonation pattern which varies from a central silica zone outward through a quartz-alunite zone, a hematite-clay zone, a high-intensity propylitic zone, and a low-intensity propylitic zone which affects nearly all of the volcanic rocks in the area. Drilling in the areas of alunite mineralization revealed that a vertical alteration pattern is also present. Based upon drill-hole data, a cross section through NG Area C is presented in Figure 10. The figure shows a vertical pattern which changes from a silica zone at the top down through a quartz-alunite zone which grades into a quartz-alunite-sericite-pyrite zone in the deepest regions explored by drilling.

In outlying altered areas, such as the small areas east of Area A, north of Areas B and C, and north of Area D, the alteration boundaries are horizontal with flat bottoms rather than funnel shaped. The vertical zonation pattern is the same as the concentrically arranged horizontal pattern described above with quartz-alunite at the top passing downwards through the hematite-clay and propylitic zones. Drilling in Area C has shown that only a small portion of the altered rocks mapped at the surface immediately overlie a deeply rooted zone

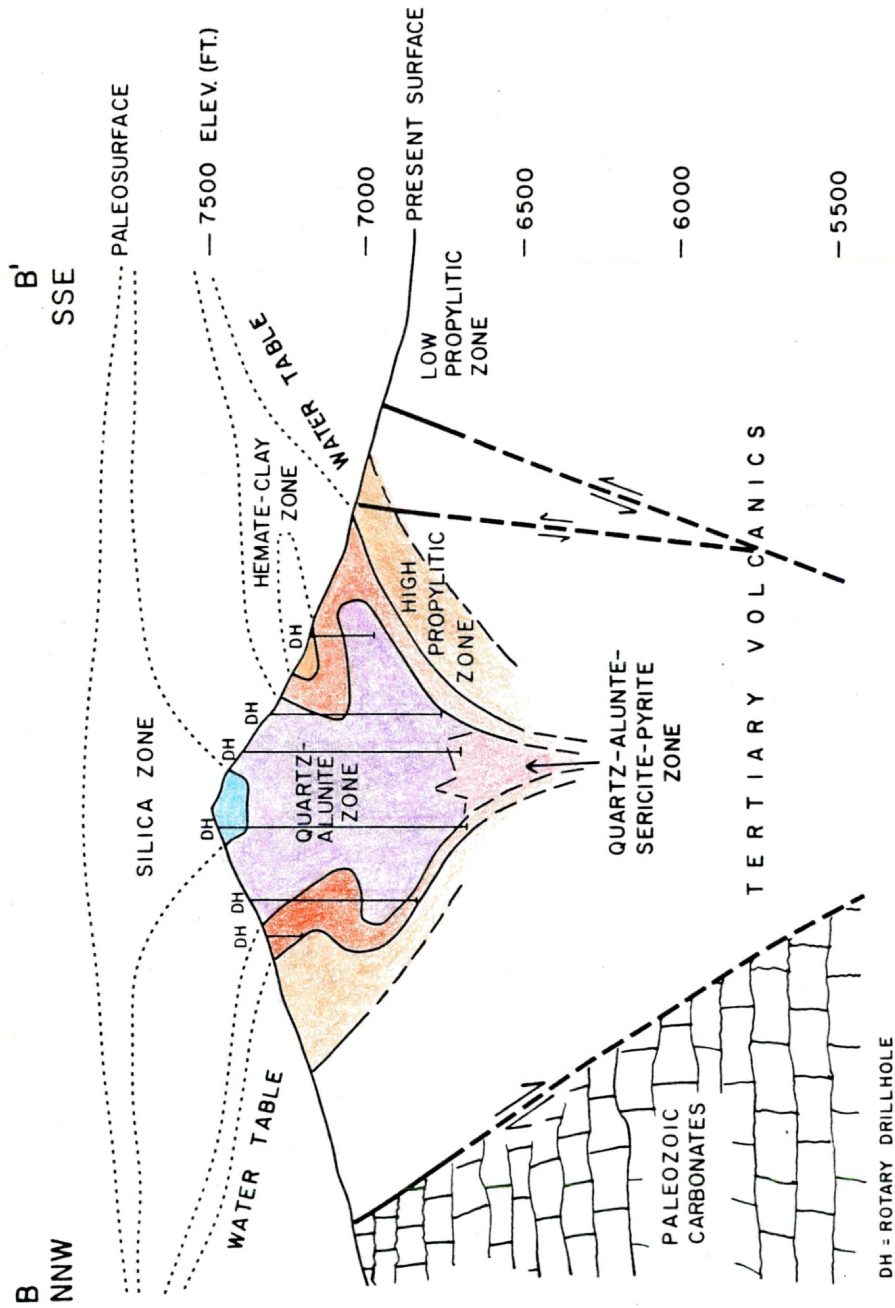


FIGURE 10. CROSS SECTION THROUGH NG AREA C,
(see PLATE 3).

and that the "rooted zones" are of relatively limited extent. Many of the marginal areas of altered rock overlie relatively unaltered volcanics.

The contact between altered and relatively unaltered volcanics, at the bottoms of these marginal areas are nearly horizontal regardless of the structure of the volcanics. To the northeast of Area C, small flat-bottomed areas of altered rock occur in steeply dipping members of the Needles Range Formation. In Areas B, C, and D, alteration boundaries cut across faults (Pl. 3). The presence of alteration boundaries that cut across structural features indicates that most of the structural development in the area was complete prior to the episode of widespread alteration.

The flat-bottomed areas of altered rocks must have formed from hydrothermal fluids which moved horizontally out from central areas underlain by root zones. Presumably, erosion has separated rootless marginal areas from the larger parent areas, which supplied the fluids.

Primary textural features of the volcanic units are largely obliterated in the areas of intense alteration. The intensity of alteration was found to vary with respect to textural variations which controlled the porosity and permeability within and between individual lithologic units. The most permeable rocks in the section are the airfall and base-surge tuff breccias and volcanic sandstones, which have well-developed primary porosity and permeability, and the strongly welded portions of ash-flow tuffs and flow units, which have well-developed

joint systems. The best example of the control of porosity on alteration intensity is at the north end of Area C. At this location, the upper weakly welded portion of the Lund Member of the Needles Range Formation is only weakly altered, while overlying tuff breccia of the Formation of Blawn Wash and the underlying, more strongly welded part of the Lund are intensely altered to quartz and alunite. The control of permeability on the degree of alteration intensity is most important near the margins of quartz-alunite altered zones. In the centers of Areas A, B, C, and D alteration is pervasive and unaffected by variations in the permeability of the host rocks. Apparently, in the centers of these systems there was sufficient time and volume of solution to alter even the least permeable parts of the section.

Application of experimentally determined phase relations to the mineralogy observed in these altered rocks put important constraints on the geochemistry of the hydrothermal fluids. Figure 11 presents phase relations in the system $K_2O-Al_2O_3-SiO_2-H_2O-SO_3$. Maintenance of the product $\log (a_{(H^+)})^2 \cdot a_{SO_4}^{-2}$ at values greater than about -11 (Fig. 11), which is necessary to stabilize alunite, requires high activities of both K^+ and H^+ . Knight (1977) estimates these activities to be attained only at pH's less than 4 and SO_4^{-2} concentrations of greater than 100 ppm. For $\log (a_{(H^+)})^2 \cdot a_{SO_4}^{-2}$ values greater than -9.5 silica is the only stable phase. Solutions associated with deposits of residual silica in active hot springs have pH's near or less than 2.0 (Ellis, 1979; White et al, 1971). At lower values of the

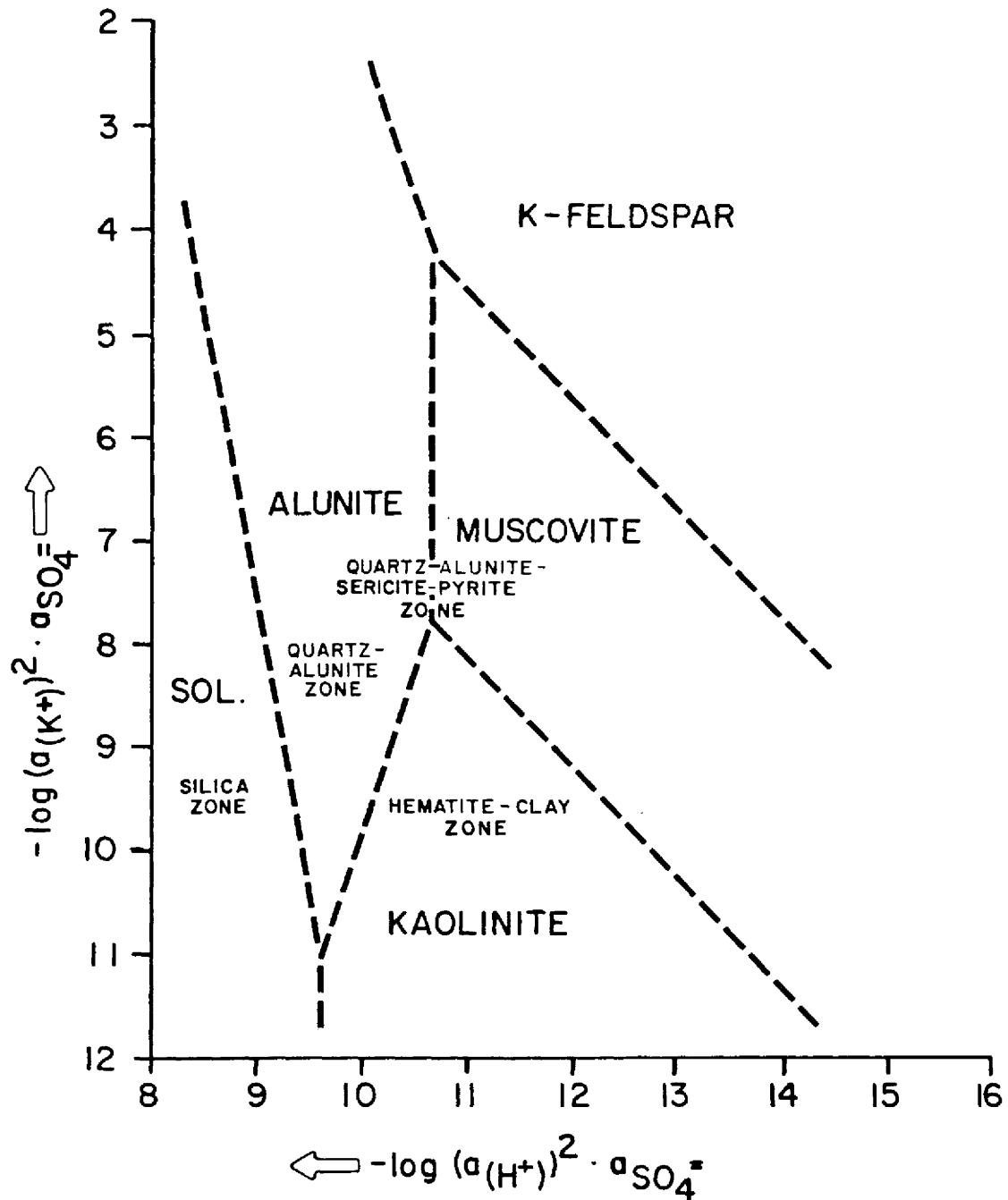


FIGURE 11. PHASE RELATIONS IN THE SYSTEM $K_2O - Al_2O_3 - SiO_2 - SO_3$, from Hemley et al, 1969 and Schoen et al, 1974.

product $\log (a_{(H^+)})^2 \cdot a_{SO_4}^{-2}$ alunite and kaolinite are stable, while at higher product $\log (a_{(K^+)})^2 \cdot a_{SO_4}^{-2}$ K-mica is stable. The phase relations indicate that the formation of the various alteration zones at NG were caused by the interaction of strong sulphuric acid solutions with the silicate minerals in the volcanic rocks.

On the northern end of Area C and on the west side of Area A, several massive pods of black iron oxide minerals are present. The iron oxides appear to have been deposited in open spaces along fault zones and in fractured and brecciated rock. These bodies often contain uranium, as indicated by scintillometer readings, and rarely contain traces of pyrite. They always occur near the margins of intensely altered rocks and are thought to be related to the episode of alunite alteration.

These deposits are presumably related to the period of alunite alteration and result from the movement of iron-rich acid solutions out of the altered areas into an environment of higher pH (Schoen et al. 1974). The neutralization of these fluids in fault zones could easily have been accomplished by mixing of the low pH hydrothermal fluids with near-neutral meteoric water that may also have been moving along these fault zones.

TRACE ELEMENT GEOCHEMISTRY

In an attempt to further define the hydrothermal system, rock samples from each stage of altered and veined rock occurring across the map area were collected and analyzed for several trace elements. The intention was to compare the trace element geochemistry of each stage and to possibly outline epigenetic leakage halos or plumes overlying buried mineralization. Samples from the silicic-alkalic rhyolite plugs were also collected and analyzed to see if they might be productive. Samples were sent to professional laboratories for analysis (see Appendix B) during the course of geologic observations in the field. One hundred samples were analyzed for Mo, Cu, Zn, Pb, Ag, and Au. Also, 22 selected samples were analyzed for As, Sb, Sn, W, and F. The method used during these analyses, the detection limits, and the results are presented in Appendix B. Sample locations are presented on Plate 4. The precision and accuracy of this data were not determined in this study, although the commercial laboratories used, guaranteed an accuracy of ± 20 percent.

Based upon a 100 sample population, threshold values for the elements Mo, Cu, Zn, Pb, Ag, and Au were determined by plotting the cumulative percent frequency versus concentration on probability paper and identifying the point of change in slope of the curve as the threshold value. Ideally, the change in slope of the curve should correspond to the point of division between samples having a normal distribution of values and samples that are anomalous. This method

of determining threshold is relatively arbitrary, and where necessary, was adjusted slightly to higher or lower values in order to better fit the data when plotted as frequency histograms. Plots of these data are available in Appendix B. The threshold was defined in this manner because these methods have proved useful for the recognition and separation of multiple populations (Levinson, 1980) and because it was anticipated that two populations would exist at NG, one reflecting the average elemental abundance of the felsic rocks, and another representing mineralization. In addition, Rose, Hawkes, and Webb (1979) have found that little appears to be gained, for most sets of geochemical data, by the use of distributions more complex than normal or log-normal ones. Too few samples were analyzed for As, Sb, Sn, W, and F to use statistical methods for threshold determinations. The values obtained for these elements have been interpreted largely on the basis of information available in the literature.

The distribution of samples across the NG Alunite Area containing anomalous values of trace elements is presented on Plate 5. Table 3 shows how the distribution of samples with anomalous trace element contents varies according to the stage of mineralization sampled.

Very few samples were collected from the areas of quartz-alunite alteration. Rocks from these areas had been previously analyzed for trace elements by Earth Sciences, Inc. and were found to have uniformly low trace element contents below the threshold values established in this study. The few samples from the alunite altered areas

TABLE 3, TRACE ELEMENT GEOCHEMISTRY, NG ALUNITE AREA

PARAGENESIS	SAMPLE MATERIAL	NUMBER OF ANOMALOUS VALUES NUMBER OF SAMPLES ANALYZED										TOTAL
		As	Au	Ag	Pb	Zn	Cu	Mo	Cu+Zn+Pb	TOTAL		
-	ALTERED SILICIC-ALKALIC RHYOLITE INTRUSIONS*	-	-	-	-	$\frac{1}{15}$	-	-	-	$\frac{2}{15}$	$\frac{2}{15}$	$\frac{2}{15}$
1	CALCITE VEINS	-	-	$\frac{1}{3}$	$\frac{2}{3}$	$\frac{1}{3}$	-	-	-	$\frac{2}{3}$	$\frac{2}{3}$	$\frac{2}{3}$
2	QUARTZ AND CALCITE VEINS	-	-	-	$\frac{1}{8}$	-	-	-	-	$\frac{2}{8}$	$\frac{2}{8}$	$\frac{2}{8}$
3	QUARTZ VEINS	$\frac{3}{49}$	$\frac{2}{49}$	-	-	$\frac{6}{49}$	$\frac{7}{49}$	$\frac{3}{49}$	$\frac{10}{49}$	$\frac{12}{49}$	$\frac{12}{49}$	$\frac{12}{49}$
4	QUARTZ-SERICITE-PYRITE VEINS	$\frac{1}{6}$	-	$\frac{1}{6}$	$\frac{1}{6}$	-	$\frac{4}{6}$	-	$\frac{2}{6}$	$\frac{5}{6}$	$\frac{5}{6}$	$\frac{5}{6}$
5	JASPEROID	$\frac{4}{10}$	-	$\frac{4}{10}$	$\frac{2}{10}$	$\frac{5}{10}$	$\frac{2}{10}$	$\frac{1}{10}$	$\frac{5}{10}$	$\frac{7}{10}$	$\frac{7}{10}$	$\frac{7}{10}$
6	QUARTZ-ALUNITE ALTERED ROCKS	-	-	-	-	-	-	-	-	$\frac{0}{2}$	$\frac{0}{2}$	$\frac{0}{2}$
7	MASSIVE BLACK IRON OXIDES	-	-	-	-	$\frac{3}{4}$	$\frac{1}{4}$	-	$\frac{3}{4}$	$\frac{3}{4}$	$\frac{3}{4}$	$\frac{3}{4}$
-	OTHER	-	-	-	$\frac{1}{3}$	$\frac{3}{3}$	$\frac{2}{3}$	-	$\frac{3}{3}$	$\frac{3}{3}$	$\frac{3}{3}$	$\frac{3}{3}$
-	TOTALS	$\frac{7}{31}$	$\frac{2}{100}$	$\frac{6}{100}$	$\frac{7}{100}$	$\frac{19}{100}$	$\frac{16}{100}$	$\frac{4}{100}$	$\frac{29}{100}$	$\frac{37}{100}$	$\frac{37}{100}$	$\frac{37}{100}$

* - Sn, W, and F were also analyzed and had uniformly low values.

analyzed in this investigation also had uniformly low values (Table 3 and Pl. 5). The alunite altered areas are largely depleted of trace metals with the exception of iron, as evidenced by trace amounts of hematite and goethite. Low trace metal values for these areas can be explained by leaching caused by the low pH fluids responsible for alunite alteration.

Plate 5 reveals an erratic distribution of samples with anomalous trace element contents. In an attempt to smooth the erratic nature of the geochemical data, the elements Cu, Zn, and Pb were added together and threshold values determined as described above. The Cu-Zn-Pb products with anomalous values were then plotted on Plate 5, along with the single element plots. From these plots (Plate 5 and Table 3), it is apparent that samples collected from quartz-sericite-pyrite veins, jasperoid, and massive iron oxide deposits have the greatest number of anomalous trace element values relative to other stages of alteration sampled. Anomalous samples from calcite veins, calcite-quartz veins, and quartz veins form a series of point anomalies with no discernable geochemical pattern. Table 3 shows that the quartz-sericite-pyrite veins are most anomalous in Cu. The jasperoid and iron oxide deposits are most anomalous in Zn, although some samples from these two materials also contained anomalous Cu.

The jasperoid deposits contain the largest percent of anomalous samples, and are anomalous in a greater variety of trace elements (Table 3). Besides Zn, the jasperoids are most commonly anomalous

in Ag and As, although Pb, Cu, or Mo may also be present. Comparison of the trace element contents of jasperoids from NG with those compiled by Lovering (1981) shows that the jasperoids at NG are most similar to the jasperoids Lovering found associated with Ag-Pb-Zn deposits. Similarly, White (1981) considered the presence of anomalous amounts of Ag and base metals to be an indication of deposition under conditions of greater depth and temperature than those occurring in shallow, Au dominant systems. He also considered As and Sb to be useful in the identification of fluid escape channels above precious metal mineralization. In view of their trace element geochemistry, the areas of jasperoid deposits at NG probably deserve more thorough study in any future investigations, such as more detailed sampling and/or drilling.

The quartz-sericite-pyrite veins are more difficult to relate to a specific type of buried mineralization, although they could possibly be indicative of Cu and/or Zn mineralization.

The anomalous character of the black iron oxide deposits is still more difficult to interpret because iron and manganese oxides tend to preferentially concentrate elements by absorption. Absorption of trace metals by goethite and other oxide minerals may very well account for the anomalous character of these deposits, although these elements and uranium may have been concentrated in these deposits during the waning stages of the hydrothermal system, as occurred at Marysvale, Utah (Cunningham, 1979a).

Quartz-sericite-pyrite veins, jasperoid, and massive iron oxide deposits were all formed during the later stages of the paragenesis (Table 3). This feature is of interest, because it suggests that deposition of most of the metals at NG occurred during the later stages of evolution of the hydrothermal system.

The intrusive rhyolite porphyries at NG were also sampled and analyzed for Mo, Cu, Zn, Pb, Ag, Au, As, Sn, W, and F. These rhyolites had uniformly low trace element contents, although one sample contained anomalous Zn. The silicic alkalic rhyolites at NG are apparently unlike the topaz rhyolites near the Staats Mine and the Tetons south of Area D, which Linsey and Osmonson (1978) described as containing anomalous amounts of lithophile elements such as F, Be, Ga, Li, Mo, Nb, and Sn. This is important because it suggests that fluorspar-uranium-beryllium mineralization, similar to that occurring at the Staats Mine is probably not present in the NG Alunite Area, or if so, is not related to the intrusions sampled, and that the two areas of mineralization may therefore be mutually exclusive. The geochemical data also suggests that the shallow level intrusion, if present, and if related to the plugs and domes at the surface, underlying the NG area is of a different character and separate from that postulated to underlie the area to the south.

FLUID INCLUSIONS

Microthermometric analysis of fluid inclusions in calcite, calcite-quartz, and quartz veins was carried out to characterize the hydrothermal fluids attending alteration and mineralization. Inclusions occurring in samples of alunite veins were also examined, but proved to be unsuitable for such measurements due to the small size, less than 6 microns, of the inclusions. Material from the other stages in the paragenetic sequence was not usable for fluid inclusion study because of the microgranular-character and/or mineralogy of the samples. In all, over 40 samples were examined on the heating/freezing stage microscope. Of these, 22 yielded 118 homogenization temperature measurements. Freezing temperatures of 25 inclusions from six selected samples were also measured to characterize the salinity of the hydrothermal fluids. The results of this work are presented in Figure 12 and tabulated in Appendix A. Sample locations are shown on Plate 4. Information on the procedure used during the collection of fluid inclusion data and on the calibration of the heating/freezing stage microscope is presented in Appendix A.

Inclusions occurring in calcite, quartz, and alunite were classified as primary, pseudosecondary, or secondary using criteria presented in Roedder (1979). The inclusions were also classified as liquid-dominant or vapor-dominant, based on the ratio of liquid to vapor in

- ▣ SALINITIES < 2 EQ. WT. % NaCl
- ▣ SECONDARY INCLUSION IN QUARTZ
- PRIMARY INCLUSION IN QUARTZ
- ▤ SECONDARY INCLUSION IN CALCITE
- PRIMARY INCLUSION IN CALCITE

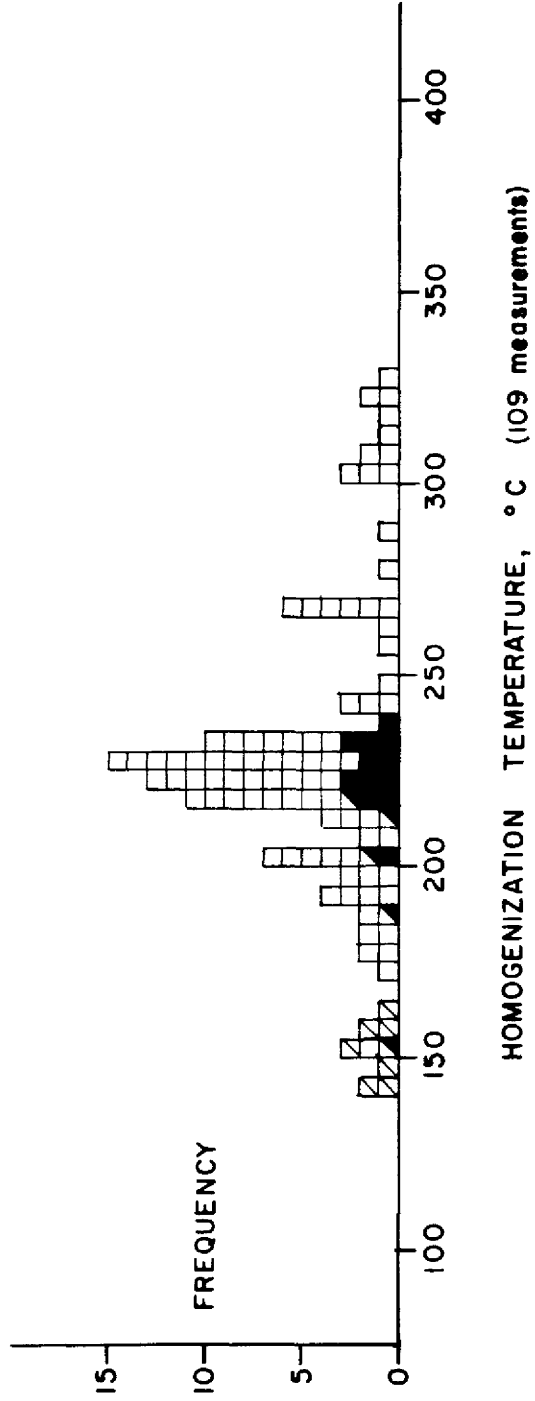


FIGURE 12. FLUID INCLUSION DATA

the inclusion at room temperature. None of the inclusions were found to contain daughter minerals.

Liquid-dominant inclusions containing liquid plus a vapor bubble occupying less than 30 volume percent of the total inclusion volume were the most common. Liquid-dominant inclusions were the only type of inclusion observed in calcite (Fig. 13 and 14), the most common type occurring in quartz (Fig. 15 and 16), and were absent from alunite. All of the homogenization and freezing temperatures measured during this investigation are from these liquid-dominant inclusions.

Vapor-dominant inclusions containing more than 70 volume percent vapor were commonly observed in quartz (Fig. 17) and were the only type of inclusion observed in alunite (Figs. 18 and 19). Measurement of the homogenization and melting temperature of these inclusions proved to be impossible--in quartz, due to difficulties in observing phase disappearance caused by internal reflections; and in alunite, due to the small size (less than 6 microns) of the inclusions.

In calcite, the first stage in the paragenesis, the homogenization temperature of primary and secondary inclusions range from 150°C to 240°C. Primary inclusions cluster around 225°C and range from 200°C to 240°C. (Fig. 12). All have salinities of less than 2 equivalent weight percent NaCl (Table A-2). These values are similar to those obtained from quartz occurring in the same propylitically altered zones, suggesting that calcite and quartz veining took place under

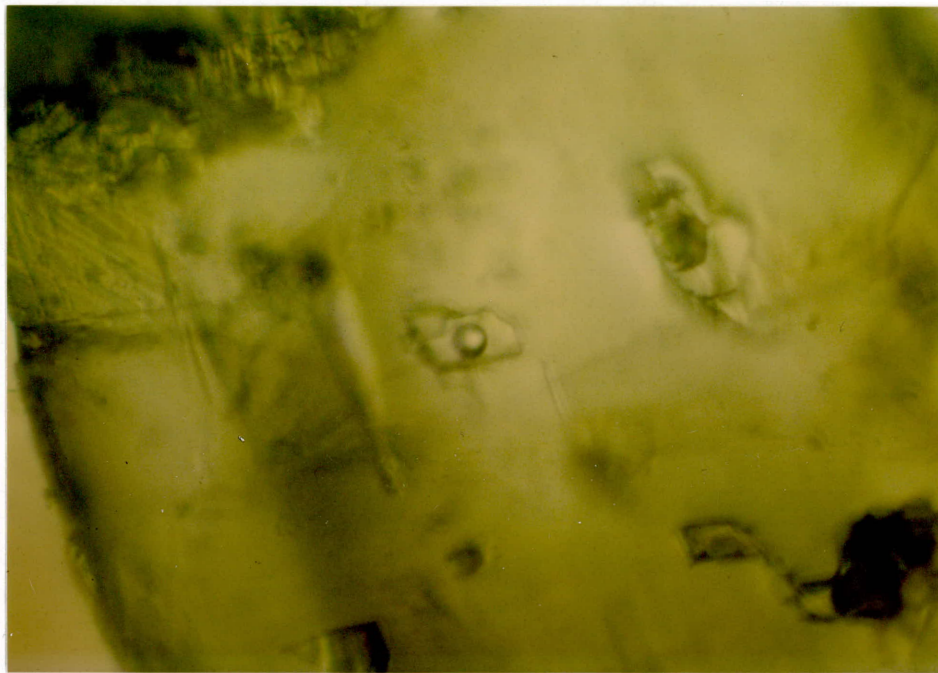


Figure 13. Primary Liquid-Dominant Inclusion in Calcite, at 25°C. The inclusion is approximately 15 microns in length and homogenized at 233.2°C. Sample number 29A15 (Plate 4).

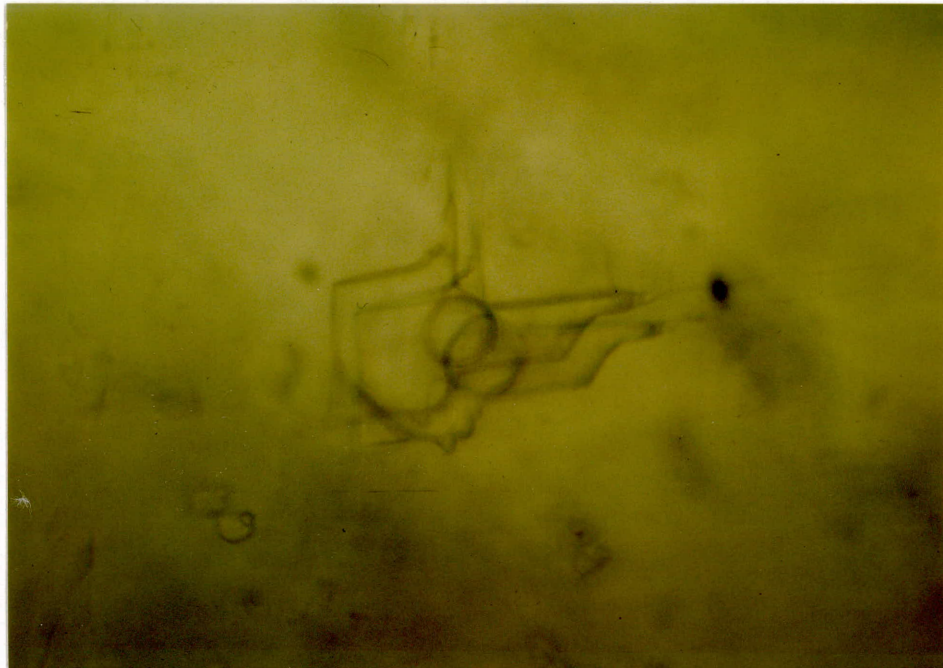


Figure 14. Secondary Liquid-Dominant Inclusion in Calcite, at 25°C. The inclusion is approximately 22 microns in length and homogenized at 210.7°C. The double image is due to refraction. Sample number 29A15 (Plate 4).

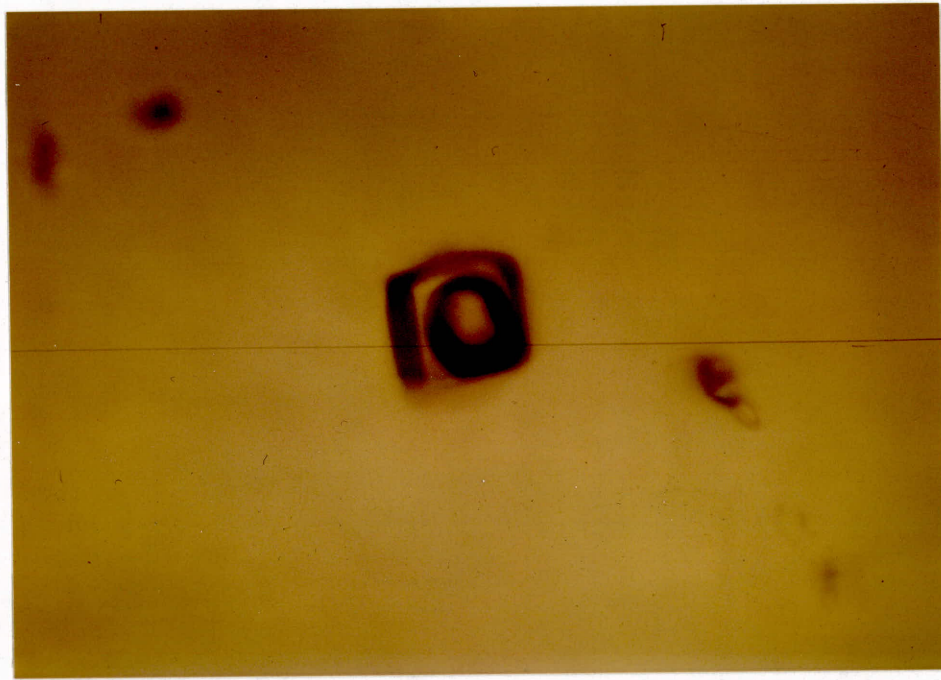


Figure 15. Primary Liquid-Dominant Inclusion in Quartz, at 25°C. The inclusion is approximately 27 microns across, homogenized at 301.8°C, and had a salinity of 1.5 eq. wt. % NaCl. Sample number 19A1S (Plate 4).

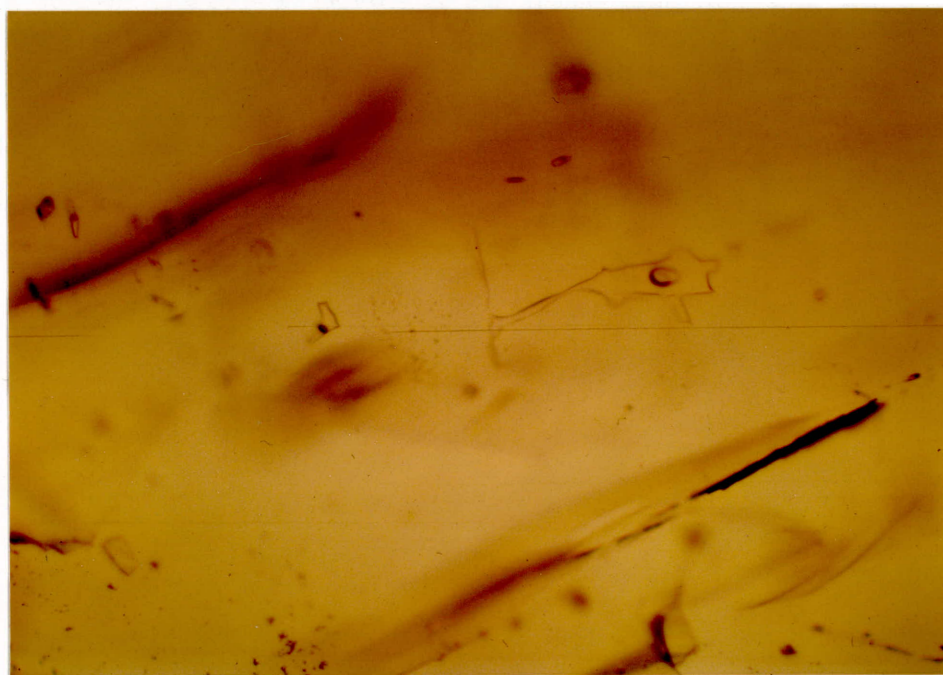


Figure 16. Secondary Liquid-Dominant Inclusions in Quartz, at 25°C. The largest inclusion is approximately 20 microns in length, homogenized at 187.2°C, and had a salinity of 1.9 eq. wt. % NaCl. The inclusions occurring along this secondary plane have necked down and some may have leaked along fractures. Sample number 29A9N (Plate 4).

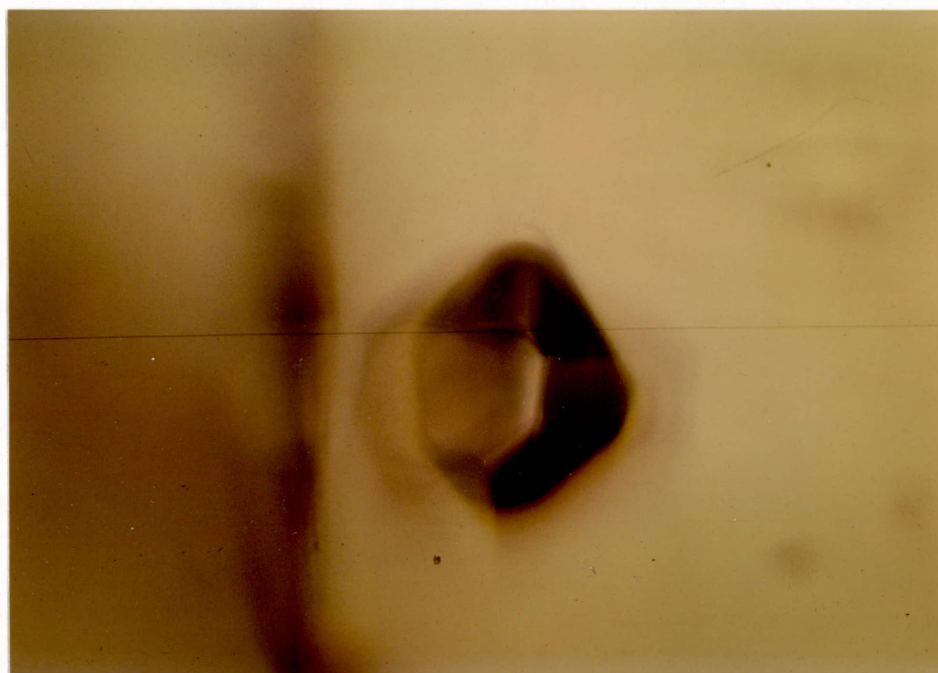


Figure 17. Primary Vapor-Dominant Inclusion in Quartz, at 25°C. The inclusion is approximately 39 microns in length. Sample number 19A1S (Plate 4).

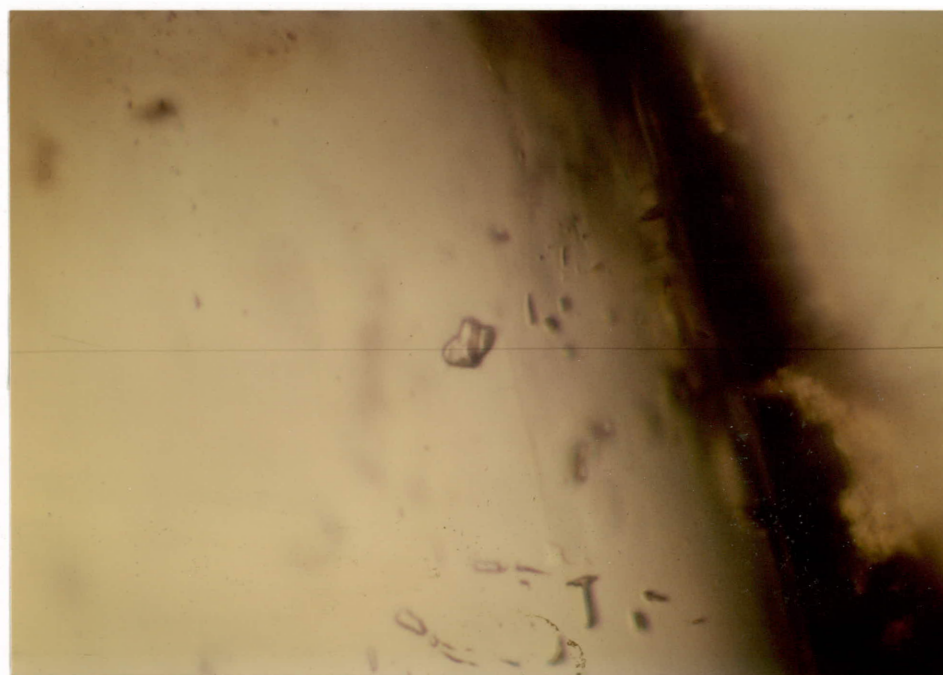


Figure 18. Primary Vapor-Dominant Inclusion in Alunite, at 25°C.
The inclusion is approximately 6 microns across.
Sample number 21XT11 (Plate 4).

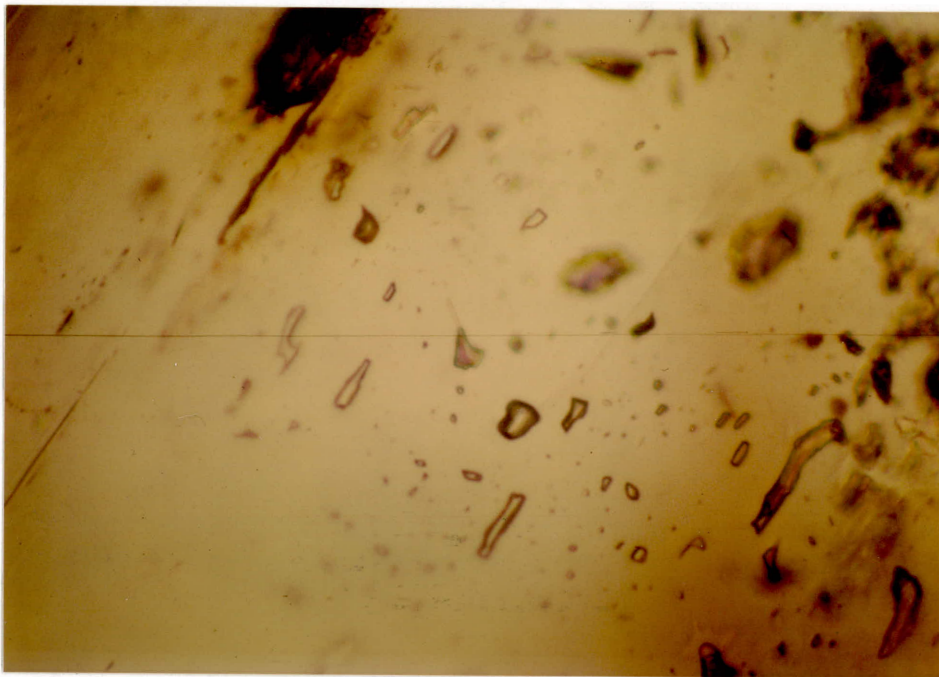


Figure 19. Pseudosecondary Vapor-Dominant Inclusions in Alunite. The bottle-shaped inclusion in the center of the photo contains a liquid phase. The inclusion is approximately 6 microns in length. Sample number 21XT11 (Plate 4).

similar conditions and from similar fluids during the evolution of the hydrothermal system.

Evidence of boiling was not observed in any of the calcite examined, indicating that calcite veining took place at a pressure greater than that at the liquid-vapor curve in the H_2O -NaCl system for a given temperature. Primary inclusions homogenize near $225^{\circ}C$ and have salinities near 1 eq. wt. % NaCl. In the H_2O -NaCl system a fluid of this character intersects the liquid-vapor curve at 25 bars pressure.

Stratigraphic reconstruction of the section at the time of mineralization and alteration indicates the most deeply exposed parts of the hydrothermal system in the field area were buried no more than about 1500 feet (500 meters). This corresponds to a maximum pressure of 150 bars under lithostatic conditions and 45 bars if hydrostatic.

Homogenization temperatures from inclusions trapped above the liquid-vapor curve require a correction for pressure to obtain the true trapping temperature. The maximum pressure of 150 bars would require these data to be corrected at the very most by $+10^{\circ}C$. Because this value is small with respect to the range of homogenization temperatures, no corrections were made on the data.

Most of the inclusions measured in quartz were considered to be primary inclusions (e.g., Figs. 15 and 17) as evidenced by the common negative crystal shape characteristic of inclusions occurring on growth planes, the large size (up to 100 microns) of individual inclusions, and by their 3-dimensional distribution throughout the crystals.

Primary inclusions from throughout the study area have homogenization temperatures that range from about 175°C to 325°C, and salinities of less than 2 equivalent weight percent.

Secondary inclusions (e.g., Fig. 16) occur along conchoidal fractures, are generally irregular in shape, and are smaller, normally reaching sizes of only about 5 to 15 microns. These inclusions have lower homogenization temperatures than primary inclusions, most clustering near 150°C (Fig. 12).

A few of the inclusions measured were arranged in patterns possibly indicative of necking. Some of these inclusions have homogenization temperatures of more than 350°C (Table A-2). Necked inclusions are not plotted on Figure 12.

Many of the quartz crystals examined contained large, primary, liquid-dominant (Fig. 15) and vapor-dominant (Fig. 17) inclusions distributed 3-dimensionally throughout the crystal. In one sample, both types were observed in a cluster of inclusions. Roedder (1979) has shown that the close association of both types of primary inclusions is evidence for boiling of the hydrothermal fluid at the time of entrapment. There were also many samples of quartz that didn't contain vapor-dominant inclusions, but contained only liquid-dominant ones. These observations suggest that the hydrothermal fluids underwent at least episodic boiling, although, perhaps only locally, during

quartz deposition. The maximum pressure corrections for inclusions in quartz are the same as those for calcite and therefore not made.

Examination of Figure 12 reveals a peak in the data. This is due to a sampling bias caused by examining more samples from the propylitically altered portions of the area. However, Figure 20 shows that homogenization temperatures of primary inclusions in quartz increase towards the more intensely altered zones. A horizontal temperature gradient existed in the area that varied from a low of about 175-225°C in the low-intensity propylitic zone up to 275-325°C in the silica zone indicating that one of the factors controlling alunite alteration was temperature. The horizontal temperature gradient was probably due to upwelling of hydrothermal fluids in the silica and alunite zones of the altered areas.

The inclusions observed in alunite veins are vapor-dominant and primary or pseudosecondary in origin, as evidenced by their occurrence in the cores of individual crystals, in clusters and/or along planes, that are enclosed by a clear unfractured rim. The occurrence, of vapor-dominant inclusions in alunite veins is important because it indicates that alunite was deposited from vapor-dominant fluids.

Vapor-dominant conditions may occur either below the water table in vapor-dominated reservoirs, or above a water table that is boiling. James (1968) and White et al. (1971) have shown that vapor-dominated conditions arise below the water table in circulating hydrothermal systems when the amount of water entering the system at the margins

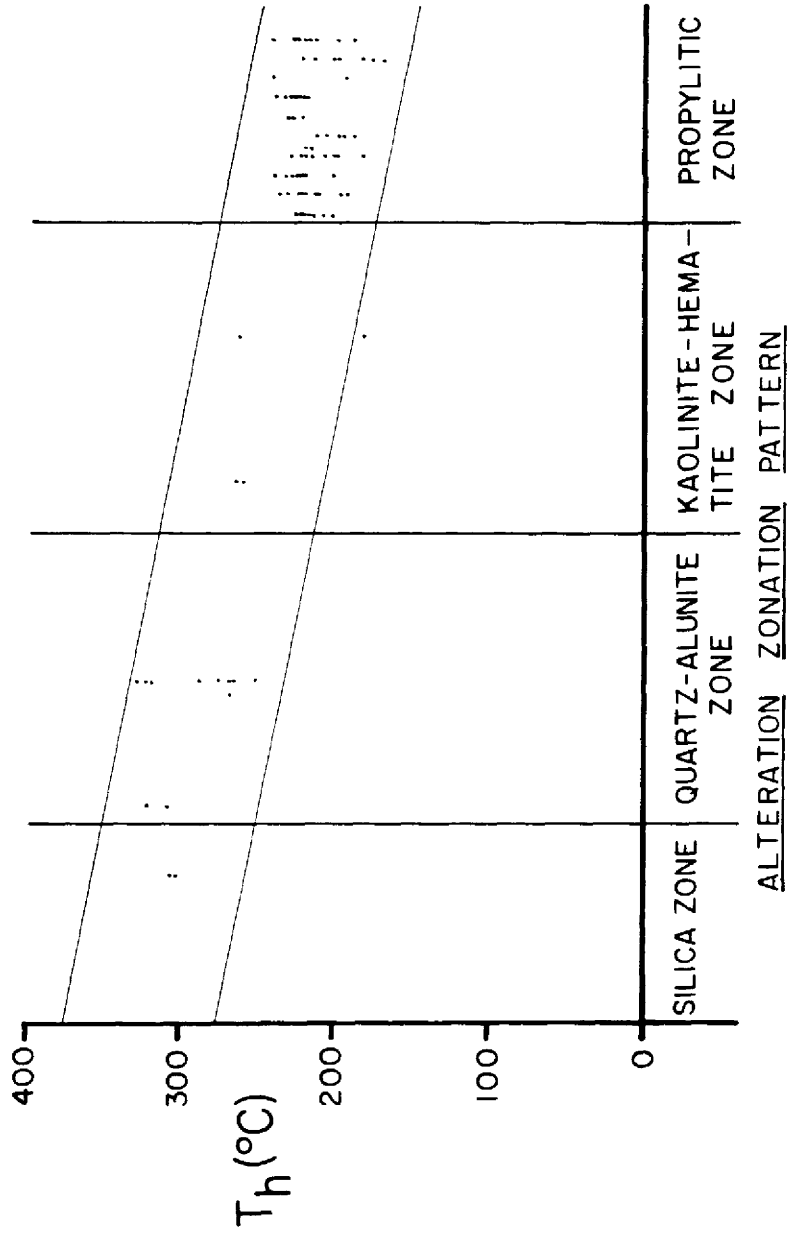


FIGURE 20, LATERAL TEMPERATURE GRADIENT BASED UPON FLUID INCLUSIONS

is less than the water discharged at the top. In such cases, the heat transfer capacity of the system is increased by the development of a vapor-dominant zone in which heat is absorbed during vaporization at the level of boiling, and then released at shallower levels by condensation. Within this zone, steam may be rising while condensed water is descending. White et al. (1971) found that, compared to hot water systems, the major reservoirs in explored vapor-dominated systems have low salinities, and temperatures and pressures near 240°C and 34 bars. This is close to the temperature (236°C) and pressure (31.8 bars) of vapor of maximum enthalpy (670 cal/gm) (James, 1968). James (1968) proposed that, below the critical point of water, the temperature and pressure in these reservoirs is buffered to near the maximum enthalpy of vapor due to the higher heat content of vapor during condensation. In most vapor-dominant reservoirs as steam rises to shallower levels and decreases in temperature and pressure it begins to condense, thus increasing the enthalpy of the remaining rising vapor until the pressure and temperature of maximum enthalpy is attained.

White et al. (1971) suggested that the temperature and pressure in these reservoirs may differ from that of maximum enthalpy steam because of the effects of dissolved salts and partial pressures of other gases; components likely to occur in natural systems. He also suggested that over-pressures could occur in these reservoirs if the supply of heat produced more steam than can escape through available channels.

If the hydrothermal system at NG developed a vapor-dominated zone, under the conditions described by White et al. (1971) and James (1968), the top of the vapor-dominated reservoir, at 236°C and 31.8 bars, would from the hydrostatic boiling condensation curve, have been near 360 meters (1,100 feet) below the paleowater table. Stratigraphic reconstruction of the area indicates that much of the alunite altered rocks formed at no more than 160 meters (500 feet) below the paleosurface. Therefore, alunite alteration occurred at levels above that where a vapor-dominant reservoir, if present, could exist, at pressures and temperatures less than maximum enthalpy vapor.

Alternatively, vapor-dominated conditions could also exist at the top of a hydrothermal system in the rocks occurring at and above the surface of a boiling water table. In this case the pressure would be near atmospheric and the temperature near 100°C. This model seems the most reasonable because it explains the flat-bottomed morphology of some of the alunite altered areas, the bottoms of which presumably record the position of the paleowater table, and provides atmospheric oxygen which could have produced H_2SO_4 from H_2S released during boiling, a product necessary to form alunite. Accordingly, alunite may have been deposited at temperatures near 100°C and pressures near 1 atmosphere.

The composition, temperature, and pressure of the fluids depositing quartz-sericite-pyrite veins and jasperoid could not be determined. However, based on paragenetic relations it is reasonable to assume

that they were deposited within the temperature and pressure range defined by quartz veins and alunite alteration. Therefore, boiling may also have been a factor in their formation.

In summary, fluid inclusion evidence records the evolution of the hydrothermal system from an early nonboiling, hot-water system, to an episodically boiling, hot-water system, and finally to a boiling hot-water system.

The exact cause or causes of boiling of the hydrothermal fluids is unknown. Regardless, boiling is important because of its marked effect on the physical and chemical conditions of the hydrothermal fluid and because it has been recognized in numerous hydrothermal deposits (Buchanan, 1981). Drummond and Ohmoto (1979) showed that, in the $\text{H}_2\text{O}-\text{NaCl}-\text{CO}_2-\text{CH}_4-\text{H}_2\text{S}-\text{SO}_2$ system, isoenthalpic boiling, the most common type, results in an increase in oxygen fugacity, decrease in sulfur fugacity, increase in pH, and an increase in the concentration of chloride and metals in the residual liquid relative to the initial liquid. Conversely, the vapor phase has a lower oxygen fugacity, higher sulfur fugacity, and lower chloride and metal concentration than the initial solution. They suggested that these shifts should result in changing mineral solubilities, promoting the deposition of quartz, gold and silver metals, and possibly sulfates. Vapor phase condensation, at higher levels should result in intense hydrogen metasomatism due to the low pH of these solutions.

The very low salinity of the fluids, less than 2 eq. wt. % NaCl, agrees with the results of other studies (see Buchanan, 1981) that show that hydrothermal fluids in epithermal systems are generally of low salinity. Oxygen and hydrogen isotopic work by Taylor (1973) on similar epithermal systems, such as Goldfield, Nevada, showed that the water associated with these low salinity systems is dominantly of meteoric origin. This may have also been the case at NG, although a sulfur isotope value, discussed in a later section, indicates some components of the fluid were derived from other sources.

ISOTOPIC COMPOSITION OF SULFUR

A sample of relatively pure, fine-grained replacement alunite from the main metallurgical test pit (Area C, Pl. 4) was obtained by C. G. Cunningham of the U.S. Geological Survey and analyzed for ^{34}S and ^{32}S (pers. commun., 1982). The alunite was found to have a $^{34}\text{S}/^{32}\text{S}$ ratio of +1.45 per mil nearly the same as the Canon Diablo meteorite standard (Cunningham, pers. commun., 1982). Ohmoto and Rye (1979) have shown that the observed S per mil values of hydrothermal minerals reflect the varied geochemical history of the sulfur in hydrothermal fluids, and the proper interpretation of the significance of the S isotopic composition can be made only through understanding the geology of the deposit and the many processes of isotopic fractionation likely to occur.

Based on geologic considerations there are three possible sources for sulfur; Mesozoic evaporites, S-bearing volcanics, and magmatic fluids. Sulfur in evaporites could be incorporated into a hydrothermal fluid by movement of the fluids through an evaporite. Isotopic fractionation of S would take place during incorporation of sulfate into the fluid. Ohmoto and Rye (1979) demonstrated that when sulfur species in solution are introduced through dissolution of another compound, such as anhydrite or gypsum, isotopic fractionation is controlled by reaction kinetics. They also noted that the kinetic

affect is most pronounced when the rupturing of a chemical bond involving the isotopes in question is the rate controlling step of the reaction. This arises because reaction rates are mass dependent; with molecules containing the lighter isotopes generally having the fastest reaction rates. Consequently, the product, in this case H_2S , tends to be enriched in the lighter isotope, although fractionation becomes less pronounced at successively higher temperatures. For sulfate having an S isotopic value of +20 per mil, the average value for Mesozoic evaporites (Ohmoto and Rye, 1979), the isotopic value of S in H_2S produced by reduction could range between +20 and -5 per mil, depending on the extent to which the original sulfate was reduced and the temperature. Partial reduction of seawater sulfate could result in the formation of an H_2S -bearing fluid with an apparent "magmatic" S isotopic composition, but only during the initial stages of reduction. It seems unlikely that at the temperatures observed in these fluids that large volumes of H_2S would have been produced that had values near zero per mil, although it is possible. It is unlikely, therefore, that evaporites were the major source of sulfur.

It is also possible that sulfur was leached from sulfide minerals in volcanics exposed in the area. Based on experimental data, Ohmoto and Rye (1979) suggest that kinetic isotopic effects during leaching of sulfide minerals are small and that hydrothermal fluids that obtained H_2S by decomposition of sulfides in igneous rocks would have S values nearly identical to magmatic fluids. Although some of

the sulfur in the hydrothermal fluid may have been derived from near-surface volcanic rocks, given the large quantities of sulfur added to the rocks, about 30 million metric tons, and the average abundance of S in igneous rocks of 300 ppm (Rose et al. 1979), it appears likely that another source was involved.

Alternatively, sulfur may have been derived from an H₂S-bearing hydrothermal fluid exsolved from a cooling magma. Ohmoto and Rye (1979) have shown that very little isotopic fractionation occurs, during any reactions likely to proceed, in rising hydrothermal fluids. However, upon oxidation of the fluid, kinetic isotopic effects tend to produce sulfate that is successively lighter until most, or all, of the H₂S is oxidized, in which case the isotopic composition of SO₄ approaches that of the original magmatic hydrothermal H₂S. The absence of sulfide minerals, evidence of high fO₂, and a δS value of +1.45 per mil suggest that a similar process may have operated during formation of alunite. Of the three possibilities, a magmatic source for S appears the most likely and is consistent with earlier interpretations suggesting that a shallow level intrusion is closely related to alteration and mineralization in the area.

SUMMARY AND GENETIC MODEL

Any model describing the genesis of the NG Alunite Area must consider the following observations.

1. The spatial coincidence of the alunite altered volcanics with local volcanic centers and local uplift and extension.
2. The coincident age of alunite alteration, approximately 20 m.y., with a belt of rhyolitic volcanic centers 23 to 18 m.y. old.
3. The onset of alteration after an episode of local deformation, but before emplacement of the rhyolitic volcanic centers observed at the surface.
4. A likely magmatic source of sulfur in alunite.
5. The zoning, morphology, and size of the altered areas.
6. The paragenesis and accompanying physico-chemical evolution of the hydrothermal system (see Table 4).
7. The higher temperatures of fluid inclusions in quartz veins in the most intensely altered areas.
8. The low trace element content of the altered areas.

Observations 1-4 are consistent with the idea that hydrothermal activity at NG was initiated following emplacement of a shallow level intrusion. Assuming that an intrusion is present, it is thought to have been involved in development of the hydrothermal system in the following manner: it disrupted and fractured the overlying rocks promoting free fluid circulation to deep levels; the heat provided

Table 4. Summary of Physical and Chemical Conditions Attending Alteration and Mineralization

Order in Paragenetic Sequence	1	2	3	4	5	6	7
	Calcite Veins	Cc - Qtz Veins	Quartz Veins	QSP Veins	Jasperoid	Alunite Alteration	Massive Iron Oxides
T °C	200-235*	200-235* 175-350*	130?	?	?	100 ±***	?
P bars	25-150*	25-150* 20-150* Hydrostatic? Atmospheric*** Hydrostatic?	Hydrostatic?	Hydrostatic?	Hydrostatic?	Atmospheric*** Hydrostatic?	Hydrostatic?
Boiling	No*	No* Episodic*	?	?	?	Yes***	?
Salinity	<2*	<2*	<2*	?	?	Low?	Low?
pH	6-7**	6-7** 6-7**	3.5-6.5***	?	?	<2-4**	4 ±**
Stable Form of Excess Iron	Py	Py	Py	Py	Py	Hm	Hm

*Based on fluid inclusion measurements.

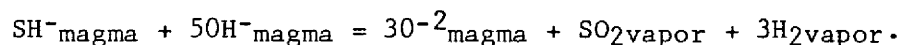
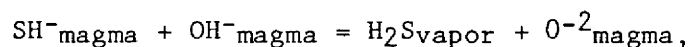
** Based on mineral phase equilibria.

***Based on fluid inclusion observations and interpretation.

Py = Pyrite; Hm = Hematite

produced density differences in ground waters resulting in the convective circulation of these fluids; and last S, and possibly other dissolved constituents were derived from the cooling magma.

The evolution of the hydrothermal system is summarized on Figure 21 based on the assumption that an intrusion is present. Experimental evidence (Brimhall and Ghiorso, 1983), demonstrated that during cooling and solidification of an intrusion, a magmatic aqueous phase may be generated through the partitioning of water, sulfur, chlorine, carbon dioxide, and heavy metal complexes from the silicate melt. On the basis of experimental data and thermodynamic calculations, Burnham (1979) has shown that the most likely S species formed on exsolution are H_2S and SO_2 (Fig. 21-1 and 2), which are formed through the reactions



He further demonstrated that the equilibrium distribution of these species in solution, at magmatic temperatures and pressures, is a function of fO_2 which in turn depends on the composition and water content of the magma. This is due to the likely loss of H_2 from the hydrous magma to the wallrocks during formation of an aqueous phase (Fig. 21-2). This results in an fO_2 increase in the magma that causes the ratio of SO_2 to SH^- in the magma to increase. Because of the low solubility of SO_2 in the magma, nearly all of the S can be partitioned into the vapor phase. Accordingly, most water-rich silicic magmas tend to

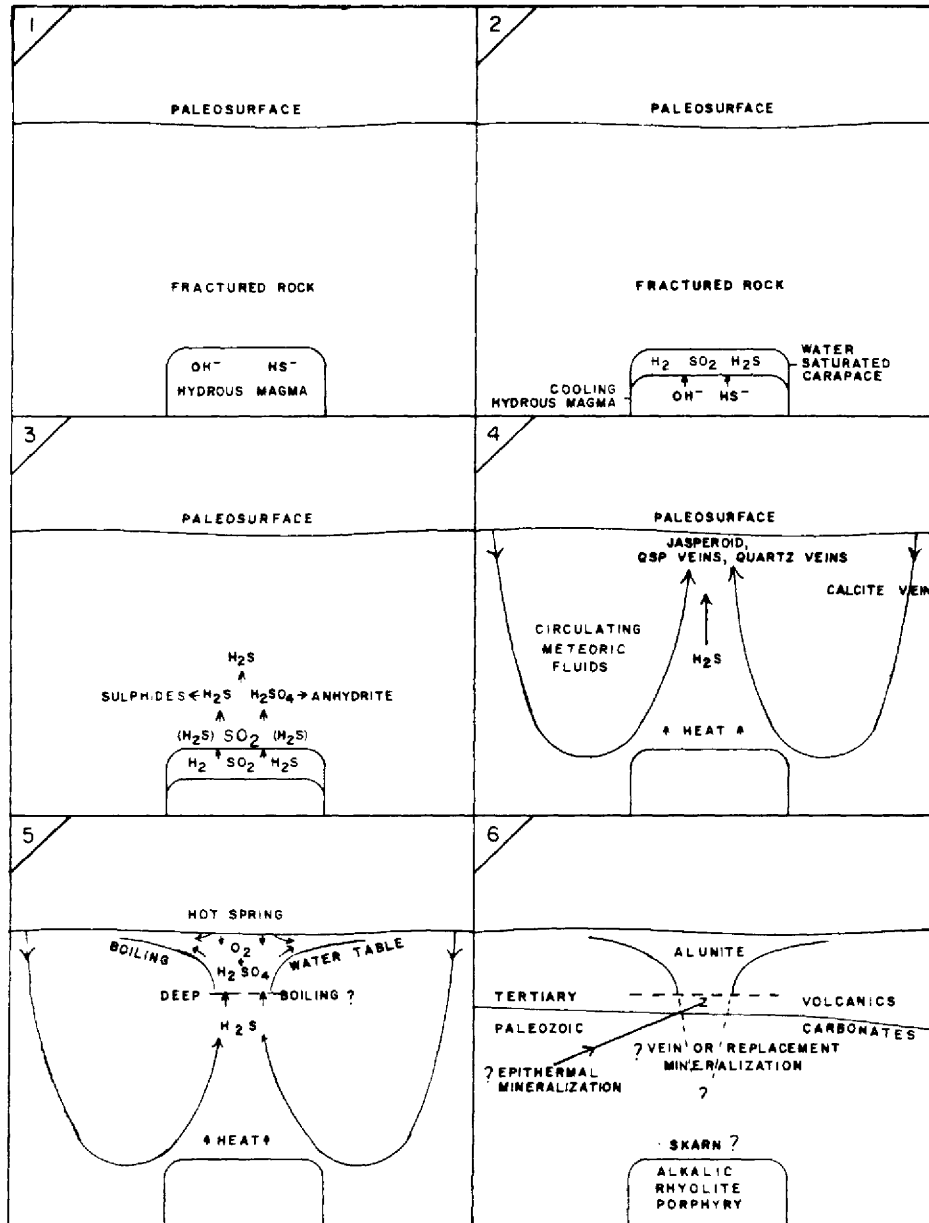
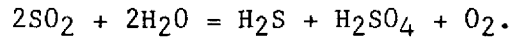


FIGURE 21. HYPOTHETICAL EVOLUTION OF THE HYDRO-THERMAL SYSTEM, NG ALUNITE AREA

exsolve SO₂-dominant fluids (Fig. 21-3). Burnham (1979) reports that as the SO₂-dominant fluid moves away from the magma to lower temperature conditions, the SO₂ hydrolyzes to produce H₂S and H₂SO₄ (Fig. 21-3) according to the reaction



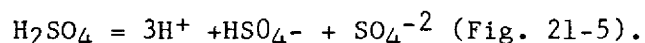
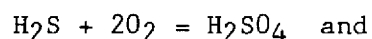
The resulting increase in the fugacity of H₂S may cause precipitation of sulfide minerals from any metal-chloride complexes present in the fluid (Fig. 21-3). A factor not considered by Burnham (1979) is the possible reduction of H₂SO₄ and loss of O₂ from the fluid through oxidation of ferrous iron to ferric iron in the wallrocks. This would result in the formation of a reduced H₂S-rich brine (Fig. 21-4). The fluid continued to rise to shallower levels where it was diluted and incorporated into meteoric fluids circulating over the heat source (Fig. 21-4).

In the near surface regime, it is likely that alteration and mineralization took place under the influence of a circulating meteoric hydrothermal system. The pressure drive that initiated convection in the water-saturated rocks is thought to have resulted from a decrease in density of the heated water, due to thermal expansion, relative to the surrounding cooler water. Cool, dense waters descended around the margins of the heat source while hot, low density fluids rose above it (Fig. 21-4 and 5). The veined and altered rocks observed at the surface today provide evidence of the fluid circulation paths. The sites of upwelling fluids are recorded by the quartz veins,

quartz-sericite-pyrite veins, jasperoid bodies, and alunite altered areas (Fig. 21-4). Lateral temperature gradients indicate that the sites of alunite alteration were located where the upwelling fluids were the hottest.

During the early stages of mineralization, prior to alunite alteration, the rocks were apparently sufficiently permeable, the rate of fluid flow high enough, and the supply of conducted heat from below, low enough for most of the water flowing through the system to remain liquid. However, as evidenced by fluid inclusions in quartz veins, temperatures were locally high enough, pressures low enough, or both, for some boiling to occur as the fluids rose. This eventually led to formation of a vigorously boiling system as evidenced by vapor-dominant inclusions in alunite.

Upward movement of vapor into the cool rocks overlying the boiling water table resulted in condensation of the vapor phase, oxidation of H_2S , and formation of sulfuric acid through reactions such as



Vigorous boiling eventually caused large amounts of acid-condensates to accumulate in the rocks above the boiling water table. As boiling continued, the rocks became saturated with acid-condensates resulting in expansion of the saturated zone laterally in permeable rocks at and above the water table to produce the near horizontal, flat-bottomed alunite altered areas. With a decreasing rate of recharge water, and

a sufficiently potent heat supply, vapor loss at sites of most vigorous boiling eventually led to depression of the water table above hot zones of fluid upwelling. The low-pH condensates percolated downward into the depressions to produce the funnel-shaped altered areas (Fig. 21-5).

The affects of movement of these acid-condensates through the volcanic rocks can be thought of as the movement of a hydrolysis front (Schoen et al. 1974). Ions released by dissolution of minerals accumulate in the pore liquid and move in response to gravity, concentration, pressure, and temperature gradients. Depending on the composition of the pore liquid, alteration minerals may precipitate from some of the ions in solution, while other ions will continue to move in the pore solution. In the central areas, at high temperatures and low pH, only silica is stable, with the remaining elements diffusing away from the hot, low pH portions of the system. Further out, first alunite and then kaolinite form in response to a decrease in pH. As pH rises, due to reaction of the fluids with fresh rock and by mixing with ground water, iron precipitates at a pH of 4 (Schoen et al. 1974) to form the hematite-clay zone around the margins of the quartz-alunite altered areas. The massive iron oxide deposits formed by the same process in open fissures adjacent to the altered areas. Beyond the hematite halo, solutions enriched in silica and alumina, derived from alteration near the center of the system, combine with solutions containing magnesium, calcium, and iron, derived from the alteration occurring at the margins. Here, montmorillonite is stable forming

the high propylitic zone. Acid-condensates containing iron that percolated down below the level of oxidation of H_2S to H_2SO_4 , contributed to the precipitation of the pyrite found in the quartz-alunite-sericite-pyrite root zones. Sericite may have formed due to some combination of the following: higher pH, higher K^+ activity, or higher temperature.

During the waning stages of the hydrothermal system, as the solutions cooled, minor amounts of uranium and other trace elements were precipitated along cracks and fissures at previous sites of massive iron oxide deposition.

The hydrothermal system at NG differs from most other epithermal systems in that larger volumes of rock were altered to advanced argillic assemblages (Hall, 1978). This may have been promoted by the forceful emplacement of a shallow level intrusion that fractured the country rocks thus allowing more fluid contact. The hydrothermal system may also have been active for a longer period of time because the intrusion was capable of sustaining boiling conditions long enough to produce the large amounts of acid condensate necessary to alter the large volumes of rock occurring at NG.

The low trace element content of the alunite altered areas is thought to be due to leaching under the low pH, high fO_2 conditions that formed these deposits. Outside of the altered areas, the earlier stages of quartz-sericite-pyrite veining and jasperoid formation

deposited anomalous concentrations of trace elements possibly due to higher pH and lower fO_2 conditions at these sites.

Given the character of the hydrothermal system, it is considered likely that mineralization is present at depth. Likely loci (Fig. 21-6) include: the contact zone of the intrusive, the carbonate rocks overlying the intrusive, and along fractures at the level where boiling occurred.

REFERENCES CITED

- Anderson, J. J., 1971, Geology of the Southwestern High Plateaus of Utah: Bear Valley Formation, an Oligocene-Miocene Volcanic Arenite: Geological Society of America Bulletin, Vol. 82, p. 1179-1206.
- Anderson, J. J. and Rowley, P. D., 1975, Cenozoic Stratigraphy of Southwestern High Plateaus of Utah: Geological Society of America, Special Paper 160, p. 1-51.
- Armstrong, R. L., 1968, Sevier Orogenic Belt in Nevada and Utah, Geological Society of America Bulletin, Vol. 79, p. 429-458.
- _____, 1970, Geochronology of Tertiary igneous rocks, eastern Basin and Range Province, western Utah, eastern Nevada, and vicinity, U.S.A.: Geochimica et Cosmochimica Acta, Vol. 34, p. 203-232.
- Best, M. G.; Shuey, R. T.; Caskey, C. F.; Grant, S. K., 1973, Stratigraphic relations of Members of the Needles Range Formation at Type Localities in Southwestern Utah: Geological Society of America Bulletin, Vol. 84, p. 3269-3278.
- Best, M. G. and Brimhall, W. H., 1974, Late Cenozoic Alkalic Basaltic Magmas in the Western Colorado Plateaus and the Basin and Range Transition Zone, U.S.A., and Their Bearing on Mantle Dynamics: Geological Society of America Bulletin, Vol. 85, p. 1677-1690.
- Best, M.G. and Keith, J.D., 1979, Map Showing Volcanic Geology of the Observation Knoll and the Tetons Quadrangles, Beaver and

- Iron Counties, Utah: U.S. Geological Survey Open-File Report 90-1611, 5 pp.
- Best, M. G. and Mehnert, H. H., 1983, Miocene Magmatism and Tectonism in the southern Wah Wah Mountains and Needle Range, Southwestern Utah, Geological Society of America Abstracts with Programs, Rocky Mtn. and Cordilleran Sections, Vol. 15, p. 402.
- Botinelly, T., 1976, A Review of the Minerals of the Alunite-Jarosite, Beudantite, and Plumbogummite Groups: Geological Survey Journal of Research, Vol. 4, p. 213-216.
- Brophy, G. P., Scott, E. S., Snellgrove, R. A., 1962, Sulfate Studies II. Solid Solution Between Alunite and Jarosite: The American Mineralogist, Vol. 47, p. 112-126.
- Buchanan, L. J., 1981, Precious Metal Deposits Associated With Volcanic Environments in the Southwest: Arizona Geological Society Digest, Vol. 14, p. 237-262.
- Burchfiel, B. C. and Davis, G. A., 1972, Structural Framework and Evolution of the Southern Part of the Cordilleran Orogeny, Western United States: American Journal of Science, Vol. 272, p. 97-118.
- Burnham, C. W., 1979, Magmas and Hydrothermal Fluids, in Geochemistry of Hydrothermal Ore Deposits, 2d ed., Chapter 10, edited by H. L. Barnes, published by John Wiley and Sons, Inc., New York, U.S.A.

- Burt, D. M., Sheridan, M. F., Bikun, J. V., and Christiansen, E. H., 1982, Topaz Rhyolites--Distribution, Origin, and Significance for Exploration: Economic Geology, Vol. 77, pp. 1818-1836.
- Clarke, D. B., 1981, The Mineralogy of Peraluminous Granite: A Review: Canadian Mineralogist, Vol. 19, p. 3-17.
- Cunningham, C. G., 1976, Field and Laboratory Tests for the Detection of Alunite and Determination of Atomic Percent Potassium: Economic Geology, Vol. 71, p. 1596-1598.
- Cunningham, C. G. and Steven, T. A., 1979a, Uranium in the Central Mining Area, Marysvale District, West-Central Utah: U.S. Geological Survey Map I-1177.
- _____, 1979b, Mount Belknap and Red Hills Calderas and Associated Rocks, Marysvale Volcanic Field, West-Central Utah: U.S. Geological Survey Bulletin 1468.
- Drummond, S. E. and Ohmoto, H., 1979, Effects of boiling on mineral solubilities in hydrothermal solutions: Geological Society of America Abstracts with Programs, Vol. 11, p. 416.
- Ellis, A. J., 1979, Explored Geothermal Systems, in Geochemistry of Hydrothermal Ore Deposits, chapter 13, 2d ed., edited by H. L. Barnes, John Wiley and Sons, Inc., New York, U.S.A.
- Fahley, M. P., 1981, Fluid Inclusion Study of the Tonopah District, Nevada: Unpublished Masters Thesis, No. 2468, Colorado School of Mines, Golden, Colo.

- Fleck, R. J., Anderson, J. J., and Rowley, P. D., 1975, Chronology of mid-Tertiary volcanism in the High Plateaus region of Utah, in Cenozoic geology of the southwestern High Plateaus of Utah: Geological Society of America Special Paper 160, p. 53-62.
- Hall, R. B., 1978, World Nonbauxite Aluminum Resources--Alunite: U.S. Geological Survey Professional Paper 1076-A.
- Hemley, J. J., Hostetler, P. B., Gude, A. J., Mountjoy, W. T., 1969, Some Stability Relations of Alunite: Economic Geology, Vol. 64, p. 599-612.
- Hemley, J. J., Montoya, J. W., Marinenk, J. W., Luce, R. W., 1980, General Equilibria in the System Al_2O_3 - SiO_2 - H_2O and Some Implications for Alteration/Mineralization Processes: Economic Geology, Vol. 75, p. 210-228.
- Holland, H. D., and Malinin, S. D., 1979, The solubility and occurrence of non-ore minerals, in Geochemistry of Hydrothermal Ore Deposits, 2d ed., chapter 9, edited by H. L. Barnes, John Wiley and Sons, Inc., New York, U.S.A.
- James, Russell, 1968, Wairakei and Larderello; geothermal power systems compared: New Zealand Journal of Science and Technology, Vol. 11, p. 706-719.
- Keith, J. D., 1979, Miocene volcanism hosting porphyry-molybdenum and epithermal vein mineralization, Southwestern Utah and Nevada: Geological Society of America Abstracts with programs, Vol. 11, no. 7, p. 455.

- Kesler, S. E., Russell, N., Seaward, M., Rivera, J., McCurdy, K., Cumming, G. L., Sutter, J. F., 1981, Geology and Geochemistry of Sulphide Mineralization Underlying the Pueblo Viejo Gold-Silver Oxide Deposit, Dominican Republic: Economic Geology, Vol. 76, p. 1096-1117.
- Knight, J. E., 1977, A Thermochemical Study of Alunite, Energite, Luzonite, and Tennantite Deposits: Economic Geology, Vol. 72, p. 1321-1336.
- Lemmon, D. M., and Morris, H. T., 1979, Preliminary Geologic Map of the Frisco Quadrangle, Beaver County, Utah: U.S. Geological Survey Open-File Report 79-724, 17 pp.
- Levinson, A. A., 1980, Introduction to Exploration Geochemistry, 1st and 2d eds., Applied Publishing, Ltd., Wilmette, Ill., U.S.A.
- Lindsey, D. A., and Osmonson, L. M., 1978, Mineral Potential of Altered Rocks near Blawn Mountain, Wah Wah Range, Utah: U.S. Geological Survey Open-File Report 78-114, 18 p.
- Lovering, T. G., 1972, Jasperoid in the United States--its characteristics, origin, and economic significance: U.S. Geological Survey Professional Paper 710, 164 p.
- _____, 1981, Jasperoid Float and Stream Cobbles as Tools in Geochemical Exploration for Hydrothermal Ore Deposits: Journal of Geochemical Exploration, Vol. 14, p. 69-82.

- Mackin, J. H., 1960, Structural Significance of Tertiary Volcanic Rocks in Southwestern Utah: American Journal of Science, Vol. 258, p. 81-131.
- Mehnert, H. H., 1978, K-Ar Ages and Geothermal Implications of Young Rhyolites in West-Central Utah: ISOCHRON-West, no. 21, p. 3-7.
- Miller, G. M., 1966, Structure and Stratigraphy of Southern Part of Wah Wah Mountains, Southwest Utah: Bulletin of the American Association of Petroleum Geologists, Vol. 50, p. 858-900.
- Ohmoto, H., and Rye, R. O., 1979, Isotopes of sulfur and carbon, in Geochemistry of Hydrothermal Ore Deposits, 2d ed., chapter 10, edited by H. L. Barnes, John Wiley and Sons, Inc., New York, U.S.A.
- Perry H. A. and Walker, W. W., 1974, Summary Report of Results of Development Work on the NG Alunite Property, Southern Wah Wah Mountains, Beaver County, Utah: Unpublished Earth Sciences, Inc., company report.
- Perry, H. A., Walker, W. W., Tipton, W. R., 1977, Mining Plan for NG Alunite Area C - First Five Years: unpublished Alumet Company report.
- Potter, R. W. II, Clynne, M. A. and Brown, D. L., 1978, Freezing Point Depression of Aqueous Sodium Chloride Solutions: Economic Geology, Vol. 73, p. 284-285.

- Roedder, E., 1979, Fluid Inclusions as Samples of Ore Fluids, in Geochemistry of Hydrothermal Ore Deposits, 2d ed., chapter 14, edited by H. L. Barnes, John Wiley and Sons, Inc., New York, U.S.A.
- Rose, A. W., and Burt, D. M., 1979, Hydrothermal Alteration, in Geochemistry of Hydrothermal Ore Deposits, 2d ed., chapter 5, edited by H. L. Barnes, John Wiley and Sons, Inc., New York, U.S.A.
- Rose, A. W., Hawkes, H. E., Webb, J. S., 1979, Geochemistry in Mineral Exploration, 2d ed., Academic Press, Inc., New York, U.S.A.
- Rowley, P. D., Anderson, J. J., Williams, P. L., Fleck, R. J., 1978a, Age of Structural Differentiation Between the Colorado Plateaus and Basin and Range Provinces in Southwestern Utah: Geology, Vol. 6, p. 51-55.
- Rowley, P. D., Lipman, P. W., Mehnert, H. H., Lindsay, D. A., Anderson, J. J., 1978b, Blue Ribbon Lineament, an east-trending structural zone within the Pioche Mineral Belt of southwestern Utah and eastern Nevada: U.S. Geological Survey Journal of Research, Vol. 6, p. 175-192.
- Schoen, R., White, D. E., Hemley, J. J., 1974, Argillization by Descending Acid at Steamboat Springs, Nevada: Clays and Clay Minerals, Vol. 22, p. 1-22.

- Shawe, D. R. and Stewart, J. H., 1976, Ore Deposits as Related to Tectonics and Magmatism, Nevada and Utah: A.I.M.E. Transactions, Vol. 260, p. 225-232.
- Sheridan, M. F., and Updike, R. A., 1975, Sugarloaf Mountain tephra—a Pleistocene rhyolitic deposit of base-surge origin in northern Arizona: Geological Society of American Bulletin, Vol. 86, p. 571-581.
- Shuey, R. T., Caskey, C. F., Best, M. G.; 1976, Distribution and Paleomagnetism of the Needles Range Formation, Utah and Nevada: American Journal of Science, Vol. 276, p. 954-968.
- Sillitoe, R. H., 1973, The Tops and Bottoms of Porphyry Copper Deposits: Economic Geology, Vol. 68, p. 799-815.
- Slack, J. F., 1980, Multistage Vein Ores of the Lake City District, Western San Juan Mountains: Economic Geology, Vol. 75, p. 963-991.
- Steven, T. A., Rowley, P. D., Hintze, L. F., Best, M. G., Nelson, M. G., and Cunningham, C. G., 1978, Preliminary Geologic Map of the Richfield 1° x 2° Quadrangle, Utah: U.S. Geological Survey Open-File Report 78-602.
- Steven, T. A., Cunningham, C. G., Naeser, C. W., Mehnert, H. H., 1979, Revised Stratigraphy and Radiometric Ages of volcanic Rocks and Mineral Deposits in the Marysvale Area, West-Central Utah: U.S. Geological Survey Bulletin 1469.

- Steven, T. A., Cunningham, C. G., Machette, M. N., 1980, Integrated Uranium Systems in the Marysvale Volcanic Field, West-Central Utah: U.S. Geological Survey Open-File Report 80-524, 39 pp.
- Stewart, J. H., Moore, W. J., Zietz, I., 1977, East-West Patterns of Cenozoic Igneous rocks, Aeromagnetic Anomalies, and Mineral Deposits, Nevada and Utah: Geological Society of America Bulletin, Vol. 88, p. 67-77.
- Taylor, H. P., 1973, O^{18}/O^{16} Evidence for Meteoric-Hydrothermal Alteration and Ore Deposition in the Tonopah, Comstock Lode, and Goldfield Mining Districts, Nevada: Economic Geology, Vol. 68, p. 747-765.
- Tolman, C. F. and Ambrose, J. W., 1934, The Rich Ores of Goldfield, Nevada: Economic Geology, Vol. 29, p. 255-279.
- Walker, W. W., 1971, Summary Report of Results of Phase I Exploration Program on the NG Alunite Property Beaver County, Utah: unpublished Earth Sciences, Inc. company report.
- Walker, W. W., and Stevens, D. N., 1972, Report of Results Phase III Exploration Program on the NG Alunite Property, Beaver County, Utah: unpublished company report for National-Southwire Aluminum Co and Earth Sciences, Inc.
- Westra, G., and Keith, S. B., 1981, Stockwork Mo Deposits: Classification and Genesis: Economic Geology, Vol. 76, pp. 844-873.

White, D. E., Muffler, L. J. P., Truesdell, A. H., 1971, Vapor Dominated Hydrothermal Systems Compared with Hot-water Systems: Economic Geology, Vol. 66, p. 75-97.

White, D. E., 1981, Active Geothermal systems and hydrothermal ore deposits; Economic Geology, 75th Anniversary Volume, pp. 392-423.

APPENDIX A

Calibration of the Heating/Freezing
Stage Microscope

A gas-flow, dual-purpose, heating/freezing stage microscope was used to measure the temperatures of phase changes in fluid inclusions reported in this paper. A description of the system used is given in Fahley (1981), as well as calibration data which are presented in Table A-1 and outlined below. The stage was calibrated at the temperatures of fluid inclusion homogenization using TEMPILAQ organic melting point standards at 101, 198, 253, and 302 degrees C. Calibration of the stage at freezing temperatures was made by observing the melting point of triple distilled water and n-tridecane placed in sealed capillary tubes. The heating runs conducted by Fahley (Table A-1) demonstrated that the equipment could measure homogenization temperatures to accuracies within ± 1 percent of the measured value. In view of this accuracy, the homogenization temperatures obtained during the course of this study have not been adjusted or corrected. However, freezing runs (Table A-1) show that near 0 degrees C, temperature measurements are about 0.7 degrees C higher than the true value. Accordingly, the freezing points reported in Table A-2 have been corrected by 0.7°C. The corrected freezing point measurements are considered to be accurate to within 0.5°C of the true freezing point of the inclusions, or 1.0 wt. percent of the true salinity of the fluids.

During the course of the present study, measurements of the temperatures of phase changes in individual inclusions were generally found to be reproducible to within 0.5 to 1.0°C during successive heating runs and to within 0.1 to 0.3°C during successive freezing runs.

Procedure

Samples of calcite and quartz were first described and classified according to their paragenesis. In order to obtain mineral chips suitable for viewing on the heating/freezing stage microscope, selected samples were crushed to obtain thin chips about 0.5 to 0.2 cm across. The chips were then examined under the microscope for the presence of fluid inclusions. Chips containing fluid inclusions were then separated for heating/freezing runs. Prior to heating or freezing, each inclusion was drawn to scale, phase relationships noted, and classified as primary, pseudosecondary, or secondary in origin based upon criteria presented in Roedder (1979). Because gas-flow stages of this type have been shown to develop a thermal gradient from the center of the sample chamber to the wall of the chamber of about 0.25 degrees C per mm (manufacturer's specifications), sample chips were positioned as close to the center of the stage as possible. The thermocouple junction was then placed in physical contact with the chip under observation. During heating runs, the chip was rapidly heated until the temperature approached the homogenization temperature when the heating rate was reduced to about 4 degrees C/minute

(in order to minimize error due to thermal gradients within the chip) until the homogenization temperature was reached.

The freezing points of inclusions were measured by dropping the temperature to around -30°C to freeze the inclusions. They were then heated to nearly the melting point when the heating rate was reduced to about $1^{\circ}\text{C}/\text{minute}$ until the last ice crystal melted (if visible) or until rapid expansion of the vapor bubble occurred. The vapor bubble expansion method yields only a minimum estimate of the melting point because small crystals of ice may be present after the bubble expands. However, in inclusions where melting at the last ice crystal was observed, bubble expansion occurred within 0.1 to 0.2 degrees C of the final melting temperature of the ice. Salinities were calculated from the freezing point depression of ice using the following equation:

$$\begin{aligned} \text{Wt. \% NaCl} &= 0.00 + 1.76958F - 4.2384 \times 10^{-2} F^2 \\ &+ 5.2778 \times 10^{-4} F^3 \pm 0.028 \end{aligned}$$

where the variable "F" equals the Freezing point depression in degrees C (Potter et al, 1978).

TABLE A-1

RESULTS OF HEATING FREEZING CALIBRATION RUNS

<u>HEATING CALIBRATION</u>					
<u>Melting Point</u> <u>Standard</u>	<u>Observed</u>	<u>T_{melting}</u>		<u>AVERAGE</u>	<u>Δ T</u>
TEMPILAQ 101°C	101.6	100.6	100.2	100.8	-0.2°C
TEMPILAQ 198°C	197.3	198.0	197.0	197.4	-0.6°C
TEMPILAQ 253°C	252.7	253.4	253.2	253.1	+0.1°C
TEMPILAQ 302°C	304.6	303.7	304.1	304.1	+2.1°C
<u>FREEZING CALIBRATION</u>					
<u>Material</u>	<u>True</u> <u>T_{freezing}</u>	<u>Observed</u> <u>T_{freezing}</u>		<u>AVERAGE</u>	<u>ΔT</u>
Triple distilled H ₂ O	-0.1°C	+0.8,+0.4,+0.6		+0.6°C	+0.7°C
n-tridecane	-5.4°C	-5.4,-5.4,-5.4		-5.4°C	0.0°C

TABLE A-2

Fluid Inclusion Data

<u>Sample Number</u>	<u>Inclusion Number</u>	<u>Material</u>	<u>Th</u>	<u>Tf</u>	<u>Origin</u>
19A15	a	Quartz	303.0	--	Primary
	b	Quartz	301.8	-0.8	Primary
19A9	a	Calcite	152.4	--	Secondary
	b	Calcite	350	--	Necked
19A10	a	Quartz	155.5	--	Secondary
29A2	a	Quartz	355.7	--	Necked
29A3	a	Quartz	181.4	--	Secondary
	b	Quartz	260.6	--	Primary
29A4	a	Quartz	99.8	--	Necked
29A5	a	Quartz	232.9	--	Primary
	b	Quartz	220.6	--	Primary
	c	Quartz	225.6	--	Primary
	d	Quartz	234.5	--	Primary
	e	Quartz	241.0	--	Primary
	f	Quartz	226.8	--	Primary
	g	Quartz	228.3	--	Primary
	h	Quartz	228.4	--	Primary

Sample	Inclusion				
<u>Number</u>	<u>Number</u>	<u>Material</u>	<u>Th</u>	<u>Tf</u>	<u>Origin</u>
29A9N	a	Quartz	177.6		Secondary
	b	Quartz	187.2	-1.1	Secondary
	c	Quartz	266.1	-0.5	Primary
	d	Quartz	266.6	-0.4	Primary
	e	Quartz	266.0		Primary
	f	Quartz	264.4		Primary
	g	Quartz	249.9		Primary
	h	Quartz	275.4		Primary
	i	Quartz	266.8		Primary
	j	Quartz	327.2		Primary
	k	Quartz	285.4		Primary
	l	Quartz	266.3		Primary
	m	Quartz	320.8		Primary
	n	Quartz	323.6		Primary
	o	Quartz		-0.5	Primary
p	Quartz		-0.8	Primary	
29A13(B)	a	Quartz	225.7		Primary
	b	Quartz	232.6		Primary
	c	Quartz	227.6		Primary
	d	Quartz	229.0		Primary

<u>Sample Number</u>	<u>Inclusion Number</u>	<u>Material</u>	<u>Th</u>	<u>Tf</u>	<u>Origin</u>
29A13(B) (cont.)	e	Quartz	229.0		Primary
	f	Quartz	240.9		Primary
	g	Quartz	226.4		Primary
	h	Quartz		-0.2	Primary
	i	Quartz		-0.2	Primary
	j	Quartz		-0.3	Primary
29A14	a	Quartz	223.6		Primary
	b	Quartz	191.1		Primary
	c	Quartz	192.0		Primary
	d	Quartz	221.1		Primary
	e	Quartz	231.8		Primary
	f	Quartz	152.7		Secondary
	g	Quartz	227.1		Primary
	h	Quartz	216.4		Primary
	i	Quartz	200.0		Primary
	j	Quartz	244.2		Necked ?
29A15	a	Calcite	210.7		Secondary
	b	Calcite	185.0		Secondary

<u>Sample Number</u>	<u>Inclusion Number</u>	<u>Material</u>	<u>Th</u>	<u>Tf</u>	<u>Origin</u>
29A15	c	Calcite	204.7		Secondary
(cont.)	d	Calcite	217.2		Secondary
	e	Calcite	225.4		Primary
	f	Calcite	202.1		Primary
	g	Calcite	217.6		Primary
	h	Calcite	233.2		Primary
	i	Calcite	234.4		Primary
	j	Calcite	222.3		Primary
	k	Calcite	221.8		Primary
	l	Calcite		-0.9	Primary
	m	Calcite		-0.8	Primary
	n	Calcite		-0.8	Primary
	o	Calcite		-0.8	Primary
	p	Calcite		-0.2	Primary
	q	Calcite		-0.4	Primary
	r	Calcite		-0.9	Primary
29A17	a	Quartz	209.6		Primary
	b	Quartz	194.6		Primary
	c	Quartz	190.0		Primary

<u>Sample Number</u>	<u>Inclusion Number</u>	<u>Material</u>	<u>Th</u>	<u>Tf</u>	<u>Origin</u>
29A17	d	Quartz	216.1		Primary
(cont.)	e	Quartz	200.2		Primary
	f	Quartz	216.2		Primary
29A22	a	Quartz	155.0		Secondary
29A23	a	Quartz	348.8		Necked
	b	Quartz	369.2		Necked
	c	Quartz		-0.8	Necked
	d	Quartz		-0.65	Necked
	e	Quartz		-0.75	Necked
	f	Quartz		-0.9	Necked
29A25	a	Quartz	140.7		Secondary
	b	Quartz	219.9		Primary
	c	Quartz	206.5		Primary
	d	Quartz	147.8		Secondary
	e	Quartz	143.0		Secondary
29AL4	a	Quartz	162.9		Secondary
	b	Quartz	229.1		Primary
	c	Quartz	226.2		Primary
	d	Quartz	309.0		Primary

<u>Sample Number</u>	<u>Inclusion Number</u>	<u>Material</u>	<u>Th</u>	<u>Tf</u>	<u>Origin</u>
29AL4	e	Quartz	319.0		Primary
(cont.)	f	Quartz	221.6		Primary
	g	Quartz	378(+)		Leaked
38A3	a	Quartz	200.3		Primary
	b	Quartz	195.3		Primary
	c	Quartz	199.7		Primary
	d	Quartz	217.5		Primary
	e	Quartz	213.1		Primary
	f	Calcite	220.9		Primary
	g	Calcite	226.2		Primary
	h	Calcite	216.6		Primary
	i	Calcite	238.9		Primary
	j	Calcite	232.6		Primary
38A6	a	Quartz	205.2		Primary
	b	Quartz	221.7		Primary
	c	Quartz	226.1		Primary
	d	Quartz	220.6		Primary
	e	Quartz	217.5		Primary
	f	Quartz	223.3		Primary

<u>Sample Number</u>	<u>Inclusion Number</u>	<u>Material</u>	<u>Th</u>	<u>Tf</u>	<u>Origin</u>
38A6	g	Quartz	223.3		Primary
(cont.)	h	Quartz	211.1		Primary
	i	Quartz	305.0		Primary
	j	Quartz	300.0		Primary
	k	Quartz	347.0		Necked
	l	Quartz	311.0		Primary
38A7	a	Quartz	255.0		Primary
	b	Quartz	234.3		Primary
	c	Quartz	232.6	-0.5	Primary
	d	Quartz	234.9	-0.5	Primary
38A8B	a	Quartz	219.0		Primary
38A13	a	Quartz	196.5		Primary
	b	Quartz	242.4		Primary
38A19	a	Quartz	224.5		Primary
	b	Quartz	216.6		Primary
	c	Quartz	172.3		Primary
	d	Quartz	179.4		Primary
	e	Quartz	150.0		Primary
	f	Quartz	200.8		Primary
	g	Quartz	201.7		Primary
	h	Quartz	184.2		Primary

APPENDIX B

TRACE ELEMENT GEOCHEMISTRY

All analyses were performed by Bondar-Clegg, Inc., except for those samples designated with a "*" which were analyzed by Cone Geochemical, Inc. The method of extraction, analysis and the detection limit for each element is presented for both companies. Although the accuracy and precision of the geochemical data was not determined, both geochemical laboratories consider their analyses accurate within ± 20 percent.

TABLE B-1
Analytical Results
Trace Element Geochemistry

SAMPLE NUMBER	PPM Cu+Zn+Pb	PPM Cu	PPM Zn	PPM Pb	PPM Ag	PPB Au	PPM As	PPM Sb	PPM Mo	PPM Sn	PPM W	PPM % F
8A1	14	7	5	2	0.2	5	NA	NA	10	NA	NA	NA
15XT6	46	43	1	2	0.2	5	NA	NA	2	NA	NA	NA
15XT7	7	4	1	2	0.2	5	NA	8	8	NA	NA	NA
15TBT6	746	5	91	650	1.4	10	100	2	7	NA	NA	NA
15TBT6*	40	5	5	30	0.8	20	77	NA	9	NA	NA	NA
15TBT9	7	4	1	2	0.2	5	NA	NA	NA	NA	NA	NA
15TBT16	6	3	1	2	0.2	5	NA	NA	10	NA	NA	NA
15TBT19*	16	6	6	4	0.9	20	84	NA	15	NA	NA	NA
15NGSK*	333	12	320	1	2.8	20	66	13	6	NA	NA	NA
17T13	9	12	12	6	0.2	5	NA	NA	1	NA	NA	NA
17XT5A	7	4	1	2	0.2	5	NA	NA	3	NA	NA	NA
17XT5C	16	4	1	11	0.2	5	NA	NA	13	NA	NA	NA
17XT14	5	2	1	2	0.2	5	NA	NA	2	NA	NA	NA
17XT23	6	3	1	2	0.2	5	NA	NA	1	NA	NA	NA
17XT26	41	4	1	36	0.2	5	NA	NA	11	NA	NA	NA
19A1S	-6	-3	-1	-2	-0.2	-5	NA	NA	-2	NA	NA	NA
19A1N	36	6	22	8	0.2	5	NA	NA	6	NA	NA	NA
19A2N	11	5	4	2	0.2	5	NA	NA	2	NA	NA	NA
19A5	40	11	25	4	0.2	5	NA	NA	3	NA	NA	NA
19A6B	39	22	12	5	0.2	5	NA	NA	5	NA	NA	NA
19A6C	9	6	1	2	0.2	5	NA	NA	5	NA	NA	NA
19A7	50	11	32	7	0.6	5	NA	NA	9	NA	NA	NA
19A8	21	6	11	4	0.2	5	NA	NA	2	NA	NA	NA
19A10	25	10	11	4	0.2	5	NA	NA	6	NA	NA	NA
21A1N	12	7	3	2	0.2	5	NA	NA	2	NA	NA	NA
21A2N	39	18	17	4	0.2	5	NA	NA	7	NA	NA	NA
21A3	41	32	1	8	0.2	5	NA	NA	7	NA	NA	NA
21PP1	363	6	353	4	0.2	5	NA	NA	3	NA	NA	NA
21PP3	183	6	173	4	0.2	5	NA	NA	3	NA	NA	NA
21XT7	48	33	10	5	0.2	5	NA	NA	4	NA	NA	NA
21XT20	32	8	18	6	0.2	5	NA	NA	8	NA	NA	NA
21NGM19*	427	6	420	1	2.0	20	383	NA	7	6	1	.03
21NGM20*	1665	34	1630	1	1.9	20	118	NA	5	2	2	.06
21NGM21*	412	8	400	4	2.0	20	70	NA	5	2	2	.05
27XT3	273	20	85	168	1.7	10	2	2	2	NA	NA	NA

TABLE B-1 (continued)

SAMPLE NUMBER	PPM Cu+Zn+Pb	PPM Cu	PPM Zn	PPM Pb	PPM Ag	PPB Au	PPM As	PPM Sb	PPM Mo	PPM Sn	PPM W	% F
27XT16	25	4	1	20	0.2	5	NA	NA	5	NA	NA	NA
27XT21	6	2	2	2	0.2	5	NA	NA	1	NA	NA	NA
27XT26W	5	2	1	2	0.2	5	NA	NA	2	NA	NA	NA
29A1	14	4	4	6	0.2	5	NA	NA	3	NA	NA	NA
29A4	6	3	1	2	0.2	5	NA	NA	8	NA	NA	NA
29A7	106	3	17	86	0.6	5	NA	NA	5	NA	NA	NA
29A9N	12	5	5	2	0.2	5	NA	NA	14	NA	NA	NA
29A9S	43	10	27	6	0.2	5	NA	NA	7	NA	NA	NA
29A12	526	82	362	82	1.3	5	NA	NA	8	NA	NA	NA
29A13A	254	53	179	22	1.4	5	NA	NA	5	NA	NA	NA
29A13B	29	7	7	15	0.9	5	NA	NA	4	NA	NA	NA
29A16	44	11	25	8	0.2	10	NA	NA	1	NA	NA	NA
29A18	349	108	235	6	0.2	10	NA	NA	13	NA	NA	NA
29A19	108	9	40	59	2.2	10	205	19	6	NA	NA	NA
29A21	36	10	24	2	0.2	5	NA	NA	3	NA	NA	NA
29Tnwp3	92	23	51	18	1.3	5	NA	NA	4	NA	NA	NA
31A1	186	65	106	15	0.2	5	390	10	5	NA	NA	NA
31A2	12	8	2	2	0.2	5	NA	NA	1	NA	NA	NA
31A3	46	9	29	8	0.2	5	NA	NA	7	NA	NA	NA
31A5	205	7	191	7	0.2	5	NA	NA	1	NA	NA	NA
31A7	136	65	64	7	0.2	5	NA	NA	8	NA	NA	NA
31A9	73	19	39	15	0.2	5	NA	NA	66	INT	3	.02
31A10	33	10	17	6	0.2	5	NA	NA	4	NA	NA	NA
31A11	158	150	6	2	0.2	5	NA	NA	1	NA	NA	NA
31A12	76	27	46	3	0.2	5	NA	NA	6	NA	NA	NA
31A12	57	11	25	21	0.4	5	NA	NA	5	NA	NA	NA
31A13	18	8	8	2	0.2	5	NA	NA	1	NA	NA	NA
31A14	66	9	14	43	1.4	5	NA	NA	6	NA	NA	NA
31A14A	18	9	5	4	0.2	5	NA	NA	3	NA	NA	NA
31XT30	5	2	1	2	0.2	5	NA	NA	1	NA	NA	NA
31SK	495	36	440	19	1.5	5	NA	NA	6	NA	NA	NA
31QV	76	33	13	30	1.0	5	NA	NA	5	NA	NA	NA
31NGM18*	113	35	64	14	0.9	20	209	NA	2	2	1	.03
38A4	48	16	23	9	0.2	5	NA	NA	1	NA	NA	NA
38A6	33	4	12	17	0.5	5	NA	NA	1	NA	NA	NA

TABLE B-1 (continued)

SAMPLE NUMBER	PPM Cu+Zn+Pb	PPM Cu	PPM Zn	PPM Pb	PPM Ag	PPB Au	PPM As	PPM Sb	PPM Mo	PPM Sn	PPM W	% F
38A7	19	2	8	9	0.3	5	NA	NA	3	NA	NA	NA
38A8	47	9	30	8	0.2	20	205	2	11	NA	NA	NA
38A13	41	8	26	7	0.2	5	NA	NA	5	NA	NA	NA
38A16	13	4	5	4	0.2	5	NA	NA	3	NA	NA	NA
38A17	23	8	13	2	0.5	30	123	19	393	5	4	.01
38QV1	55	11	33	11	0.2	5	NA	NA	5	NA	NA	NA
38NGM15*	22	7	12	3	0.3	20	10	NA	2	1	1	.01
38NGM16*	27	6	18	3	0.4	20	43	NA	8	3	1	.02
38NGM17*	31	7	19	5	0.4	20	52	NA	1	4	1	.01
40A2	10	5	2	3	0.2	5	NA	NA	7	NA	NA	NA
40A6	22	7	10	5	0.2	5	NA	NA	2	NA	NA	NA
40A7B	69	4	31	34	1.4	5	NA	NA	6	NA	NA	NA
40A8S	10	6	2	2	0.2	5	NA	NA	5	NA	NA	NA
40A10	71	15	45	11	0.2	5	NA	NA	20	NA	NA	NA
40A11	73	35	32	6	0.2	5	NA	NA	3	NA	NA	NA
40A14	5	2	1	2	0.2	5	NA	NA	1	NA	NA	NA
40S1B	43	3	18	22	0.6	5	NA	NA	2	NA	NA	NA
40NGM1*	43	6	20	17	0.7	20	3	NA	1	3	1	.03
40NGM2*	57	8	27	22	0.7	20	5	NA	1	1	1	.04
40NGM3*	54	5	34	15	0.6	20	4	NA	2	3	2	.02
40NGM4*	37	5	22	10	0.8	20	8	NA	1	2	2	.02
40NGM5*	35	5	12	18	0.7	20	17	NA	1	4	1	.03
40NGM6*	31	4	12	15	0.5	20	8	NA	1	4	1	.03
40NGM7*	48	5	28	15	0.8	20	42	NA	3	5	2	.02
40NGM9*	58	4	30	24	0.6	20	4	NA	2	2	2	.04
40NGM10*	51	5	17	29	0.7	20	6	NA	1	3	2	.05
40NGM11*	70	10	38	22	0.8	20	2	NA	1	2	2	.04
40NGM12*	74	5	50	19	0.9	20	2	NA	1	2	1	.02
40NGM13*	58	4	39	15	0.8	20	3	NA	1	3	1	.04
40NGM14*	56	5	32	19	0.8	20	4	NA	1	2	2	.04
BLANK	12	5	5	2	0.2	0.5	NA	NA	5	NA	NA	NA

NA = Not Analyzed

INT = Interference

**TABLE B-2. ANALYTICAL PROCEDURE,
CONE GEOCHEMICAL INC.**

Minus 100 Mesh Fraction Used for Analysis

<u>Element</u>	<u>Extraction</u>	<u>Method of Analysis</u>	<u>Detection Limit</u>
Mo	4 Acid	Atomic Absorption	1 ppm
Cu	do.	do.	1 ppm
Zn	do.	do.	1 ppm
Pb	do.	do.	1 ppm
Ag	do.	do.	.02 ppm
Au	Agua Regia	do.	.02 ppm
As	do.	do.	2 ppm
W	do.	Colorimetric	1 ppm
F	Fusion	Specific Ion	.01 %
Sn	Iodide Fusion	Atomic Absorption	1 ppm
Sb	do.	X-ray Fluorescence	1 ppm

TABLE B-3. ANALYTICAL PROCEDURE,
BONDAR-CLEGG INC.

Fraction Used for Analyses: Rocks - 100 mesh

<u>Element</u>	<u>Extraction</u>	<u>Method of Analysis</u>	<u>Detection Limit</u>
Mo	Hot Lefort Agua Regia	Atomic Absorption	1 ppm
Cu	do.	do.	1 ppm
Zn	do.	do.	1 ppm
Pb	do.	do.	2 ppm
Ag	do.	do.	0.1 ppm
Au	Fire Assay and Hot Agua Regia	do.	5 ppb
As	Perchloric Nitric	Colorimetric	2 ppm
W	Basic Oxidizing Fusion	Colorimetric	2 ppm
F	Basic Fusion	Citrate Buffer-Specific Ion	20 ppm
Sn	do.	X-ray Fluorescence	1 ppm
Sb	do.	X-ray Fluorescence	1 ppm

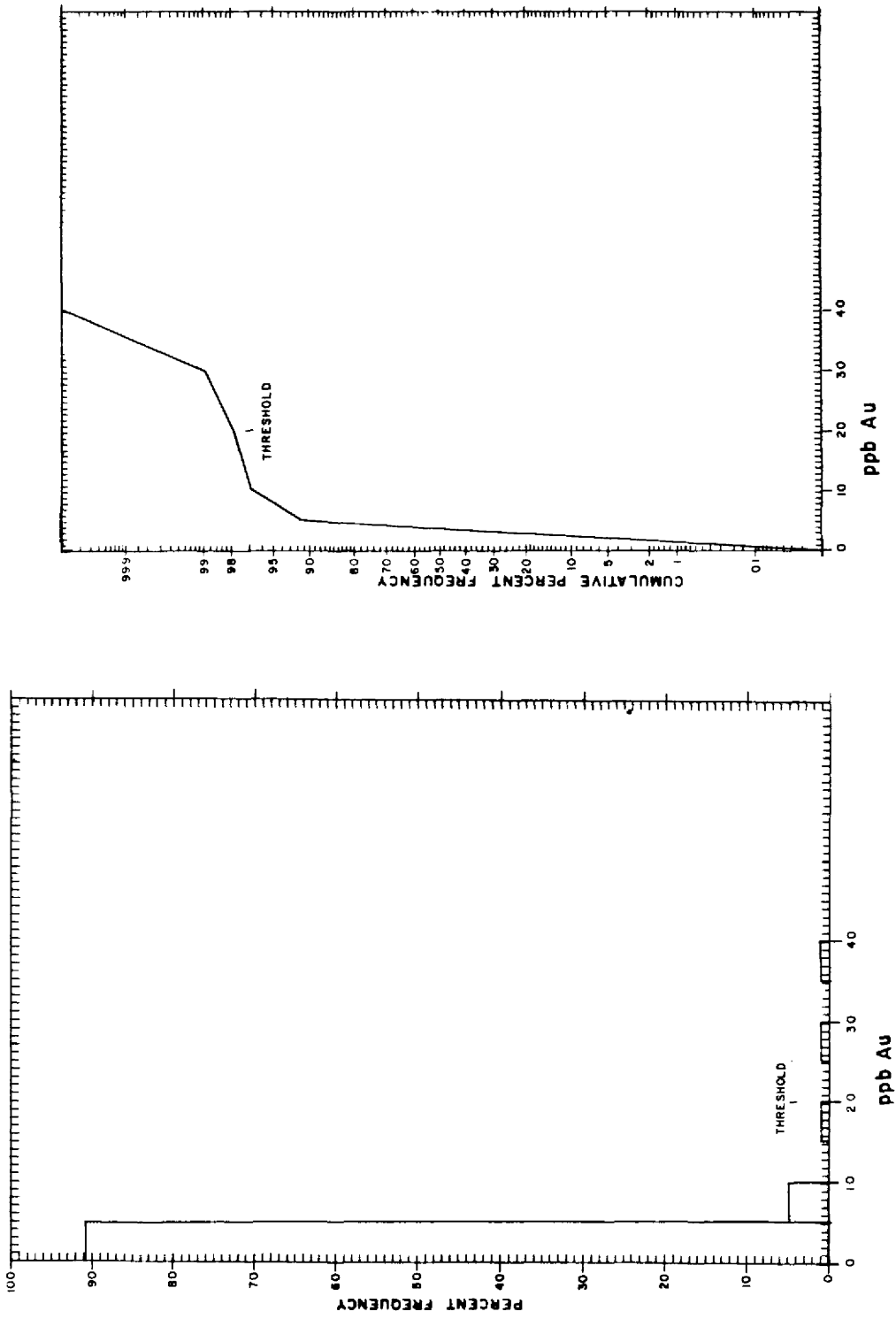


Figure B-1. Percent Frequency Histogram and Cumulative Percent Frequency Probability Plot - Gold

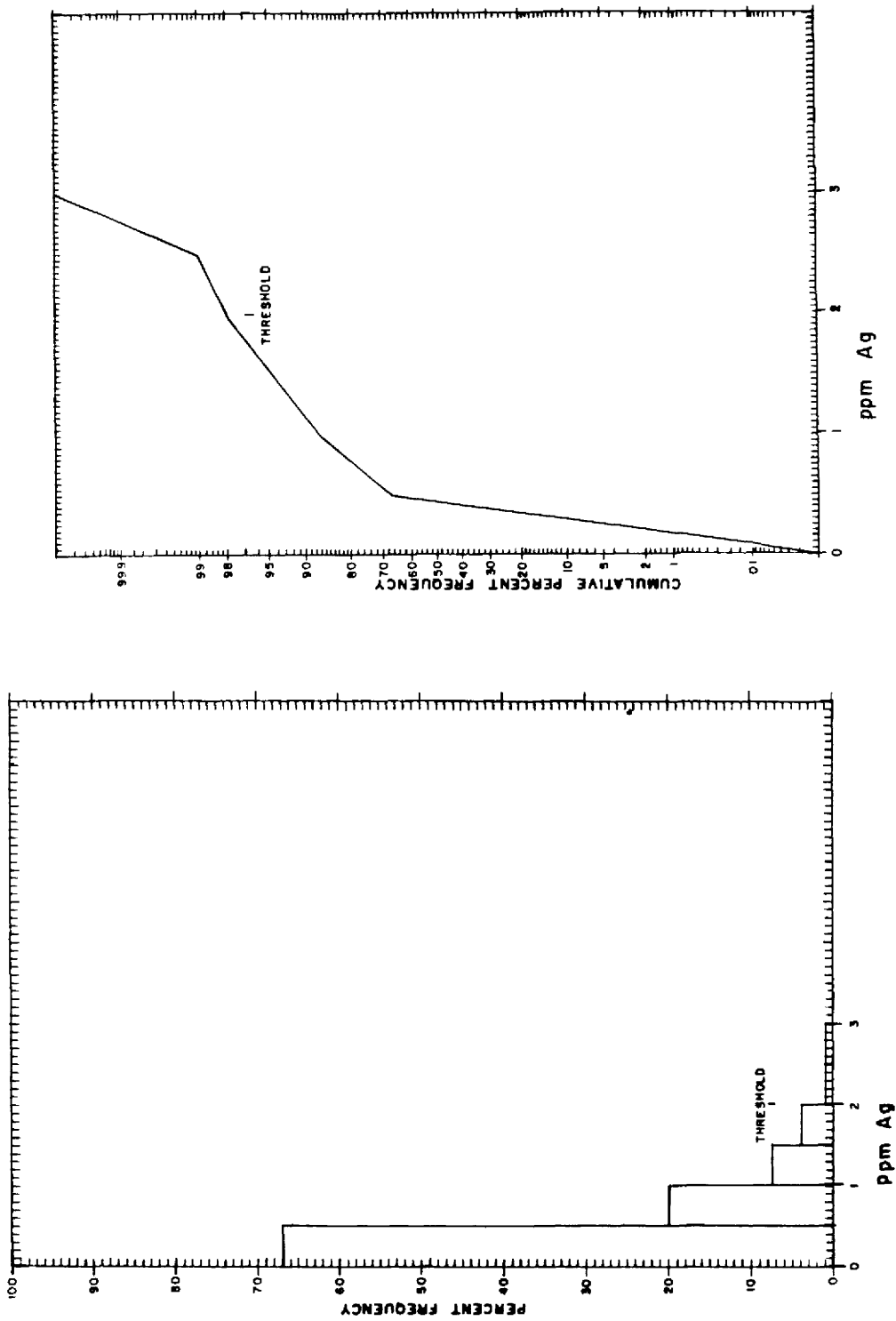


Figure B-2. Percent Frequency Histogram and Cumulative Percent Frequency Probability Plot - Silver

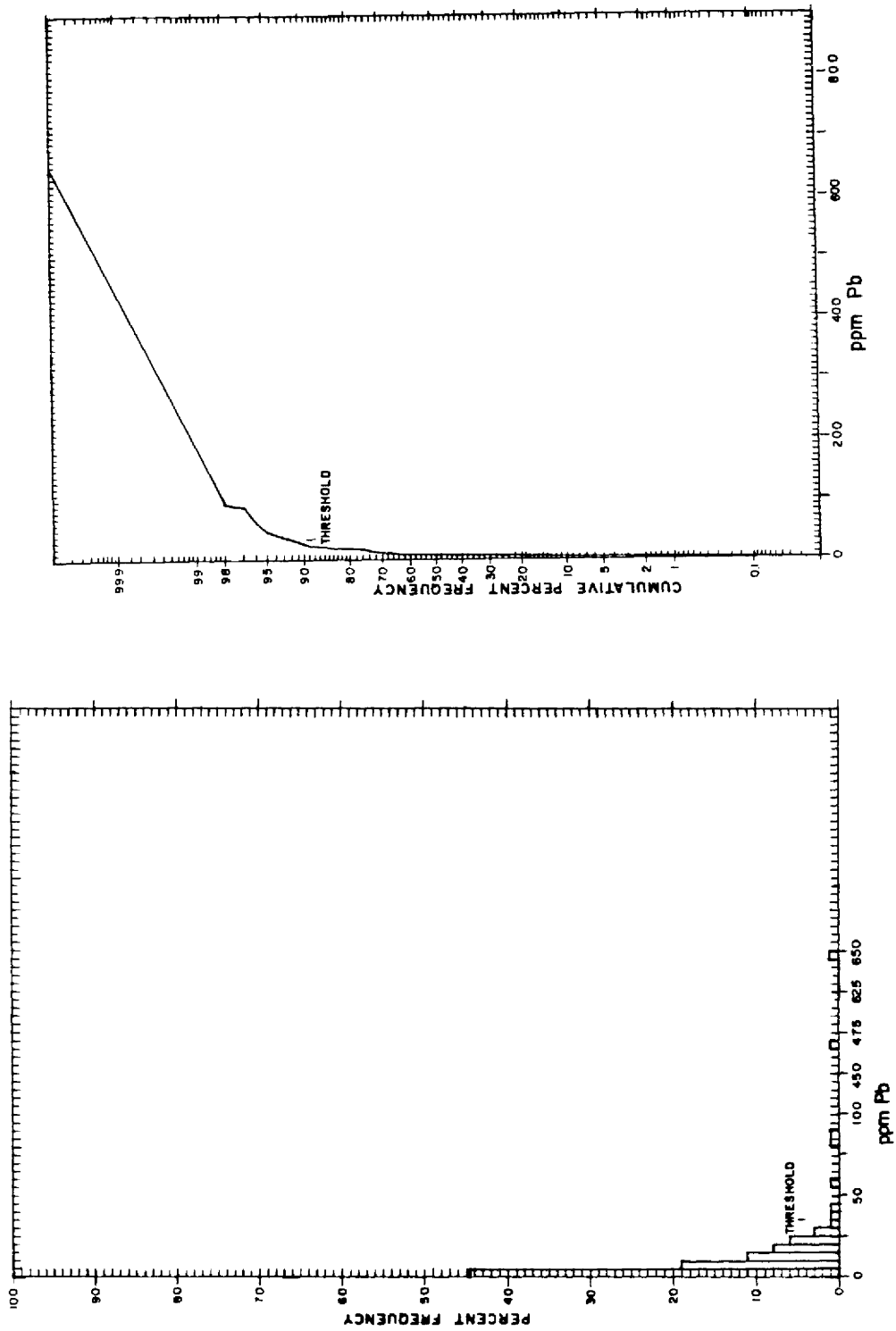


Figure B-3. Percent Frequency Histogram and Cumulative Percent Frequency Probability Plot - Lead

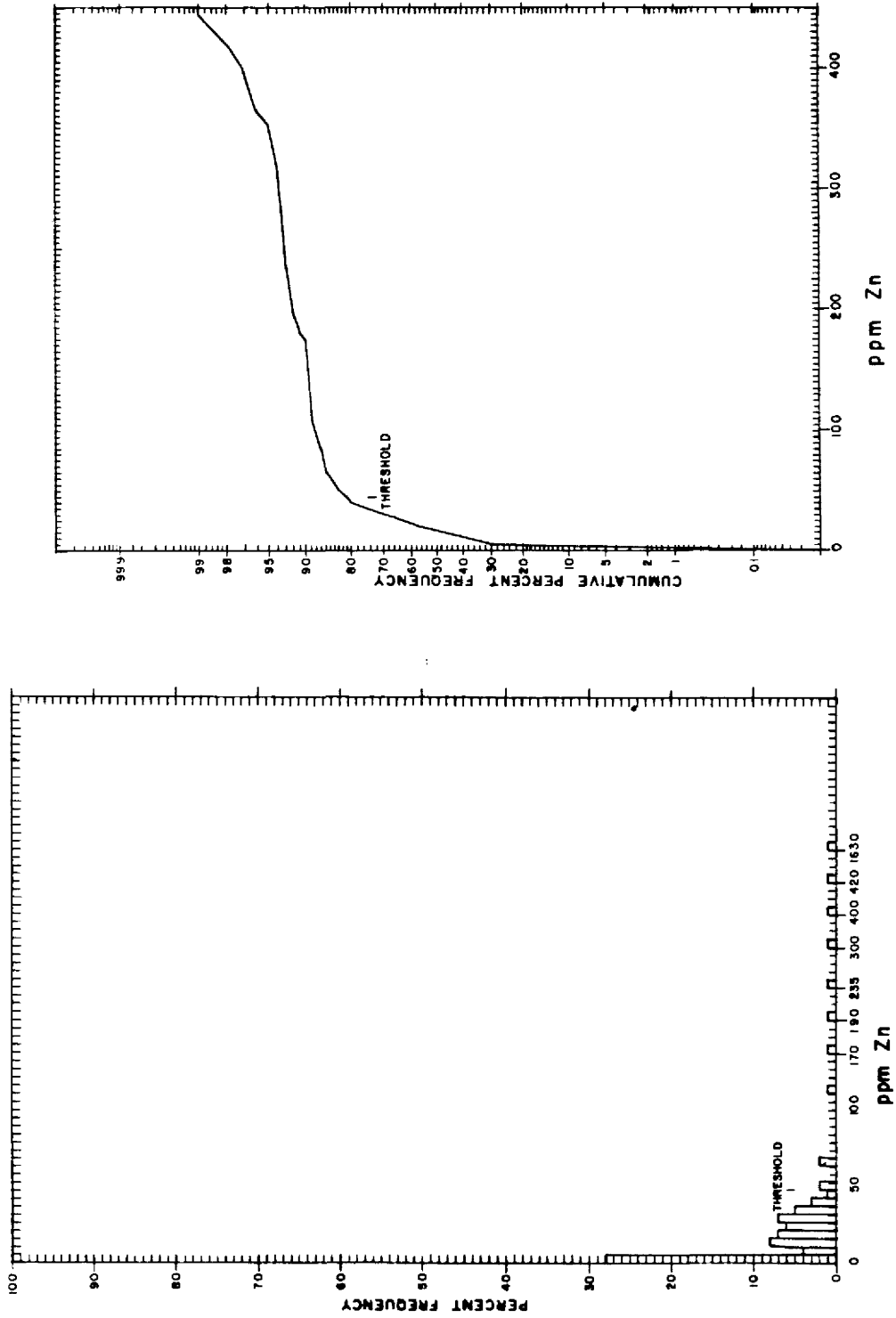


Figure B-4. Percent Frequency Histogram and Cumulative Percent Frequency Probability Plot - Zinc

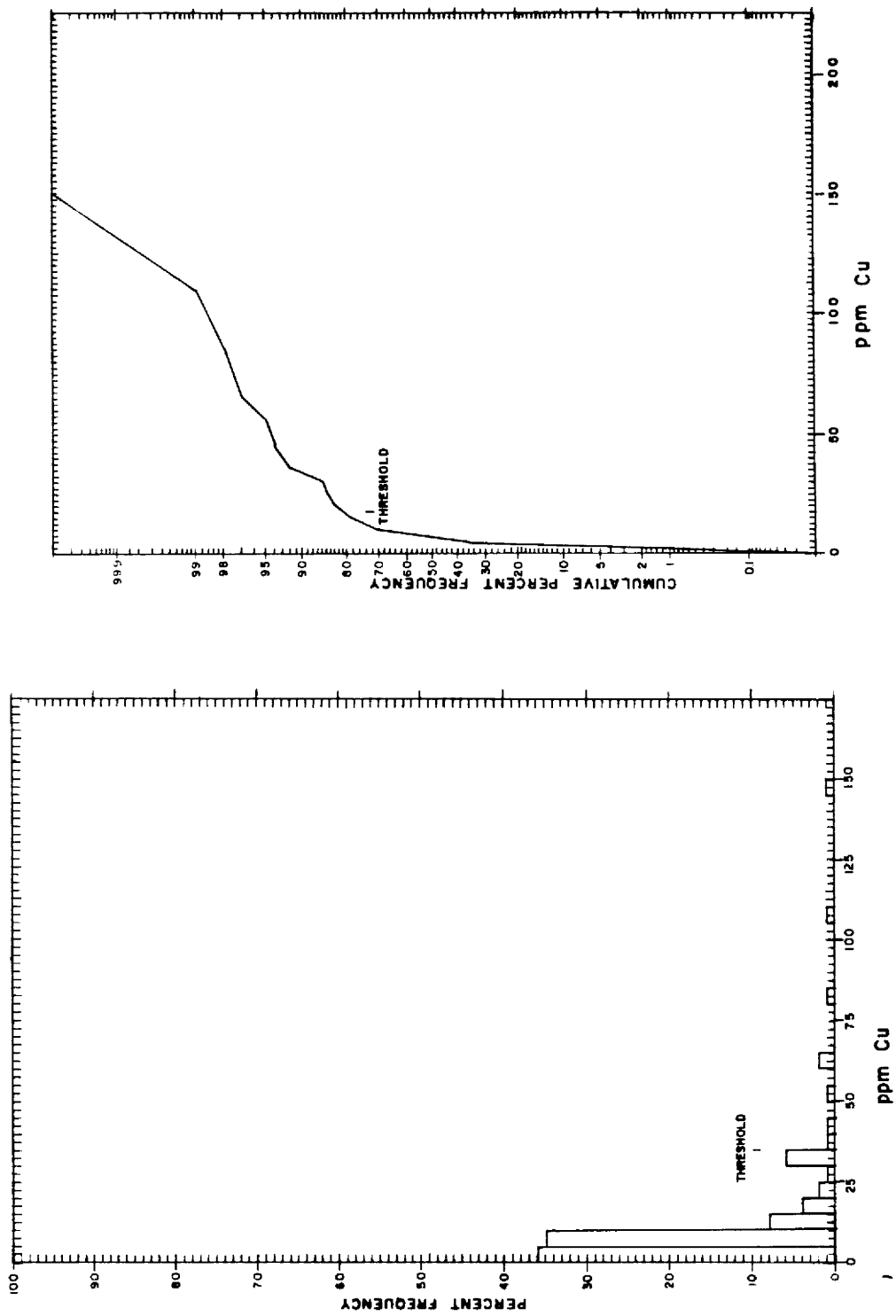


Figure B-5. Percent Frequency Histogram and Cumulative Percent Frequency Probability Plot - Copper

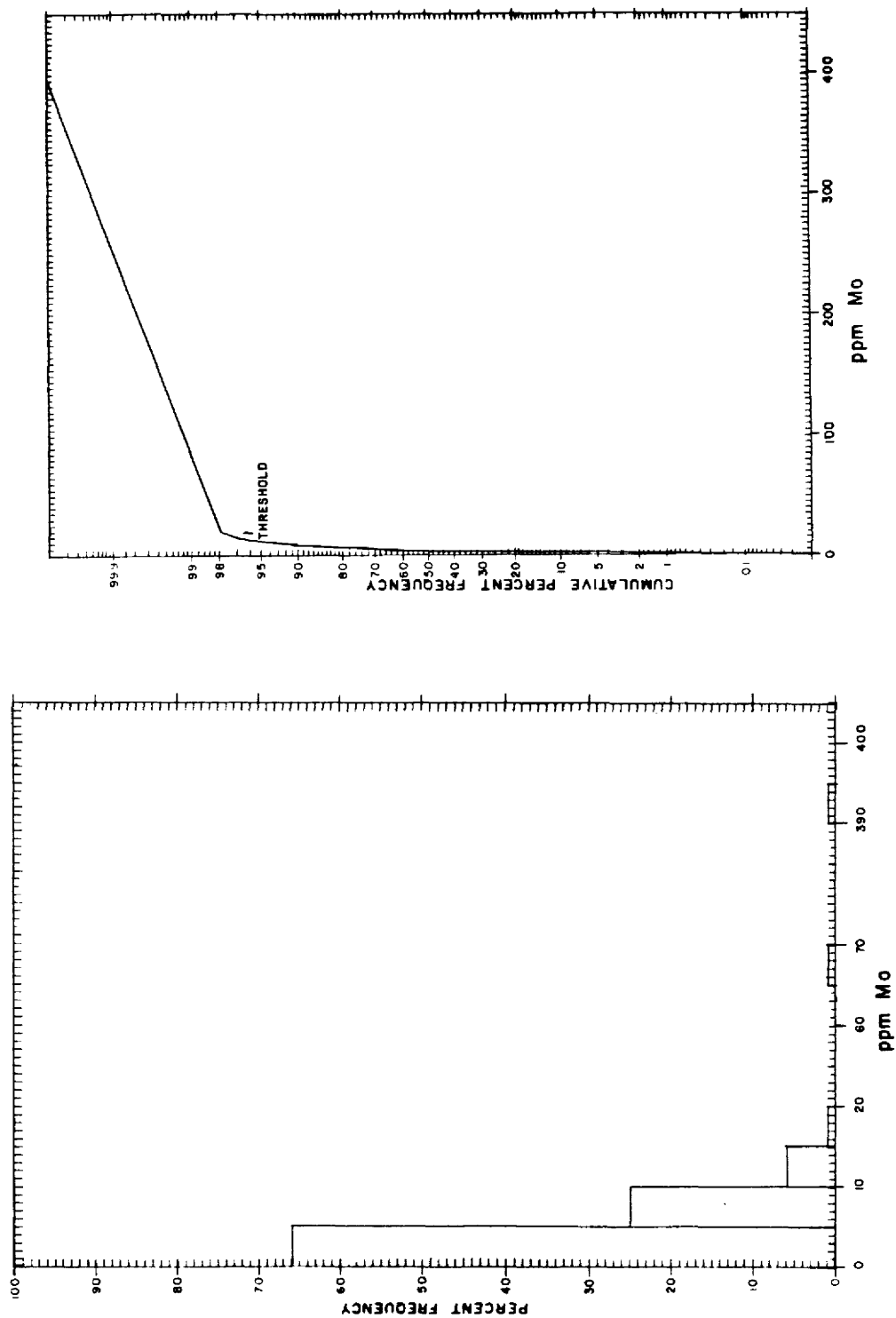


Figure B-6. Percent Frequency Histogram and Cumulative Percent Frequency Probability Plot - Molybdenum

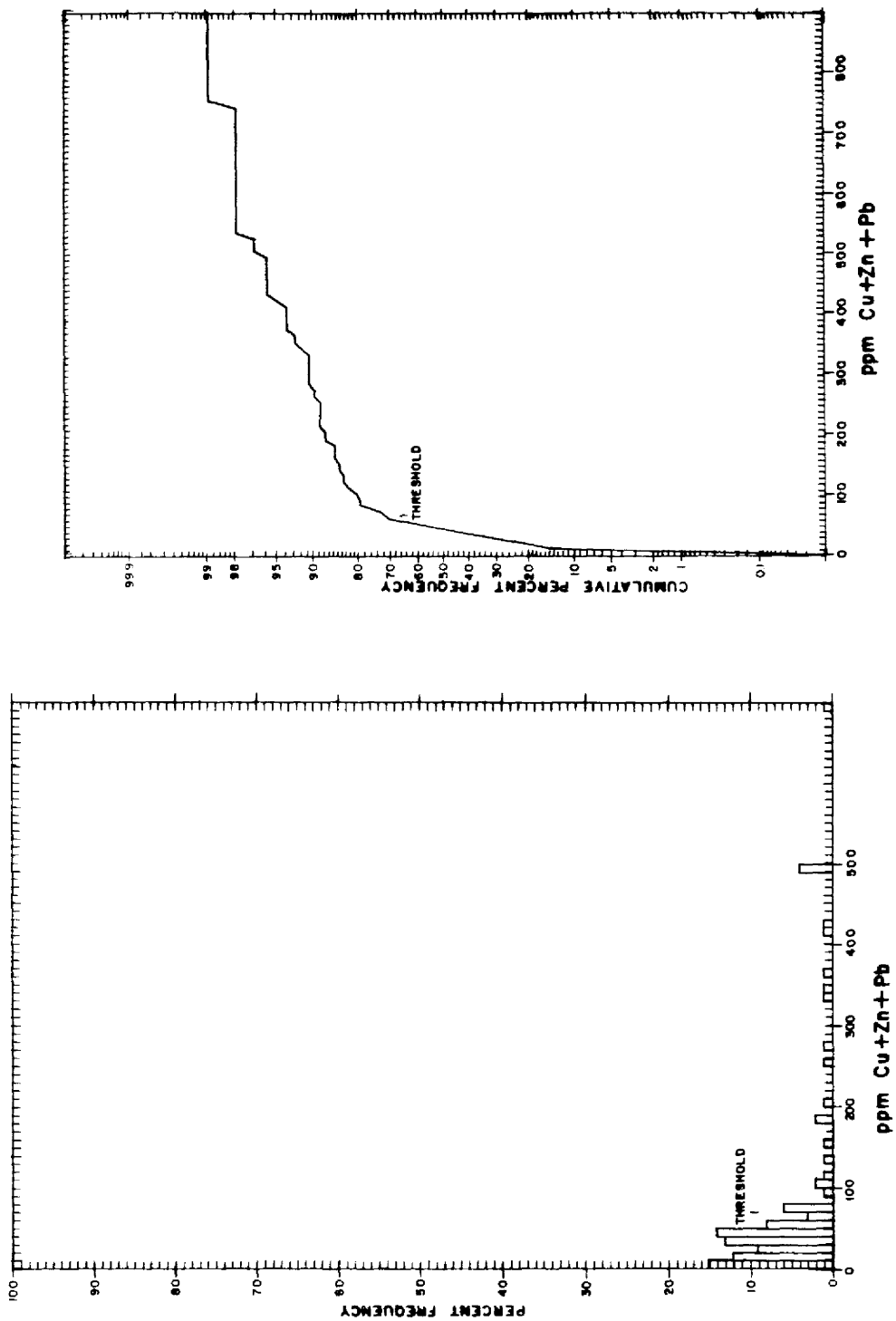


Figure B-7. Percent Frequency Histogram and Cumulative Percent Frequency Probability Plot - Copper, Zinc, and Lead Product

EXPLANATION, GEOLOGIC MAP

QUATERNARY		ALLUVIUM AND COLLUVIUM	20	STRIKE AND DIP OF BEDS
PLIOCENE		BASALT OF BRIMSTONE RESERVOIR	35	STRIKE AND DIP OF FOLIATION
		RHYOLITE PLUS, DOME, AND FLOW MEMBER, FORMATION OF BLAWN WASH		VERTICAL FOLIATION
MIOCENE		LATITE ASH-FLOW TUFF MEMBER, FORMATION OF BLAWN WASH		
		BAUERS TUFF MEMBER, CONDOR CANYON FORMATION QUICHAPA GROUP		
		MAFIC DIKE AND FLOW MEMBER, FORMATION OF BLAWN WASH		
		RHYOLITE TUFF MEMBER, FORMATION OF BLAWN WASH		
		BALDHILLS TUFF MEMBER, ISOM FORMATION		
		WALLACES PEAK TUFF MEMBER, NEEDLES RANGE FORMATION		
		LUND TUFF MEMBER, NEEDLES RANGE FORMATION		
		WAH WAH SPRINGS MEMBER, NEEDLES RANGE FORMATION		
		COTTONWOOD WASH MEMBER, NEEDLES RANGE FORMATION		
		LAMERDORF TUFF MEMBER, ESCALANTE DESERT FORMATION		
OLIGOCENE		UNDIVIDED PALEOZOIC CARBONATES		
		FAULT - DASHED WHERE APPROXIMATELY LOCATED, DOTTED WHERE CONCEALED		
TERTIARY		FAULT - "D" ON DOWNTHROWN SIDE		
		TRUST FAULT - TEETH ON UPPER PLATE		
		CONTACT - DASHED WHERE APPROXIMATELY LOCATED, DOTTED WHERE CONCEALED		

A — A'
LINE OF CROSS SECTION PRESENTED ON PLATE 2

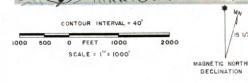


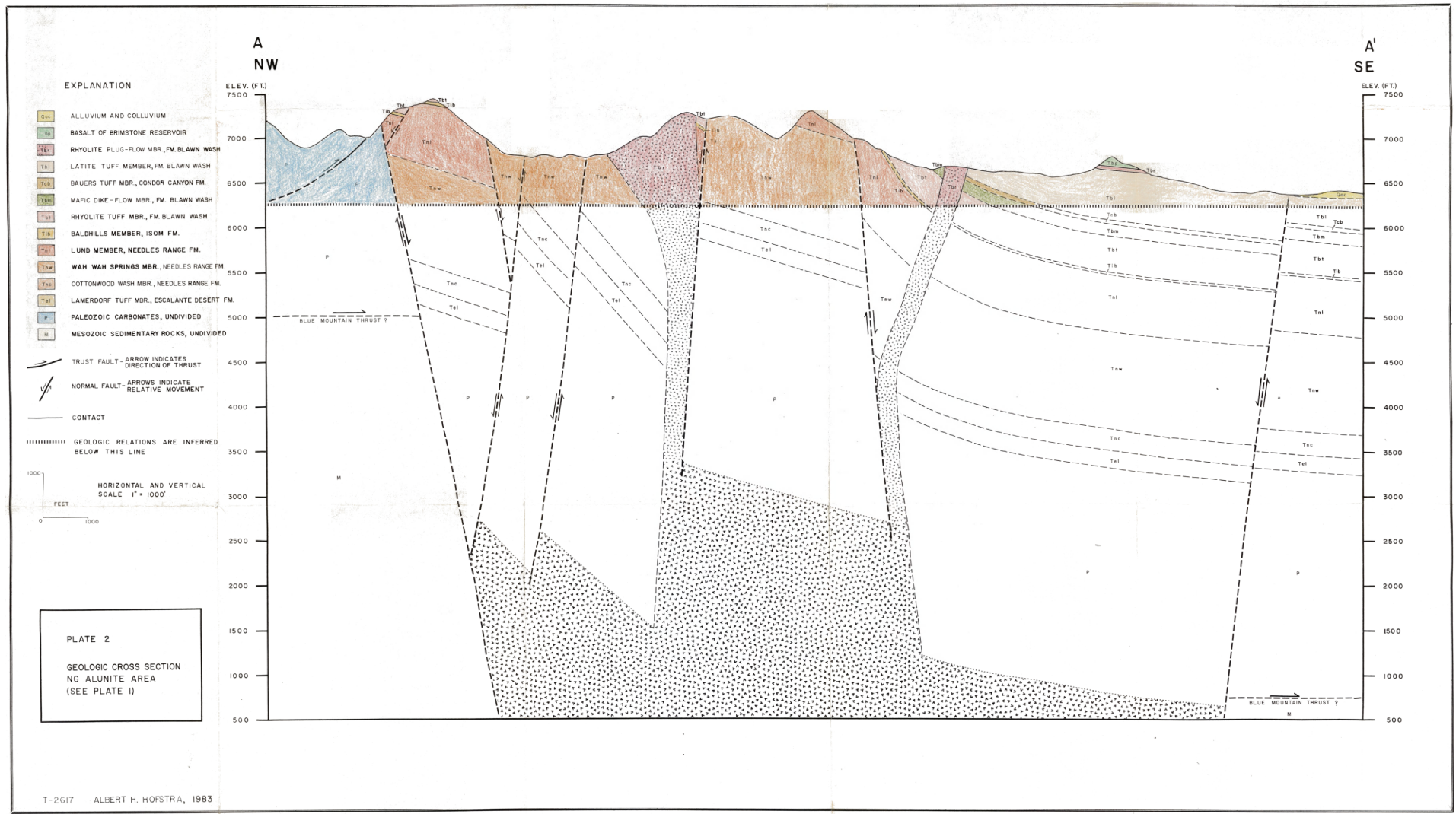
PLATE I
GEOLOGIC MAP
NG ALUNITE AREA

NOTE: The geology of NG AREA D and of the PALEOZOIC CARBONATES is adapted from Miller (1966), Best (1968), written common (Lund, 1968) and (Gardner) (1970).




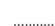
T-2617 ALBERT H. HOFSTRA, 1983



XANTHUS LAKES LIBRARY
COLORADO SCHOOL of MINES
GOLDEN, COLORADO 80401



- EXPLANATION**
- ALLUVIUM AND COLLUVIUM
 - BASALT OF BRIMSTONE RESERVOIR
 - RHYOLITE PLUG-FLOW MBR., FM. BLAWN WASH
 - LATITE TUFF MEMBER, FM. BLAWN WASH
 - BAUERS TUFF MBR., CONDOR CANYON FM.
 - MAFIC DIKE-FLOW MBR., FM. BLAWN WASH
 - RHYOLITE TUFF MBR., FM. BLAWN WASH
 - BALDHILLS MEMBER, ISOM FM.
 - LUND MEMBER, NEEDLES RANGE FM.
 - WAH WAH SPRINGS MBR., NEEDLES RANGE FM.
 - COTTONWOOD WASH MBR., NEEDLES RANGE FM.
 - LAMERDORF TUFF MBR., ESCALANTE DESERT FM.
 - PALEOZOIC CARBONATES, UNDIVIDED
 - MESOZOIC SEDIMENTARY ROCKS, UNDIVIDED

-  TRUST FAULT - ARROW INDICATES DIRECTION OF THRUST
-  NORMAL FAULT - ARROWS INDICATE RELATIVE MOVEMENT
-  CONTACT
-  GEOLOGIC RELATIONS ARE INFERRED BELOW THIS LINE

HORIZONTAL AND VERTICAL SCALE 1" = 1000'

FEET

0 1000 2000

PLATE 2











GEOLOGIC CROSS SECTION
NG ALUNITE AREA
(SEE PLATE I)

T-2617 ALBERT H. HOFSTRA, 1983

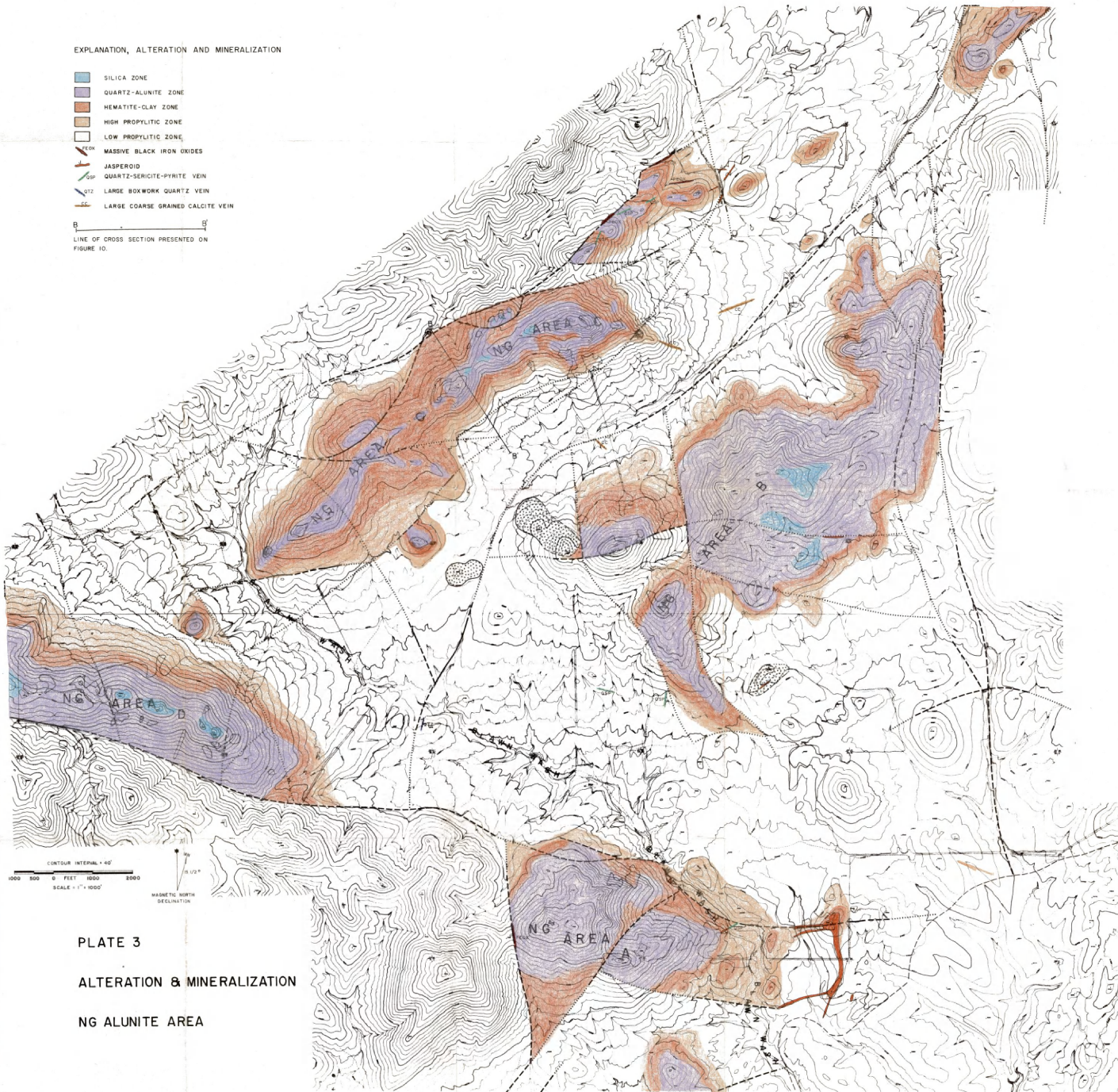
ARTHUR LAKES LIBRARY
COLORADO SCHOOL OF MINES
GOLDEN, COLORADO 80401



EXPLANATION, ALTERATION AND MINERALIZATION

-  SILICA ZONE
-  QUARTZ-ALUNITE ZONE
-  HEMATITE-CLAY ZONE
-  HIGH PROPYLITIC ZONE
-  LOW PROPYLITIC ZONE
-  MASSIVE BLACK IRON OXIDES
-  JASPEROID
-  QUARTZ-SERICITE-PYRITE VEIN
-  LARGE BOXWORK QUARTZ VEIN
-  LARGE COARSE GRAINED CALCITE VEIN

B
LINE OF CROSS SECTION PRESENTED ON
FIGURE 10.



CONTOUR INTERVAL = 40'
0 500 1000 1500 2000
SCALE = 1" = 1000'

MAGNETIC NORTH
DECLINATION

PLATE 3
ALTERATION & MINERALIZATION
NG ALUNITE AREA

EXPLANATION, SAMPLE LOCATIONS

- 21X77 TRACE ELEMENT GEOCHEMISTRY SAMPLE LOCATION
- 40478 FLUID INCLUSION SAMPLE LOCATION
- 31X79 K-Ar AGE DATE SAMPLE LOCATION
- ▲ 21X70 SULPHUR ISOTOPE SAMPLE LOCATION

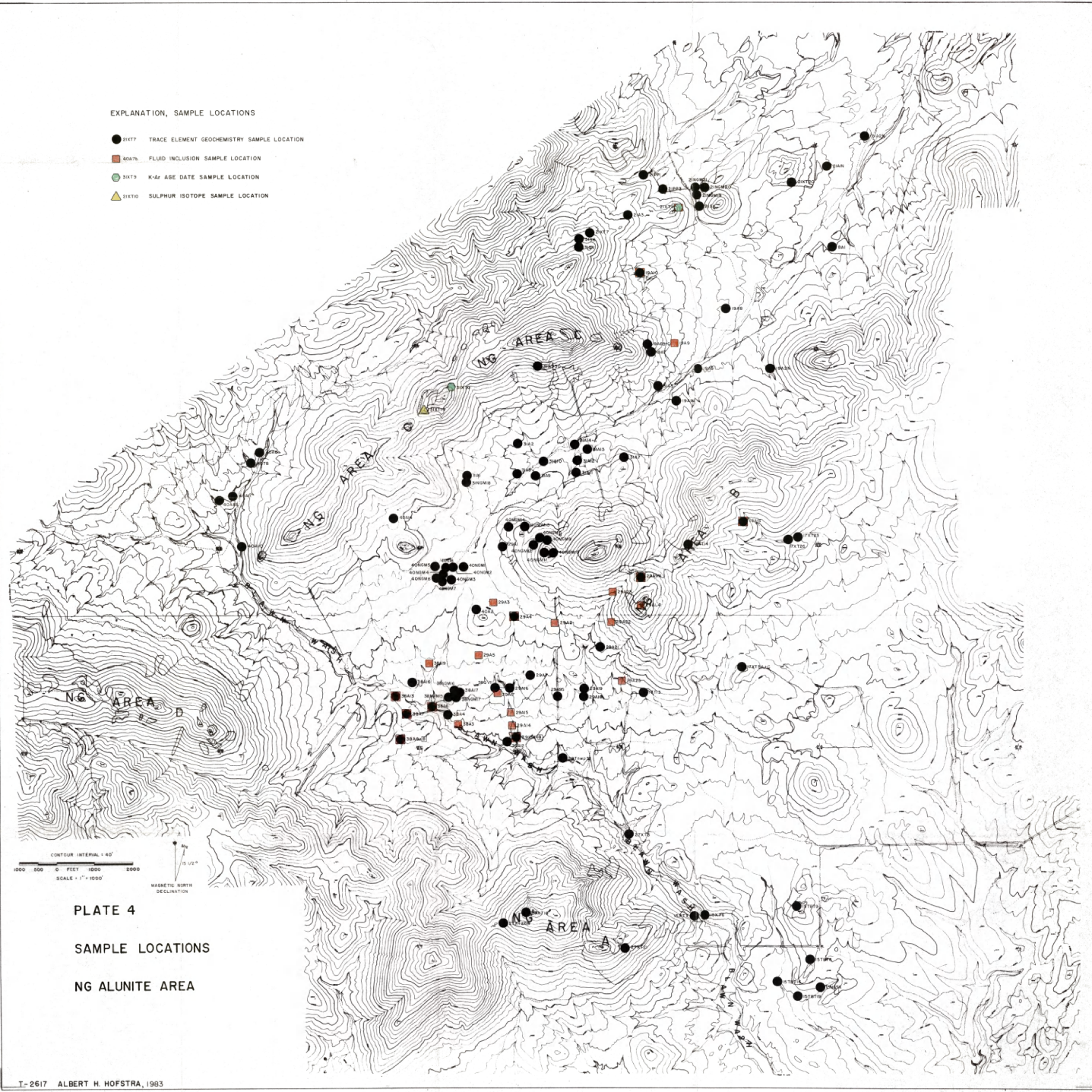


PLATE 4
SAMPLE LOCATIONS
NG ALUNITE AREA

T-2617 ALBERT H. HOFSTRA, 1983

ARTHUR LEXER LIBRARY
COLORADO SCHOOL OF MINES
GOLDEN, COLORADO 80401



EXPLANATION, TRACE ELEMENT GEOCHEMISTRY

- ^{Q1} Quartz-Sericite-Pyrite Vein Showing Anomalous Au/Ag Values
- Cu+Zn+Pb > 65 ppm ▲ ALTERED VOLCANICS
- Cu > 35 ppm ▲ JASPEROID
- Zn > 45 ppm ▲ BLACK Fe-OXIDES
- Pb > 35 ppm ○^{Q2} QUARTZ SERICITE VEIN
- Ag > 2 ppm ○ QUARTZ VEIN
- Au > 20 ppb ○ CALDERA
- Mo > 20 ppm

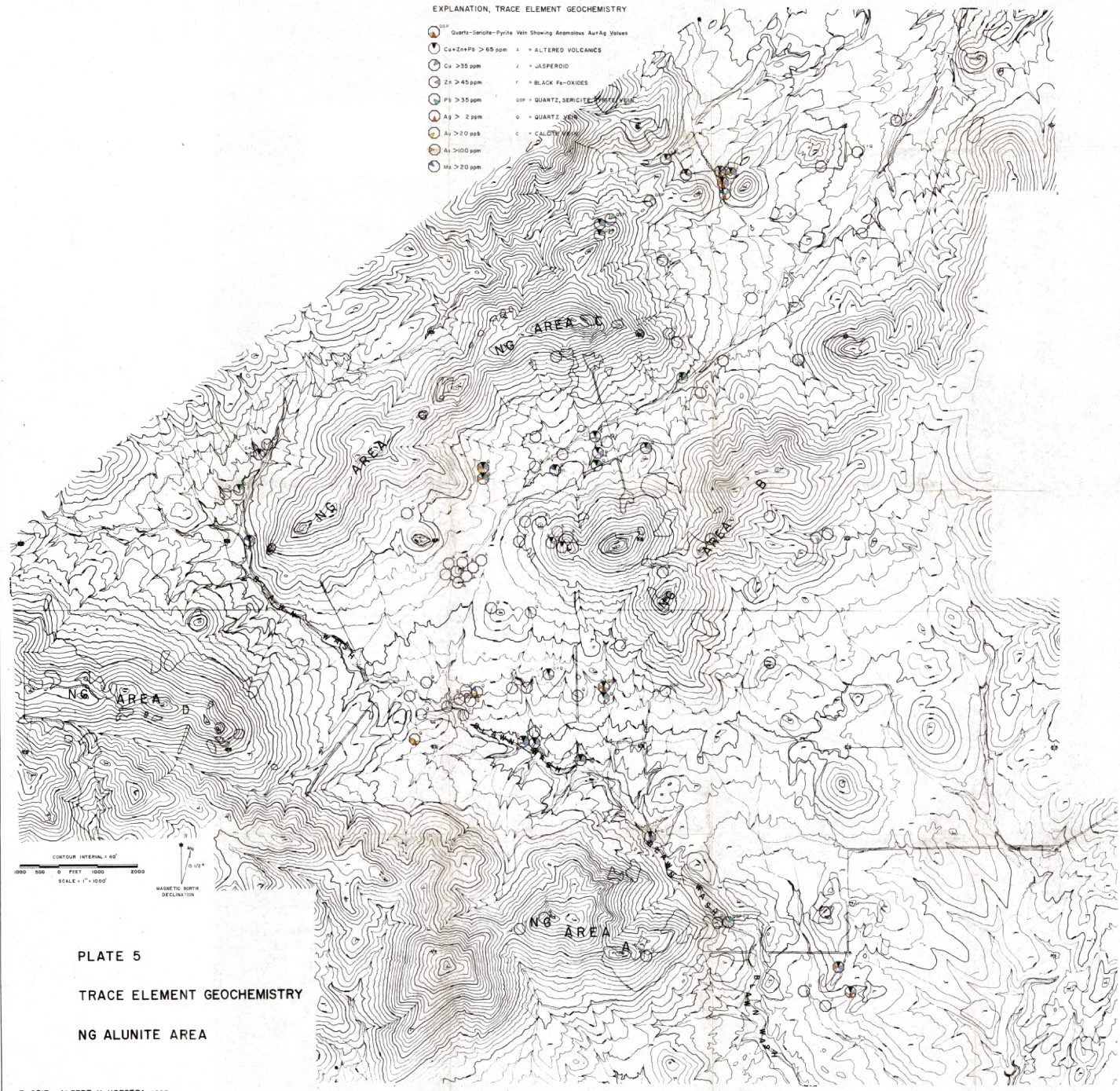


PLATE 5
TRACE ELEMENT GEOCHEMISTRY
NG ALUNITE AREA

T-2617 ALBERT H. HOFSTRA, 1983



ARTHUR LAKES LIBRARY
COLORADO SCHOOL OF MINES
GOLDEN, COLORADO 80408